AD-A204 736 METHODS FOR STUDYING EFFECTS OF HIGH-ENERGY IRRADIATION ON THE MECHANICAL..(U) HACETTEPE UNIV ANKARA (TURKEY) P MEDUIG 1987 R/D-5980-CH-02 DAJA45-88-M-0294 1/1

UNCLASSIFIED F/G 7/6 NL

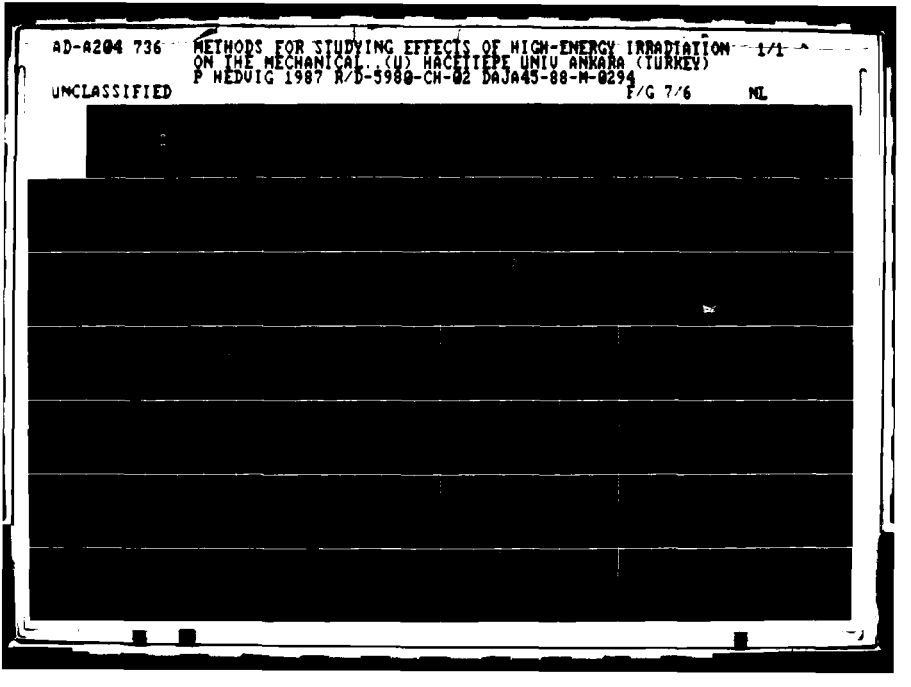

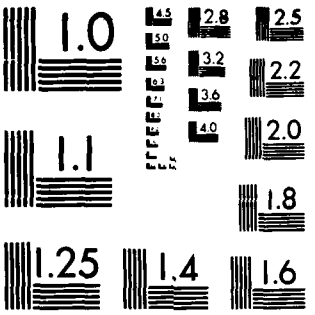
1.0
1.1
1.25
1.4
1.6
1.8
2.0
2.2
2.5
2.8
3.2
3.6
4.0
4.5
5.0
5.6
6.3

Methods for studying ~~the~~ effects of high-energy irradiation on the mechanical and electronic properties of polymers

Péter Hedvig
~~Research Institute for Plastics~~
Budapest 1950, Hungary

INTRODUCTION

High energy electron-, X-ray- or gamma-irradiation is known to result in degradation and/or crosslinking of polymers [1]. Crosslinking usually dominates when the polymer is irradiated in the absence of oxygen while degradation is overwhelming when oxygen is present.

The aim of this paper is to discuss how to measure the effects of high energy irradiation on the main mechanical and electric properties of polymers.

In the following sections the most important properties will be defined and the methods of their measurement discussed with illustrative experimental examples.

MECHANICAL PROPERTIES

The response of a material to a ~~external~~ mechanical load is expressed in terms of a response function which describes how the system would reach thermodynamical equilibrium after being subjected to ~~external~~ mechanical action. This action may be a constant strain, ε_o, which results in a decaying stress, $\sigma(t)$. This stress may be expressed in terms of the time-dependent stress-relaxation response function $\phi_\sigma(t)$ as

$$\sigma(t) = \sigma(\infty) + [\sigma(0) - \sigma(\infty)]\,\phi_\sigma(t) \qquad (1)$$

where $\sigma(\infty)$ is the stress at $t \to \infty$; $\sigma(0)$ is that just after straining; $\phi_\sigma(t)$ is dimensionless and is normalized as $\phi_\sigma(0) = 1$; $\phi_\sigma(\infty) = 0$. This function is independent on strain in the so called "rheologically linear" range which is for elastomers ε_o = 100-400 %, for uncrosslinked polymers up to about 50 % in certain temperature ranges, for semi-crystalline polymers up to about 2 %. Amorphous polymers below their glass-transition temperature are essentially rheologically nonlinear systems.

Equation (1) describes the response of the material to a step-function strain. When the strain is time-dependent, $\varepsilon(t)$, the response is expressed as

$$\sigma(t) = \dots \int_{t'=0}^{t} \frac{d\phi_\sigma(t-t')}{dt'} \dots dt' \qquad (2)$$

where constants $E(0)$ and $E(\infty)$ are referred to as limiting moduli. This expression can be derived by assuming that the response to any change of strain is indspendent on previous straining, i.e. the system has completely forgotten its history. (Boltzmann's superposition principle, see e.g. in Ref. [2].) This is another important condition of rheological linearity besides the independency of ϕ_σ on the strain.

Nonlinear cases can also be handled, but the expression is more complicated than Equ. (2). In the case of rheological linearity by Equ.(2) the response (stress) to any strain function can be calculated provided that the response to a step-function is known.

When, for example, the strain is a harmonic (sinusoidal) function with an amplitude ε_o and angular frequency ω

$$\varepsilon(t) = \varepsilon_o \exp(i\omega t) \qquad (3)$$

the response (stress) is expressed by using Equ. (2) as

$$\sigma(t) = \sigma(o)\exp(i\omega t) + \left[\sigma(o) - \sigma(\infty)\right] \int_{t'=0}^{t} \left[-\frac{d\phi_\sigma(t-t')}{dt'}\right] \exp(i\omega t')\, dt' \qquad (4)$$

where $\sigma(o) = \dots$, $\sigma(\infty) = \dots$

The stress-response to a harmonic sinusoidal strain is, therefore, a Fourier transform of the negative derivative of the response function $\phi_\sigma(t)$.

Similarly, when a constant stress σ_o is applied to the polymer the strain is expressed as

$$\varepsilon(t) = \varepsilon(o) + \left[\varepsilon(\infty) - \varepsilon(o)\right] \phi_\varepsilon(t) + \frac{t}{\eta}\sigma_o \qquad (5)$$

where $\phi_\varepsilon(t)$ is the creep-response function, which is dimensionless and is normalized as $\phi_\varepsilon(o) = 0$;

$\phi_\varepsilon(\infty) = 1$, the last term of Equ. 5 describes irreversible viscous flow, η being the viscosity.

In case of time-dependent stress the strain-response is expressed in the "linear" case as

$$\varepsilon(t) = D(o)\sigma(t) - \left[D(\infty) - D(o)\right] \int_{t'=0}^{t} \frac{d\phi_\varepsilon(t-t')}{dt'} \sigma(t')\, dt' \qquad (6)$$

where constants $D(o)$ and $D(\infty)$ are referred to as limiting tensile compliances extrapolated to zero respectively infinite time.

Modulus and compliance

From the above outlined picture it is clear that there are two basic experiments for characterizing the me-

chanical behaviour of a polymeric material. One is to keep the strain constant and measure the stress as a function of time (stress relaxation experiment), the other is to keep the stress constant and measure the strain as a function at the temperature (creep experiment). The characteristic parameters are the stress relaxation modulus

$$E(t) = \frac{\sigma(t)}{\varepsilon_0} \tag{7}$$

and the creep compliance

$$D(t) = \frac{\varepsilon(t)}{\sigma_0} \tag{8}$$

where ε_0 is the constant strain, σ_0 is the constant stress. The strain may be defined simply as the change of length Δl over the original length l_0. ("engineering strain") or as

$$\varepsilon_t = \ln\left(1 + \frac{\Delta l}{l_0}\right) \tag{9}$$

"true strain", in which the change of the cross-sectional area during extension is taken into account assuming that the total volume is unchanged.

Similarly the engineering stress is defined as the force, F , over the cross-sectional area, A , and the

"true stress" as

$$\sigma_t = \frac{F}{A}\left(1 + \frac{\Delta l}{l_0}\right) \tag{10}$$

σ and E are expressed in MPa (N/mm^2) units.

In torsion the deformation is measured in radians and instead of force a torque is applied. The torsional modulus can be expressed in terms of the extensional one as

$$G = \frac{E}{2(1+\nu)} \tag{11}$$

where ν is the Poisson's ratio i.e. the ratio of the strain measured in direction perpendicular to that of parallel with respect to the direction of stretching. For most polymers in extension $\nu = 0.3\text{-}0.5$, in compression $\nu = 0.5\text{-}0.7$. $\nu = 0.5$ corresponds to that case when the total volume is unchanged by deformation.

The torsional creep compliance is

$$J = 2(1+\nu)\,D \tag{12}$$

The stress relaxation modulus and creep compliance are connected by the following equations

$$\int_{t'=0}^{t} E(t-t')\,D(t')\,dt' = t$$
$$\int_{t'=0}^{t} D(t-t')\,E(t')\,dt' = t \tag{13}$$

These integrals can be calculated numerically by the method of Hopkins and Hamming [3].

Thus, in the range of rheological linearity, it is sufficient to measure either stress relaxation modulus or creep compliance because they can be transformed into each other. As a rule approximation

$E \approx 1/D$; $G \approx 1/J$

By application of harmonic load- (stress or strain) -function, as by Equ. (4) , the transformation results in real- and imaginary-parts. For stress relaxation in extension e.g.

$$E'(\omega) = E_\infty + (E_0 - E_\infty)\, f'_\sigma(\omega)$$
$$E''(\omega) = (E_0 - E_\infty)\, f''_\sigma(\omega) \qquad (14)$$

where the real part, E' , is referred to as "storage-modulus", the imaginary one, E'' , as the "loss-modulus" f'_σ and f''_σ are the Fourier transforms of the negative derivative of the stress relaxation response function $\phi_\sigma(t)$, indexes 0, and ∞ refer to $\omega \to 0$; $\omega \to \infty$ respectively. The compliances can be expressed (transformed) similarly. Since by harmonic loading the Poisson's ratio becomes also complex; the inter-relations between extensional and torsional moduli become

$$E' = 2G'(1+\nu') + 2G''\nu'' \qquad (15)$$
$$E'' = 2G''(1+\nu') - 2G'\nu''$$

The mechanical loss tangents, defined as E''/E' or G''/G', are also used. (See e.g. in Ref [2])

Ultimate mechanical properties

As was discussed in the previous section creep compliance or stress relaxation modulus are defined only within the limits of rheological linearity i.e. assuming that the creep response function is independent on strain, the stress relaxation response function is independent on stress and both response functions are independent on any previous actions ("history"). These requirements are not very often fulfilled. In many conventional quality control tests the samples are subjected to extreme loads much above linearity. In the usual stress-strain tests the strain is increased at constant rate and the stress is measured as a function of strain. At low strain-levels Equ. (2) may be used by substituting $\varepsilon(t) = \dot{\varepsilon} t$, where $\dot{\varepsilon}$ is the strain-rate. The resulting stress is obtained from Equ. (2) by integration by parts as

$$\sigma(t) = E(\infty)\dot{\varepsilon}t - \left[E(0) - E(\infty)\right] \dot{\varepsilon} \int_{t'=0}^{t} \phi_\sigma(t-t')\, dt' \qquad (16)$$

At high strains the system becomes nonlinear because its structure changes. The stress-strain curve usually reaches maximum (yielding) then a plateau or quasi-plateau is formed until rupture. The main parameters describing the ultimate properties are the

yield-stress(σ_Y) and - strain(ε_Y) and rupture-stress(σ_r) and -strain(ε_r). (See Fig.1.) In usual uncrosslinked polymers in a certain temperature range the stress--strain curve reaches maximum after which the material flows with not much change of stress until rupture. By radiation induced oxidation the yield-stress is slightly increased and the rupture-strain is drastically reduced. For crosslinked polymers above their main transition temperature there is usually no yielding: the stress continues to increase with strain almost proportionally.

From Equ.(16) it is clear that the stress-strain curve is governed by relaxation phenomena i.e. it depends on the temperature and on the strain-rate.

The Young-modulus is defined as the slope of the stress-strain curve at small strains: (cf. Equ.16):

$$E_Y = \left(\frac{d\sigma}{d\varepsilon}\right)_{t=t_o} = E(\infty) + \left[E(o) - E(\infty)\right] \phi_\sigma(t_o) \qquad (17)$$

This means, that the Young modulus determined from the stress-strain experiment is equivalent to the stress relaxation modulus determined from a step-function straining experiment at a constant time t_o.

Recovery

A very important property of most polymers is that their original shape is partially or fully recovered after certain mechanical and/or thermal loads. In practice it is important to know the load- (stress or strain) and temperature-ranges whithin which the response is fully recovered. Failure of recovery may be caused by viscous flow (usually at high temperatures), by crazeing or by structural changes at high load levels.

Fig.2. Recovery can be studied by applying a train of square load-pulses as indicated in Fig.2. and watch the recovery of deformation. Fig.2. shows schematically the extreme cases. A completely anelastic material would not recover at all. An ideal elastic material would recover completely and promptly. An uncrosslinked polymer would recover partially and relatively slowly. Besides of using force-pulses one can use a train of strain-pulses and watch the recovery inbetween them. Thus recovery may be studied after creep as well as after stress relaxation. Recovery may be described in terms of a response function $\phi_R(t)$ similarly to creep and stress relaxation. The time-dependent recovery of the strain after a certain pre-straining may be ex-

pressed as

$$\varepsilon(t) = \varepsilon(\infty) + \left[\varepsilon(0) - \varepsilon(\infty)\right] \phi_R(t) \qquad (17)$$

where the recovery function is normalized as $\phi_R(0) = 1$, $\phi_R(\infty) = 0$

$\varepsilon(0)$ is the instantaneous deformation just after pre-straining has been finished, $\varepsilon(\infty)$ is the unrecovered "anelastic" part of the deformation.

ELECTRICAL PROPERTIES

By applying an electric field to a polymer the response is <u>current</u> which arises from the displacement of charged particles within the material. There may be trapped "mono"-charges which would move by hopping from one side to another and finally to the electrodes and annihilate there. These result in irreversible current. In polymers almost always dipoles connected to the chains are found either because of the chemical construction of the material or by other effects as oxidation or diffusion of polar molecules from the environment.

Reversible chain-dipole polarization can be detected by measuring the current response to an electric field--step repeatedly till it is reversible. The response of the material to an electrical force field $\mathcal{E}$ can be treated similarly to the mechanical case if the polarization or the displacement function $\mathfrak{D}$ is regarded as response. Similarly to the mechanical case by assuming linearity, i.e. that the response (polarization) to an external field is independent on previous actions and that the dielectric response function ϕ_d is independent on the applied field, one obtains [4]

$$\mathfrak{D}(t) = \epsilon_v \epsilon(0) \mathcal{E}(t) - \epsilon_v \left[\epsilon(\infty) - \epsilon(0)\right] \int_{t'=0}^{t} \frac{d\phi_d(t-t')}{dt'} \mathcal{E}(t')\, dt' \qquad (19)$$

where ϵ_v is the permittivity of vacuum ($8.854\ 10^{-12}$ F/m), $\epsilon(0)$ and $\epsilon(\infty)$ are limiting permittivity values. ϕ_d is normalized as $\phi_d(0) = 0$; $\phi_d(\infty) = 1$

When $\mathcal{E}(t) = \mathcal{E}_o$ = constant i.e. step-function:

$$\mathfrak{D}(t) = \epsilon_v \epsilon(0) \mathcal{E}_o + \epsilon_v \left[\epsilon(\infty) - \epsilon(0)\right] \mathcal{E}_o \phi_d(t) \qquad (20)$$

Equ.(19) may be expressed in terms of time-dependent permittivity which is defined as

$$\epsilon(t) = \frac{\mathfrak{D}(t)}{\epsilon_v \mathcal{E}(t)} \qquad (21)$$

resulting in

$$\epsilon(t) = \epsilon(0) - \frac{\epsilon(\infty) - \epsilon(0)}{\epsilon_v \dot{\mathcal{E}}(t)} \int_{t'=0}^{t} \frac{d\,\dot{\phi}_d(t-t')}{dt'} \mathcal{E}(t')\, dt' \qquad (22)$$

At constant external electric field strength the time-dependent dielectric permittivity is obtained from Equ. (22) as

$$\varepsilon(t) = \varepsilon(0) + \left[\varepsilon(\infty) - \varepsilon(0)\right] \Phi_d(t) \qquad (23)$$

Equ. (23) is similar to the creep Equation (5), so the dielectric response function $\Phi_d(t)$ is analogueous to the mechanical creep response function $\Phi_E(t)$.

In order to measure Φ_d the electric charge should be measured as a function of time after the application of a voltage- (field) -step. This is technically not very easy, easier is to measure the current or current-density (current/area) which is expressed as

$$j(t) = \frac{d\mathfrak{D}(t)}{dt} + j(\infty) \qquad (24)$$

Comparison of Equ. (24) with Equ. (19) shows that the response function describing the current decay $j(t)-j(\infty)$ is the derivative of the dielectric response function (cf Equ. 20).

Thus, the dielectric response function may be measured by a "charge" experiment i.e., when the electric field is switched on suddenly and the current response is detected, and by a "discharge" experiment when the electric field is switched off and the discharge current is measured as a function of time.

By the "charge" experiment the current does not tend to ~~to~~ zero: the value extrapolated to infinite time, $j(\infty)$, is referred to as being a result of "ohmic" conductivity involving continuous charge transfer in-between the electrodes.

The transient charge- and discharge-currents are mainly due to dipole polarization. Since these dipoles are in most cases bound to the polymer molecules the dielectric response detects the mobility of such parts of the molecule which are labelled by polar groups.

The "ohmic" conductivity may be a result of intrinsic charge activation or that of injection of charge carriers from the electrodes. High energy irradiation, evidently, creates a lot of "free" charge carriers which produce current when an external electric field is applied. If an electrical field is continuously on irradiation results in a significant increase of the current. When radiation is off the current decreases. This is referred to as radiation induced conductivity and is illustrated on Fig.3. By irradiation the conductivity increases to reach a certain level. When radiation is off, the conductivity decays to reach a value which is equal, lower, or higher to the initial "dark" conductivity-level indicating irreversible change of the structure of the material. When e.g. an uncured,

Fig.3

or partially cured, resin is [illegible] with-
irradiation conductivity usually decreases because of
crosslinking. When e.g. a noncrosslinkable polymer,
as pure poly-vinylchloride (PVC) is irradiated, the
post-irradiation conductivity usually increases be-
cause of partial conjugation of the chains and because
of the presence of degradation products.

MULTIPLE TRANSITIONS AND MOLECULAR MOBILITIES

Polymers are known to exhibit several transition temperature-ranges where parts of their molecules become mobile. One of the lowest-temperature transition is connected with liberation of the rotation of methyl groups connected to the main chain. Such transitions usually occur near to the temperature of liquid Helium. Liberation of the rotational or other types of motion of larger groups are observed at higher temperatures. As there are several types of motion of the polymer molecule, including the main-chain and side-groups, it is expected and found that polymers have many transition temperature-ranges which can be assigned to liberation of motion of different parts of the molecule.

Each transition has its own response function. The mechanical methods "mechanical spectroscopy" would detect all the transitions while dielectric spectroscopy detects only those in which motion of dipoles are involved.

Transitions in polymers may be characterized by their relaxation time (τ) distribution function

$$F(\ln\tau) = \sum_{i=1}^{n} c_i \left[\frac{d^i \phi(\ln t)}{(d \ln t)^i} \right]_{t=\tau} \qquad (25)$$

where ϕ stands for the mechanical or dielectric response function, the c_i coefficients are respectively: 0.434; 2.41×10^{-2}; 5.02×10^{-3}; -3.35×10^{-4}; 2.79×10^{-5}; -7.75×10^{-7}. In practice n=3 is accurate enough. Thus, by successive derivation of the response function, the distribution can be obtained.

Fig.4

Fig.4. shows an example when the response function has the form of

$$\phi(t) = \exp\left[-\left(\frac{t}{\tau} \right)^N \right] \qquad (26)$$

with $\ln\tau = 10$. Such a function (referred to as Kohlrausch-function) is found very often useful in describing mechanical as well as dielectric responses. The distribution function calculated on the basis of Equ. (25) is also shown in Fig.4. The τ -value corresponding to the maximum of this curve may be considered as the "mean relaxation time" while exponent N determines the shape of the distribution. τ is usually strongly temperature dependent. By increasing temperature the distribution moves to shorter times.

It is found experimentally, [3][4], that the temperature dependence of τ for side-chain rotations and for local main-chain motions is Arrhenius-like; i.e.

$$\tau(T) = \tau_0 \exp\left(\frac{E_A}{RT}\right) \qquad (27)$$

where E_A is the activation energy of the transition, R is the gas constant, T is the absolute temperature. The shift of the relaxation time distribution with respect to a reference temperature T_r is described by the time-temperature shift factor

$$a_T \equiv \frac{\tau(T)}{\tau(T_r)} = \exp\left\{\frac{E_A}{R}\left(\frac{1}{T} - \frac{1}{T_r}\right)\right\} \qquad (28)$$

In the glass-transition temperature range the Arrhenius equation does not work; instead the Williams--Landel Ferry (WLF) [6] equation becomes useful. The corresponding shift factor is

$$a_T = \exp\left\{\frac{A(T-T_r)}{B+T-T_r}\right\} \qquad (29)$$

where T_r is an arbitrary reference temperature above T_g, A and B are the WLF constants.

By increasing the temperature parameter τ is decreased (E_A and A are negative); the relaxation time distribution is shifted to shorter times.

PHYSICAL AGEING

From the viewpoint of radiation chemistry it is important to realize that solid polymers exhibit considerable molecular mobility even at low temperatures. In glassy polymers there is mobility not only because of local chain- or side-group movements but by the fact that a polymeric glass is practically never in thermodynamical equilibrium. The process of approaching equilibrium, evidently, involves rearrangement of structure. When a polymer is cooled down by about $20^{\circ}C$ below T_g after processing this structural rearrangement may proceed for years; so thermodynamic equilibrium cannot be reached in a reasonable period of time. As a result of this in a glassy polymer slow, but very significant, changes of the properties occur: the specific volume decreases (volume relaxation [7]), the enthalpy also decreases (enthalpy relaxation [8]) and the mechanical and dielectric relaxation time distributions are shifted to <u>longer times</u> i.e. opposite way as by increasing the temperature. The tendency of a glass to reach equilibrium is referred to as "physical ageing" [9] because it produces similar changes in the mechanical properties as chemical ageing without any change of the chemical structure.

should influence any kind of chemical reactions in the glass including radiation chemical ones. Fig.5 also shows stress relaxation curves for semicrystalline polypropylene measured at 40°C after annealing at 100°C. 40°C is higher than T_g (-5°C) but lower then the highest transition temperature of polypropylene below crystalline melting. The similarity of the storage--time effect with that of polystyrene below T_g indicates that in semicrystalline polymers there is physical ageing even above T_g [10].

Another important feature of physical ageing is that by increasing the temperature a part or all of the ageing effect may be erased even below T_g. The time needed for this erasure, when a glassy polymer after storage for a period of time t_{s0} at temperature T_0 is heated - up to temperature $T > T_0$, is given by Struik [9] as

$$t_m = k t_{s0} \exp\left\{\frac{H}{R}\left(\frac{1}{T} - \frac{1}{T_0}\right)\right\} \qquad (31)$$

where k and H are material's constants, R is the gas-constant. For polystyrene e.g. k = 0.18, H/R = 14.2. According to Equ.(31) t_m decreases by increasing T. Above T_g the previous history is at once completely erased.

Physical ageing is a general property of glassed no matter if they are organic or inorganic; polymeric or non-polymeric; it is observed in semicrystalline materials too, even above their amorphous glass transition temperature [10].

The shift of the mechanical or dielectric relaxation time distribution due to physical ageing can be measured and calculated as

$$\ln\left[a_v(t_s, t_{sr})\right] = C\left[\ln t_s - \ln t_{sr}\right] \qquad (30)$$

where a_v is the shift factor of physical ageing, t_s is the storage time at constant temperature after processing, t_{sr} is a reference storage time, C is an experimentally determined parameter. Above T_g C=0 because there equilibrium is reached in a short time.

Below T_g C is usually in-between 0.5 and 1.2 in a rather wide temperature range. This means that in this range one decade storage time would shift the relaxation distribution by about one decade to longer times. This is a considerable effect. As an illustration Fig.5. shows the creep compliance of polystyrene at different storage times below T_g at constant temperature. It is seen that the compliance curves are shifted to longer times i.e. the mobility of the main chain segments decrease by storage. Evidently this

Fig.5

time t in the response function $\varphi(t)$ by the effective (reduced) time ξ

$$\lambda = \int_{t'=0}^{t} \left(\frac{t'}{t+t'}\right)^{c} dt' = \frac{t_0}{1-c}\left[\left(1+\frac{t}{t_0}\right)^{1-c} - 1\right] \qquad 32)$$

As a result ~~retarded~~ creep or stress relaxation is slowed down; the corresponding apparent distribution is broadened in the long-time side. As an example Fig. 7 shows stress relaxation curves for unplasticized poly vinyl chloride measured after a storage time of 17 hrs. These curves were constructed by using experimentally determined parameters and the Kohlrausch response function with the effective time according to Equ.32. The dotted line corresponds to the case when simultaneous physical ageing was not taken into account. The distribution curve calculated according to Equ.25 is also shown. The broadening of the apparent distribution to almost infinite times indicates that there is a finite probability of large scale motion within any reasonable time-interval of the measurement.

Fig. 7

To radiation chemist this means that in the glassy amorphous state there is a finite probability for reactive species to travel long-range, reactions in

the glassy or semi-crystalline polymers may be understood by this mechanism without the need of introducing quantum tunnelling or migration mechanisms.

EXPERIMENTAL TECHNIQUE AND EXAMPLES

As was discussed in the previous chapter in order to characterize the mechanical and electric properties of polymers most important is to know their response function to step-loading. At first this seems very simple. The problem is that usually one has to deal with several transitions each of them having a rather broad relaxation time distribution spectrum. In order to detect them very long measuring times would be needed in the time domain. As was also discussed previously, by Fourier transformation it is possible to transform the time-scale to the frequency-scale which is usual in spectroscopy. In principle, the frequency can be varied in a wide range, so the distribution in the frequency domain may be measured in a short period of time. The frequency domain technique is traditionally used in dielectric spectroscopy because the sinusoidal electric field "load" can be relatively easily changed by several decades. In mechanical spectroscopy the frequency domain method is technically difficult and is, correspondingly, rarely used.

Since the parameters of the response function are temperature dependent the relaxation time distribution can be continuously shifted to shorter times by increasing the temperature. This makes it possible to measure in the temperature domain i.e. at constant frequency or load-time by sweeping the temperature. This method is commonly used in mechanical spectroscopy and is also often used in dielectric spectroscopy. A very simple variation of the temperature domain method is to apply a constant load at low temperatures and, by sweeping the temperature upward, detect the reponse. Such a method is often referred to as "thermally stimulated" one.

Time-domain techniques

The time-domain method may be used in the mechanical as well as electric case. By application of a step-function load the response (mechanical stress or strain or electric current) is measured. The time-interval covered depends on the fastness of the detecting system and on the total time of the measurement. This is the most straightforward way of measuring the response function. In principle this method can be used from a few nanoseconds up to years but in practice it is mainly used to detect slow mechanical or dielectric relaxation processes. A simplified scheme is

Fig.8 shown in Fig.8.

Since the time-scale of the measurement is technically limited the best way is to fit an analytical response function, as e.g. the Kohlrausch function (Equ.26.), to the measured data. For example in the case of mechanical stress relaxation the measured time dependent modulus, according to Equs (5), (8) and (26), has four parameters: $E(o)$, $E(\infty)$, τ and N. By using approximate values for these parameters by a gradient-fitting procedure [11] it is possible to find those values which would fit best to the experimental data-points. This way an analytical form of the response is obtained which is easy to transform into the frequency scale, if needed.

Fig.9 An example is shown in Fig.9. The experimentally measured tensile modulus-values of a plasticized poly-(vinylchloride) compound (PVC) were measured as a function of ln (time) ~~(shaded area)~~. From the data by the gradient-fitting procedure the parameters of the Kohlrausch response function were obtained. The full line represents the corresponding curve. From this curve by numerical fast Fourier transformation [12] the storage E' and the loss E'' moduli were calculated and plotted against the logarithm of frequency. The relaxation time distribution spectrum was also calculated by using Equ. (25). The detected

transition is the glass-transition of plasticized PVC.

This method can be refined by repeating the measurement at different temperatures above dilatometric T_g. This results in a series of isotherms i.e. a series of parameters. Parameter τ of the Kohlrausch function is found to depend on the temperature; above T_g according to the WLF-equation (Equ.29). From this experimentally determined dependence the WLF constants are determined. Knowing them one is able to calculate any stress relaxation E(t) or creep compliance D(t) function from dilatometric T_g (-20°C in this case) up to about +150 C, where another transition occurs.

In this particular case the temperature dependence of exponent N, which determines the shape of the relaxation time distribution function, is found not significant, i.e. the spectrum is just shifted by changing the temperature without changing shape. In such cases from isotherms by "horizontal" shifting a "master curve" can be constructed. By application of the gradient fitting procedure no graphical shifting is needed; the master curve can be constructed by determining parameters τ, N, $E(o)$ and $E(\infty)$.

Fig.10 As an example Fig.10. shows stress relaxation curves of radiation crosslinked linear low density polyethylene

(X-LLDPE) above the crystalline melting temperature. At this temperature plain uncrosslinked polyethylene flows. Depending on the crosslink-density X-LLDPE above crystalline melting temperature is elastic; the deformation is almost completely recovered. From the stress relaxation curve the relaxation time distribution calculated by Equ.25. is shown in Fig.10. at different absorbed doses, i.e. crosslink-densities. The fact that there is a relatively long stress relaxation indicates the existence and importance of the entanglement network besides chemical crosslinks. The stress relaxation curves are well described by the Kohlrausch function.

Recovery of the deformation may be measured at different stages of the stress relaxation process by releasing the strain at different periods of times after loading and monitoring the time-dependent recovery. This way parts of the distribution can be sampled. A series of such curves are shown in Fig.11. for X-LLDPE. The recovery function is normalized to the original deformation and the irreversible part (flow) is subtracted. When the load time is short just the initial part of the relaxation spectrum is sampled; the corresponding recovery relaxation time distribution, $R(\ln\tau)$, is narrow. By increasing the loading time before recovery more and more of the relaxation time spectrum can be sampled.

Fig.11

The electric time-domain experiment can be performed similarly: by applying an external electric field the current is measured as a function of (time) - or rather log(time) - by using a scheme shown in Fig.12. A fitting procedure, similar to that outlined before, may be used to determine the parameters. The current response to the electric field is a decaying function ("charge" current) which tends to a constant value $I(\infty)$ which is a result of "ohmic" conductivity. When the field is made off a negative current ("discharge"--current) is observed which decays to zero. The charge period is analogueous to creep while the discharge one to recovery keeping in mind that the response function is the derivative of the mechanical one.

Fig.12

The derivative of the Kohlrausch creep function is

$$\frac{d\left[1-\phi_K(t)\right]}{dt} = \frac{N}{\tau}\left(\frac{t}{\tau}\right)^{N-1}\exp\left\{-\left(\frac{t}{\tau}\right)^N\right\} \qquad (33)$$

when $t \ll \tau$ the first term dominates in the current decay ($N<1$), ~~which~~ indeed the decay is experimentally often found a simple power function: $j(t) - j(\infty) \propto t^{-k}$ with $k = 1-N$, i.e. in the logarithmic scale the decay is approximately a straight line, as shown in Fig.13.

Fig.13

In order to transform time domain dielectric response to the frequency-domain a simplified numerical transformation may be used:[13]

$$\epsilon'(\omega) - \epsilon(\infty) = \frac{t}{C_0 V_0}\left[\frac{1000}{t}\int_{t'=0}^{\sqrt{2}t} I(t')dt' - 261.2\, I(t) - 1231\, I(4t)\right]$$
$$\epsilon''(\omega) = \frac{t}{C_0 V_0}\left[314.3\, I(t/2) + 2382\, I(2t) - 1301\, I(4t)\right] \qquad (34)$$

where C_0 is the geometrical capacitance, pF , V_0 is the applied voltage (volts), I is the current in nanoamperes, $\epsilon(0)$ and $\epsilon(\infty)$ are the $\omega \to 0$ resp. $\omega \to \infty$ limiting permittivities, $\omega = 1/t$.

Fig.14. e.g. shows a series of dielectric loss $\epsilon''(\log \omega)$ curves obtained from charge-discharge experiments by transformation (34) for low density polyethylene gamma-irradiated in air with increasing doses. The increase of the loss is a result of oxidation.

Fig.14

The time domain technique in dielectric spectroscopy is also used in the very high frequency (GHz)-range but this is of little importance for polymers. It seems to be possible to cover the frequency range from 10^{-5} Hz up to about 10^{7} Hz in one run by the time domain method because the necessary fast-response electronic parts are available. In practice, however,

the frequency band between 10^{-6} and [illegible] covered. The higher frequencies are usually measured by conventional "ac" dielectric spectroscopy using sinusoidal field. The reason of this is technical: at low frequencies relatively high time-constants are needed for the amplifiers to reduce noise level. At higher frequencies (short-times) the time constants should be reduced and no simple automatic way to do this has been developed yet.

Frequency-domain methods

Frequency-domain techniques involve measurement of the response of the material to sinusoidal (harmonic) loads as a function of the frequency. The response is also sinusoidal which can be divided into two components: one being in-phase with the load (real component) and the other is by 90^{o} out- of - phase (imaginary component). Separation of these components may be done analog way by using a phase-sensitive detector. In this case, correspondingly, instead of the time dependent response function $\phi_d(t)$ the Fourier transforms $\phi'(\omega)$ and $\phi''(\omega)$ are measured (cf Equ.13). From this, by inverse Fourier transformation, the response function may be obtained.

In the mechanical case such a measurement is rather difficult because several decades of angular frequency should be covered in order to detect a single spectrum-band. In a frequency-domain mechanical spectrometer a

mechanical, magnetic, or piezo-electric loader is used to apply a sinusoidal strain in extension. The strain, the force and the angular frequency are converted into electric signals by transducers. These signals are detected by a phase-sensitive detector which separates the force components "in-phase" and by 90^{o} out-of--phase with respect to the deformation. The signals may be printed out or just shown on a digital voltmeter display. There are many variations of this method but the principle is the same. For details see Ref [2].

In order to do a frequency domain experiment the frequency of excitation should be changed by several decades, which is technically difficult. In the dielectric case the experimental arrangement is similar to that of Fig.12. with the difference that the sinusoidal current-response signal is phase-detected by using the voltage as reference. Since the current response-function is the derivative of the polarization one, the real part of the current is proportional to the imaginary part of the permittivity (dielectric loss) and the imaginary part of the current is proportional to the real part of the permittivity.

Sinusoidal dielectric excitation is technically easy to realize from about 0.1 Hz up to 10^{5} Hz. At high

frequency range up to about 10^{11} Hz it is also possible to do dielectric experiments but the technique is not at all easy. Nevertheless, with some technical difficulties, frequency-domain dielectric spectroscopy is capable to cover the frequency range from about 0.1 Hz up to 10^{10} Hz, i.e. 11 orders of magnitude. By combination with the time domain technique and with the far infrared Fourier transform (interferometric) infrared spectroscopy it is principially possible to cover the frequency range from 10^{-5} Hz up to about 10^{14} Hz.

Temperature-domain methods

As was mentioned earlier the relaxation time distribution spectrum is shifted to *shorter times* by *increasing* the temperature. Thus, by keeping the creep or stress relaxation time (or the angular frequency) constant, "isochronous" compliances or moduli may be measured by sweeping the temperature or by changing it stepwise.

Fig.15 This situation is schematically illustrated in Fig.15. By shifting the temperature the distribution travels through the "experimental window" represented by the load-time t_0 . As a result the compliance (or modulus) exhibits a dispersion-like curve the low temperature side of which corresponding to short relaxation times while the high temperature side to longer ones.

The peak of the relaxation time distribution represented as a function of the temperature depends on the load-time or -frequency.

This method is very often used in "dynamic mechanical analysis." (DMA [14]) applying sinusoidal excitation at constant angular frequency. The resulting storage - and loss - compliances are plotted against temperature which is swept upward. By increasing the frequency the loss peak is shifted to higher temperatures.

Fig.16 As an illustrative example Fig.16. shows a typical DMA spectrum of low density polyethylene measured at a frequency of 10 Hz ($\omega = 628$) as a function of the temperature. In this case stress relaxation-mode was used so the tensile storage (E') and loss (E'') moduli are shown. The spectrum exhibits three main transitions labelled by α_c ("crystalline"), α_a ("amorphous") and γ (local motion). For details see Refs [2] and [4].

By irradiation in the absence of oxygen PE becomes crosslinked. The effect of crosslinking to the mechanical spectra is, however, very small in comparison to that of the change of the crystalline structure, "morphology". Thus, the changes of the DMA spectra observed after irradiation are mainly due

to the changes of morphology caused by the chemical processes (crosslinking or degradation). When e.g. the irradiated polymer is annealed above its crystalline melting temperature, by recrystallization the morphology becomes drastically different from the unirradiated material heat-treated the same way. ~~This change is shown in the DMA spectra of Fig.15.~~ By irradiation the spectrum is only slightly affected. After recrystallization the α_a and α_c transitions are significantly changed with respect to those of the unirradiated sample crystallized the same way.

Similarly by applying sinusoidal electric excitation of constant angular frequency the real and imaginary parts of the dielectric permittivity may be measured as a function of temperature resulting in similar curves as shown in Fig.16. Fig.17.shows a typical temperature domain dielectric spectrum of plasticized poly vinylchloride /PVC/ at 1 kHz. The real part of the dielectric permittivity and the total ac conductivity is plotted against temperature. The permittivity versus temperature curve exhibits a transition at the glass-rubber transition temperature of the compound. This is very slightly affected by irradiation. The total ac conductivity curve is a superposition of the exponentially increasing "ohmic" part, which is not frequency-dependent, and the dielectric absorption i.e. the temperature- and frequency-dependent imaginary part of the permittivity.

Fig.17

By irradiation the ohmic part increases dramatically as a result of radiation induced degradation, while the dielectric loss part is hardly affected. In order to interpret temperature domain curves, for simplicity, let us assume that in the Kohlrausch function (Equ.26) N=1, $\tau(T)$ is Arrhenius-like and, further, that the limiting moduli are independent on temperature. This is, of course, over-simplification but makes it easier to demonstrate the main tendencies. The Fourier transforms of Equ.(26) in this particular case can be expressed in analytical form, so the temperature dependence of the storage- and loss-moduli are expressed as

$$E'(\omega_o T) = E_\infty + (E_o - E_\infty)\ \frac{\omega_o \tau}{1+\omega_o^2 \tau^2} \qquad (35)$$

$$E''(\omega_o T) = (E_o - E_\infty)\ \frac{\omega_o^2 \tau^2}{1+\omega_o^2 \tau^2}$$

The maximum of the $E''(\omega_o T)$ function is when $\omega_o \tau(T_o) = 1$; T_o may be referred to as the transition temperature at ω_o. By increasing $\omega_o \tau(T_o)$ must decrease i.e. T_o increases. By introducing the temperature dependence of τ (e.g. Equ.27) the temperature dependent moduli and compliances as well as the dielectric permittivities can be analytically described.

In fact, of course, N ≠ 1 and N, as well as the limiting moduli, are temperature dependent. Consequently <u>temperature-domain mechanical or dielectric spectra are always difficult to evaluate quantitatively.</u>

The microcomputer-aided fitting-procedure is very helpful in such cases too. As an illustrative example

Fig.18 Fig.18. shows a series of temperature-domain dielectric spectra of a mixture of an unsaturated polyester resin with styrene measured at different frequencies in one run [15]. The experimental spectra (circles) were fitted to a response function introduced by Gény and Monnerie [16] . It is seen that the fit is fairly good: the temperature dependence of the limiting permettivities could also be taken into account. Such a fitting procedure was also found useful for describing dielectric transitions in radiation cured polyester resins [15].

By curing resins or by vulcanization of rubbers it is possible to keep the load-time (t_o) or the frequency (ω_o) and the temperature (T_o) constant and measure the change of the mechanical compliance or modulus or dielectric permittivity as a function of the reaction time. In such experiments the relaxation time distribution is shifted by crosslinking to <u>longer times</u> making the

compliance or permittivity decrease. The situation in this case is similar to that illustrated in Fig.15 but the distribution moves opposite way (to longer times) as a result of crosslinking and its shape is drastically changed.

Fig.19 Fig.19. shows a series of temperature-domain isochronus compliance curves measured at different stages of radiation crosslinking. It is seen that the transition is shifted to higher temperatures (longer relaxation times) and becomes broader by increasing crosslink density. Also the post-transition compliance-values are drastically reduced by crosslinking (modulus-values increased).

Temperature-domain measurements made by constant frequency (sinusoidal) or constant load-time (square--pulse) methods my be performed by stepwise or linear temperature-program; the rate of heating is only limited by the heat-capacity of the sample. By applying constant load (stress or strain) at low temperature and heating the sample up at constant rate (r) "thermally stimulated" creep or stress relaxation curves are obtained. The electrical analogue (to creep) is the thermally stimulated polarization current curve measured at constant voltage sweeping the temperature upward linearly. Another possibility is to cool a ma-

terial down in a strained state then, after removing the strain, measure the recovery (shrinkage) as a function of temperature without any load. The electrical analogue of this method is referred to as thermally stimulated dielectric depolarization (TSD) [13]. All these thermally stimulated methods are technically simple but quantitative interpretation of the obtained curves is rather complex. In the mechanical case a differential technique [18] is recommended in order to cancel-out the thermal dilatation of the sample and holder. One sample in this measurement is loaded (simply by weight or pneumatically) the other (reference) is unloaded. The true strain is calculated as

$$\varepsilon_t = \ln\left[1 + \frac{\Delta l_s}{l_{so}} - \frac{\Delta l_r}{l_{ro}}\right] \qquad (36)$$

where Δl_s and Δl_r are the deformations of the sample and reference respectively measured as a function of temperature, l_{so} and l_{ro} are the corresponding lengths at the starting (lowest) temperature.

Such an arrangement equipped with digital data-processing facility is useful to perform any thermally stimulated or pulsed-load experiments with high accuracy. Thermally stimulated electric experiments may be performed by using the simple scheme

shown in Fig.14, equipped with a temperature controller and X-Y recorder.

Thermally stimulated mechanical or electric curves are interpreted by introducing an effective time

$$\lambda = \frac{1}{r}\int_{T=0}^{T} a_T^{-1}(T, T_o) \qquad (37)$$

instead of real time into the corresponding equations. In Equ.(37) r is the rate of heating (K/sec), T_o is the starting temperature a_T is the time-temperature shift factor corresponding to the reference temperature T_o. Using this, thermally stimulated tensile creep is described as

$$D(\lambda) = D(0) + \left[D(\infty) - D(0)\right]\,\phi_\varepsilon(\lambda) \qquad (38)$$

As the effective time λ depends on the temperature according to Equ.(37) the temperature-dependent compliance can be calculated if α_T and ϕ_ε are known.

This simple method, however, works only when the limiting values D(o) and D(∞) are independent on the temperature and the conditions for shifting are fulfilled. In this case the temperature-scale can be converted into time-scale. The limitations are, however, very severe. Nevertheless, the method is very useful for detecting transitions because its effective frequency

is very low depending on the rate of heating mainly.

Fig.20 Fig.20. shows the thermally stimulated dielectric depolarization (TDS) spectrum of radiation crosslinked low density polyethylene (X-LDPE). As was discussed previously the current is proportional to the derivative of the response function so the derivative of the creep curve is similar to the TSD--spectrum. Although polyethylene is nonpolar, all the transitions are detected. The current results from the dipoles formed by oxidation during the course of processing and irradiation.

The thermally stimulated technique offers a unique way for studying relaxation time distributions. The
Fig.21 two main possibilities are shown in Fig.21. The first one, referred to as "thermal sampling" of the distribution is performed simply by loading the sample at a temperature within the transition range and quench. This way a part of the spectrum (shaded area) will be frozen-in and released by the subsequent linear heating-cycle when the temperature derivative of the strain is measured without external load. By repeating the experiment at different straining temperatures more and more of the distribution can be sampled. The other method is similar but only a small part of the distribution is frozen-in: a "temperature window". This way the whole distribution

can be sampled in small parts. Both methods can be applied in the mechanical as well as in the electric case. For a recent discussion see Ref. [18].

THERMALLY STIMULATED ELECTRICAL CURRENT-FLUCTUATIONS

By irradiation a lot of charge carriers become trapped inhomogeneously in the solid polymer. By thermal activation these carriers would produce thermally stimulated current (TSC) by heating the sample up without external field or in the presence of a small field. After this treatment the sample is "cleaned-up" from the trapped charges: no such current peaks are observed by subsequent heating-cooling cycles.

Analysis of the detrapping current-peak may be interesting in itself because of the possibility of determining the distribution of the trapping sites. Reversible current-fluctuations coming from the sample can be observed in the TDS-spectrum of radiation crosslinked low density polyethylene (Fig.20) This thermally stimulated depolarization current spectrum was obtained after previous electrical "cleaning" and after annealing the sample during polarization in

order to stabilize a certain microcrystalline structure. This way te depolarization curve is completely reproducible; the transitions marked by α_a and α_c correspond to those measured by DMA (cf Fig.16.) taking into account the difference in the effective frequencies.The current-fluctuations, which are superimposed to the depolarization-peaks in Fig. 20 , are found also reproducible.

The fluctuations can be observed without any previous polarization by increasing the temperature linearly or stepwise under chortcircuit conditions. An example
Fig.22 for this is shown in Fig.22. In this experiment the thermally treated, irradiated, and electrically cleaned sample was heated-up at a rate of 1^{o}/min without any external electric field and the short-circuit current was measured. Fig.22. shows on analog recording for illustration but in the actual experiment the current fluctuations were fed into a microcomputer for analysis of their amplitude-distribution and frequency spectrum. The analog picture is, probably, more illustrative to show that fluctuations start at about -10^{o}C where the α_c transition is located; its average intensity reaches maximum in the α_c-transition range and vanishes completely after passing through the crystalline melting temperature. By cooling the current-fluctuations reappear at the temperature of

of crystallization.

The observed current-fluctuations are interpreted as being due to large-scale motion of oxidized chains in the inter-lamellar space, governed by the re-arrangement of the structure rather than local motion, because the most intense Fourier coefficients are at very low frequencies. Experiments made with stepwise temperature-jumps support this view: fluctuations are drastically reduced after the structure reaches equilibrium after the jump [20].

CONCLUSIONS

The effect of high energy irradiation on the mechanical and electric properties of polymers is interesting from two basic viewpoints. One is radiation damage, i.e. deterioration of the properties by irradiation. This is important in such cases when plastic products are subjected to radiation, e.g. in radiation sterilization, in cases of equipment made of plastics working in the presence of radiation (reactors). The other aspect is radiation processing involving radiation polymerization, crosslinking (curing, vulcanization) and grafting.

By studying radiation damage mechanical properties are of basic importance because in every application there are requirements about mechanical properties. Radiation degradation in the presence of oxygen is known to exhibit dramatic effects to the mechanical properties. Poly(tetrafluoro-ethylene) (Teflon) e.g., which exhibits excellent thermal stability, decays into a powder by irradiation in air at a dose of a few kGreys. The reason of this apparent discrepancy is discussed in Rf. [21]. Other polymers as e.g. polyethylene, polystyrene are rather resistant to irradiation.

In order to characterize radiation damage to the mechanical properties first the limits of linearity have to be determined. A practical rule is that the load in use should be much less than the yield-stress or-strain in the service-temperature range. Sometimes radiation damage is so high that there is no yielding; rupture takes place after a short quasi-linear $\sigma(\varepsilon)$--curve section. The Young modulus or stress relaxation modulus is found not too much affected by degradation. The average molecular weight must drop tremendously to see a significant change in the modulus (or compliance) or in the relaxation time distribution.

The electrical properties are rather sensitive to radiation. These are important in such cases when electrical insulators (cables, capacitors a.s.o.) are used in radiation field. Radiation damage involves not only reduction of the molecular weight by main chain scissions but conjugation and also by splitting of by-products which might influence the electrical properties (as HCl in PVC) appreciably.

In the case of radiation polymerization, grafting, crosslinking curing, vulcanization the mechanical and electric tests are of vital importance. The crosslinking (curing) reaction e.g. can be monitored *in situ* by the dielectric technique which can be combined by differential thermal analysis [16].

By combination of the dielectric and mechanical techniques the products can be characterized even in the presence of reinforcing materials, fillers or dyes very efficiently.

REFERENCES

1. A. Charlesby: Atomic Radiation and Polymers, Pergamon Press; Oxford, London, New York 1960.

2. N.G. McCrum, B.E. Read, G. Williams: Anelastic and Dielectric Effects in Polymeric Solids. John Wiley, Sons, London, New York, Sydney 1967.

3. I.L. Hopkins, R.W. Hamming; J.Applied Phys. 28, 906, /1957/

4. P.Hedvig, Dielectric Spectroscopy of Polymers Adam Hilger Ltd, Bristol, Halsted Press, New York, /1977/

5. Yu.V. Zelenev, A.P. Molotkov: Vysokomol.Sed. 6 /8/ 1426 /1964/

6. M.L. Williams, R.F. Landel, J.D. Ferry: J.Amer.Chem. Soc. 77, 3701 /1955/ See also in Refs 2 and 4

7. A.J. Kovacs: Makromol.Chem.Suppl. 81, /1979/

8. I.M. Hodge, A.R. Berens: Macromolecules 15, 762 /1982/

9. I.C.E. Struik: Physical Aging in Amorphous Polymers and other Materials. Elsevier; Amsterdam, Oxford, New York /1978/

10. C.K. Chai, N.G. McCrum; Polymer 21, 706 /1980/ L.C.E. Struik, Polymer 28, 1521 /1987/

11. Ph.R. Bevington: Data Reduction and Error Analysis for the Physical Sciences McGraw Hill, New York, San Francisco, St.Louis, Toronto, London, Sydney, /1969/

12. L.C.E. Struik, R.F. Schwarzl; Rheologica Acta 8, 134 /1969/

13. J. van Turnhout: Thermally Stimulated Discharge of Polymer Electrets, Elsevier, Amsterdam /1974/

14. R.E. Read; Polymer, 22, 1580 /1981/

15. T. Murayama; Dynamic Mechanical Analysis of Polymeric Material, Elsevier, Amsterdam, Oxford, New York /1978/

16. Z.Jelcic, P. Hedvig, F. Ranogajec, I. Dvornik: Die Angewandte Makromolekulare Chemie, 21, 2070 /1985/

17. F. Gény, L. Monnerie; J.Polym.Sci.Phys. Ed. 15, 1974/1977/

18. P. Hedvig: Differential Thermomechanical Analysis of Polymers in "Applied Polymer Analysis and Characterization" /ed. J.Mitchell,Jr./ Hanser Publishers, München /1987/

19. N.G. McCrum: Polymer 25, 299 /1984/

20. G. Bánhegyi, P. Hedvig in the "Proc.of the 6th Symposium on Radiation Chemistry" /eds. P.Hedvig, L.Nyikos, R.Schiller/ Academic Publisher, Budapest, 1987. Vol.I., p.457.

21. P. Hedvig: J.Polymer Sci. Part A-1, 7, 1145 /1969/

DYNAMIC SHEAR COMPLIANCE OF POLYMER MELTS AND NETWORKS

W. PECHHOLD, O. GRASSL AND W. v.SODEN
Abteilung Angewandte Physik
Universität Ulm, 7900 Ulm, FRG

ABSTRACT:

The mechanical relaxation processes in polymer melts and networks are discussed. This is done by decomposition of master curves of the dynamic shear compliance into (i) the glass relaxation with its plateau compliance J_{eN}, (ii) the shearband process, the relaxation strength ΔJ_B of which is reciprocal to the total crosslink density p_c and (iii) the flow relaxation ΔJ_F and viscous flow (for uncrosslinked melts only). The plateau compliance J_{eN} is exponentially reduced only by effective crosslinks ($p_c^* = p_c/30$). This behaviour is understood on the level of a meander superstructure, including shearbands. The observed saturation in J_{eN} at higher *DCUP*-crosslinking - which doesn't appear with radiation - can be explained by the lack of chemically induced effective crosslinks across the interfaces between meander cubes (because of larger shear fluctuations in these areas). Whereas crosslinking changes strongly the form and position of the master curve, a filler content reduces the compliance but keeps its lgω-dependence about constant. Quantitatively the filler effect on the zero shear compliance is described on the level of the meander model and its coarse grain structure: the paraelasticity of a file of meanders across a coarse grain of diameter D_{CG} is blocked up, if it contains at least one filler particle (of diameter D_F).

Therefore $J(\Phi_F)/J(0) = (1-\Phi_F)^{D_{CG}/D_F}$, the probability of finding no particle in a file (Φ_F total volume fraction of filler). Analyses on 4 series of filled cis-1,4-poly(isoprenes) can be accounted for by assuming the size of the (hypothetical) coarse grains of the polymer to be some 300nm. Also the prediction (by the simple formula), that smaller filler particles should be more effective in shear compliance reduction, is most probably valid.

1. Introduction

The most remarkable property of polymer melts or networks is rubber elasticity, which can only be explained by assuming paraelastic segmental movements yielding entropic restoring forces. In order to develop a detailed model theory, it is most helpful to analyse the (low stress) complex shear compliance $J(\omega,T)$ in the frame of suitable molecular models. For melts and amorphous networks, the frequency/temperature superposition is valid, as a rule, yielding master curves $J(\omega,T_0)$ and the proper shift factors on both axes. In the first part of this paper some results of master curve analysis on polystyrene fractions and binary mixtures in the melt are summarized and interpreted in the meander model [1]. Next, the strong influence of crosslinking density on the form and position of the master curve is discussed, on radiation- as well as DCUP-crosslinked polyisoprene series as examples. Finally it will be shown, that swelling or filler content do hardly change the form but strongly the position of the master curve.

2. The master curve and its analysis

Fig.1, as an example, shows the master curve for a commercial polyisobutylene (PIB B15, M_v=83000 in isooctane, $M_w/M_n \approx 2$). It has been composed of six J',J"-curves (measured in a double sandwich sample holder automatically in the frequency range 10^{-4} to 200 Hz at 150, 80, 0, -40, -55 and -75°C)[1] by shifting them along both logarithmic scales. Curve fitting in the overlapping regions was simultaneously performed for J', J" by the computer. The vertical shift factors agree with the prediction $J',J'' \propto 1/\varrho T$. The horizontal shift factors have been used to construct the activation diagramm (Fig.2, the 3 curves from the bottom).

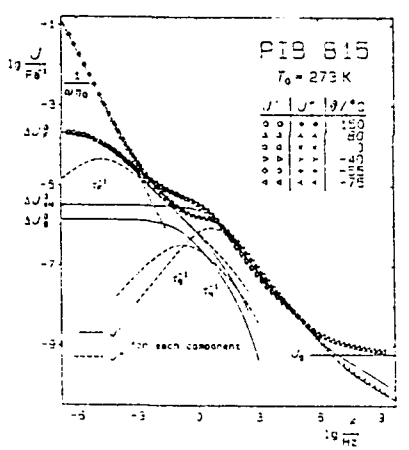

Fig. 1: Shear compliance - master curve for PIB B15 as deduced from measurements over 6 decades at 6 temperatures. Decomposition into three relaxation processes and viscous flow.

---

[1] The measurements with the mechanical spectrometer (10^{-1}-200 Hz) including different sample holders and other details of the method are published in reference [2].

3. The meander superstructure and its shear deformation modes

The meander model is quantitatively discussed in more detail in [1,4-8]. Its basic assumptions are (i) the cluster-entropy-hypothesis (CEH) and (ii) a short range order concept which favours chain parallelism across longer distances, i.e. the bundle concept. Adjusting to all energetically favoured conformations, the nearly parallel molecules are assumed to fold back and forth as defined by the free energy of a tight fold. The statistical tight folding and reptation of each molecule in the bundle results in a one-dimensional (quasi-parallel) coil appearance of its overall geometry (Fig.3, top). To gain orientational entropy of its segment lines (on the basis of CEH) a bundle (or topological tube) tightly superfolds, thereby changing its direction and becoming contracted.

The most simple and spacefilling topology of superfolding is an arrangement of meander cubes, linked together via space diagonals (serving as axes of meander cube rotation).

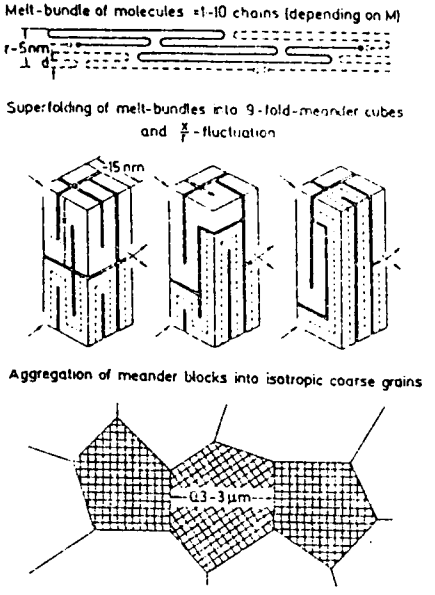

Fig.3: 3 levels of order in polymer melts or networks as described in the meander model

By minimization of the free energy per segment (including superfolding, shear fluctuation and rotation) the following results are obtained [1], which approximately read:

most probable 9-fold-meander cube, i.e.	$x/r = 2$	(1)
equilibrium bundle diameter	$r/d = (s/d)\Delta g_f^*/kT$	(2)
superfold free energy per segment	$\Delta g_N^{sf}/kT = -d/\xi r$	(3)

Δg_f^*, the free energy of one superfold in a layer of molecules, gets reduced at lower M by substitution of a pair of chain ends for the tight chain fold within the superfold. Therefore r and the meander cube size decrease at lower M. Fluctuations in x/r and r/d have to be allowed for but must not violate topology. Relying on CEH, those fluctuations can take place by reversibly coupling of any two adjacent cubes in a suitable relative orientation (x reeltuation, Fig.4, right).

For a quantitative discussion of the master curves one may try their decomposition into a few components, which may be represented by Fuoss-Kirkwood[2] or Cole-Cole[3]-functions. A high quality fit[4] was achieved for all commercial PIBs investigated [3] by choosing a decomposition of the shear compliance into

J_g		the compliance of the glass,
ΔJ_{GR}^o,	τ_N^{-1}, a_g	the glass relaxation process,
ΔJ_B^o,	τ_B^{-1}, a_B	the shearband relaxation,
ΔJ_F^o,	τ_F^{-1}, a_F	the flow relaxation and
$1/\omega\eta_o$		the loss-compliance due to viscous flow.

The ΔJ_i (relaxation strengths), τ_i (relaxation times) and a_i (widths of the distribution) as well as J_g and η_o were obtained by a least square fit of the mathematical functions [2,3] to the experimental master curve. Using these fit parameters, the 3 relaxation processes are indicated in Fig.1. Their relaxation frequencies f_{max}^i ($=1/2\pi\tau_i$), obtained from this fit (at T_o=273K) and from the frequency shift factors, are plotted in the activation diagram (Fig.2).

For comparison, glass relaxation frequencies taken from G"- and ε"-maxima as well as ε_R''-maxima from dipolar label relaxation are included [1]. One single activation curve, fitted to the dielectric frequencies [1], accounts approximately also for the other processes after vertical shifting. This means that the rapid local (segmental) movement (G", ε"-maxima) is the elementary step of larger scale (multiple step) fluctuations, to be described next.

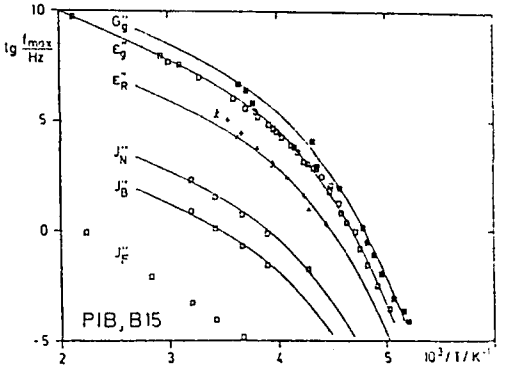

Fig. 2: Activation diagramm for PIB B15 from dielectric and mechanical measurements (cp. text).

---

[2] $J_i'' = a_i \Delta J_i / 2\cosh(a_i \ln\omega\tau_i)$; J' by Kramers-Kronig-relation

[3] $J_i = \Delta J_i / [1+(j\omega\tau_i)^{a_i}]$ (complex analytical function)

[4] The details of the decomposition procedure and the quality of the fit are also given in reference [2]

$$2s_{3131} = 2s_{3232} = \partial\gamma^{(12)}/\partial\sigma_{12} = P(\gamma_{max}^{(12)})^2 d(r+x)^4/kT \qquad (7)$$

In a similar way the shear compliance parallel to the chain direction is derived [8], and reads

$$2s_{3131} = 2s_{3232} = \partial\gamma^{(31)}/\partial\sigma_{31} = \frac{2}{3}P(\gamma_{max}^{(31)})^2 d(r+x)^4/kT \qquad (7a)$$

With $\gamma_{max}^{(31)} = \gamma_{max}^{(12)} = 1/\sqrt{3}$ one gets for the isotropic case - using Reuss-averaging -

$$J_{eN}^{o} = \frac{1}{5}\left\{\begin{matrix} s_{1212}+s_{2121} \\ +s_{3131}+s_{3232}\end{matrix}\right\} = \frac{d(r+x)^2}{9kT}P \qquad (8)$$

The plateau compliance (8) shows the 1/T-characteristic of entropy-elasticity and represents the most precise measure for the meander cube side length (r+x). The probability factor P, which, as a rule, is unity for melts, will become important for networks with medium or strong crosslinking.

In the glass relaxation process the plateau compliance gets reduced to the compliance of the glass. The relaxation frequency f_{max} (1/T) has been derived in [1,4,7], assuming an intramolecular activation energy Q_γ for the jumping segment (at the dislocation) as well as a cooperative (probability) factor for the existence of a dislocation wall structure. This expression for the activation curve reads

$$f_{max} = \frac{f_o}{\pi}\exp\left[-\frac{Q_\gamma}{kT}\right]\left[1-\left[1-e^{-\frac{\varepsilon_s}{kT}\left(\frac{3r}{d}\right)^3}\right]^3\left(\frac{3r}{d}\right)^2\frac{d}{s}\right] \qquad (9)$$

and has been applied to the glass relaxation of many polymer [1,4,7], cp. Fig.2 for PIB.

So far, the intrameander shear, i.e. shear fluctuations - restricted to one chain distance per layer of molecules - of the meander cubes have been discussed. In equilibrium, they explain the plateau compliance (8), but they account only for a maximum shear $\gamma_{max}^{intra} = 1/\sqrt{3}$ (Fig.5). Beyond these fluctuations, large scale deformations become possible by interbundle displacement, i.e. by unfolding of suitably arranged meander cubes (Fig.6). To this purpose, whole files of meander cubes or even layers of them must

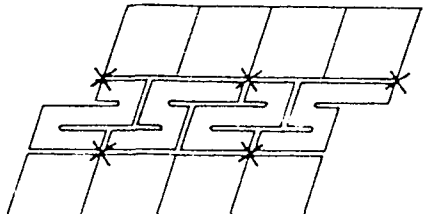

Fig.6: Interbundle shear as realized in a shearband (maximum deformation $\gamma_m = 9$)

and by changing the contour of the bundle cross-section without varying its area (r/d-fluctuation). The competition between the cube rotation entropy (the statistical element being a cube segment line) and the appropriate interaction of adjacent cubes may account for a liquid crystalline transition, in which the paracrystalline but isotropic grains (0.3 - 3µm, Fig.3, bottom) become nematically ordered [6,8].

In the meander model, the plateau compliance is explained by paraelastic intrameander shear deformation (Fig.5), mediated by dislocation movement (Fig.4), but being restricted (in the bulk) to 1d-displacements between adjacent layers of molecules in the cube ($\gamma_{max}^{intra} = 1/\sqrt{3}$).

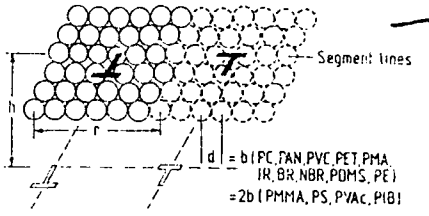

Fig.4: Dislocation wall concept of intrameander shear deformation. b, Burgers-vector; d, interchain distance.

To derive the cross-sectional shear compliance $2s_{1212}$ (3-axis in chain direction) under the assumption that only a fraction P of layers can be displaced by ±d/2 one has for the total $\gamma^{(12)}$

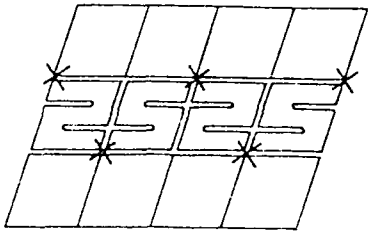

Fig.5: Intrameander shear deformation with $\gamma_{max}^{intra} = 1/\sqrt{3}$

$$\gamma^{(12)} = P\gamma_{max}^{(12)}[z-(1-z)] = P\gamma_{max}^{(12)}(2z-1) \qquad (4)$$

with z, (1-z) as the probabilities for the isoenergetic +,- positions. The statistical element for shear deformation now is larger than one layer, $d(r+x)^2$, by 1/P, and its free energy of deformation becomes

$$\frac{\Delta g_{def}}{kT} = z\ln z+(1-z)\ln(1-z)+\frac{d(r+x)^2\sigma_{12}}{P\,kT}-[\gamma^{(12)}-P\gamma_{max}^{(12)}(2z-1)] \qquad (5)$$

the last term takes into account condition (4), with a Lagrangian multiplier directly connected to the shear stress σ_{12} via its definition $\sigma = \partial(g/V)/\partial\gamma$.
Minimization of (5) for z yields

$$\gamma^{(12)} = P\gamma_{max}^{(12)}\tanh\left[d(r+x)^2\gamma_{max}^{(12)}\sigma_{12}/kT\right] \qquad (6)$$

In the limit of small amplitudes ($\sigma \to 0$) the anisotropic compliance becomes

In the meander model, this paraelastic deformation is attributed to an extra shear γ_e (Fig.8) caused by the reptating chains, when leaving one junction and entering a neighbouring one.

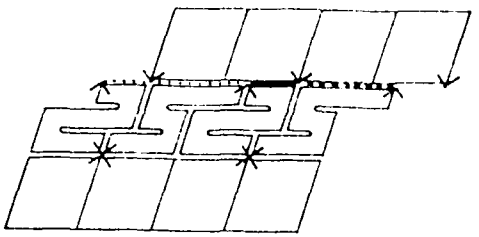

Fig. 8:
2-dimensional sketch of the paraelastic deformation on the upper interface of a shearband, caused by spread junctions.

To minimize interfacial energy of these spread junctions, two assumptions are made:
(i) Only the upper and lower interface of a shearband is appropriate to adapt extra chain sections with a minimum of chain crossing.
(ii) The extra sections (fully drawn, dashed and dotted lines in Fig.8) are the shortest bridges between the respective junctions (with no back and forth folding). On this basis the flow relaxation strength has been derived [1]

$$\Delta J_F^0 = \frac{2}{5}\beta \cdot 216 \frac{qd^2 r/kT}{1+(q-1)p} F(Q,m) \qquad (11)$$

with β shearband concentration, q average number of parallel stems/molecule, r bundle diameter, d interchain distance, l_o monomer length, p_f^0 tight fold probability (per monomer), p probability of a tight fold to bridge a junction (Fig.9), M_o molecular weight of the monomer, $m=(l_o/6r)M/M_o$, $Q=\exp[-6rp_f^0/l_o]$. The analytical function F is given in [1].
To predict the zero shear rate viscosity

$$\eta_o = 2\tau_F/\Delta J_F^0 \qquad (12)$$

one has to derive the flow relaxation time τ_F. This can be done as follows: The flow relaxation requires disentanglement of shearband junctions and hence reptation of the chains across half of their lengths L on the average.
For fractions one may use the simple formula $x^2=2D_1t$, and gets for τ_F

$$\tau_F = (L/2)^2/2D_1 \qquad (13)$$

D_1 being the curvilinear diffusion constant.

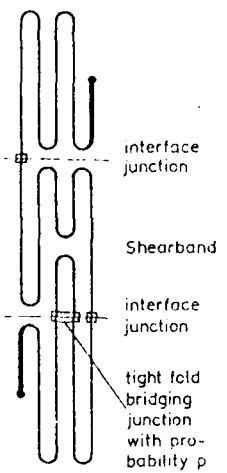

Fig.9: Shorthand sketch of a tight folded molecule, crossing two shearband interfaces.

cooperate in a shearband process, the stress-strain behaviour of which was first derived in [5].
This model theory was generalized in reference [1] taking into account rearrangements within the shearband which reduce its orientation correlation and therefore increase its compliance as well as its probability $\beta(\sigma)$: (i) only the polymer fraction ϕ, which cannot recover its cube rotation mode by reptation (at the time scale of interest), may maintain its shearband orientation. (ii) Part of this fraction, $(1-\xi)$, may albeit rearrange (by movement of folds) and reduce the orientation (x_2-x_1) (Fig. 7b), the origin of the restoring force. For statistical networks a simple picture to estimate ξ will be used later on. Fig.7 may elucidate the meaning of ϕ and ξ with 3 examples.

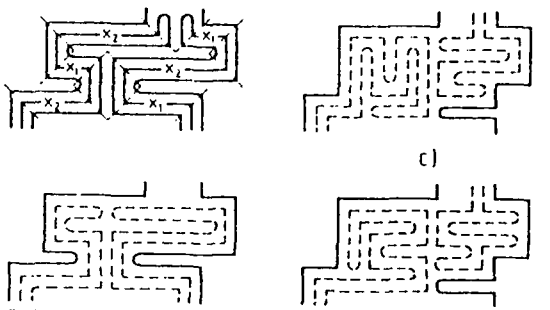

Fig. 7: *2-dimensional sketch of a shearband unit.*
a: Without any loss of orientation correlation (ϕ=1,ξ=1)
b: Only the fully drawn part of the polymer is keeping the orientation (ϕ=1,ξ=1/3).
c: A lower-M component $(1-\phi)$ = 2/3 (dashed) has recovered its cube rotation. The high-M fraction (ϕ) has not yet reduced (x_2-x_1), therefore ξ = 1.

The strength of the relaxation process due to shearband deformation can be written in the linear case after Reuss-averaging [1]

$$\Delta J_B^0 = \frac{\beta(\phi)}{\phi \cdot \xi} \frac{s \cdot d(r+x)^2 \gamma_m^2}{5xkT} \qquad (10)$$

$\beta(\phi)$ is the shearband concentration, derived in [1, Equation 25], and amounts to some 2 per cent for dry rubber at $\sigma \to 0$.

Besides plateau compliance and shearband relaxation (i.e. rubber-elasticity), polymer melts show viscous flow and a simultaneous recoverable strain if the stress is released. In dynamic mechanical investigations, the latter corresponds to a paraelastic relaxation process taking place in the same frequency range as the onset of a $J''=1/\omega\eta$ behaviour, i.e. when chain reptation becomes effective.

with Φ=1, ξ=1, to estimate the shearband relaxation strength for fractions. Assuming for aPS: $-\Delta g_{tot}/kT$=2/3, γ_m=9, d=2s=41$_o$=0.88nm, x/r=2, r_∞/d=6, we get $\beta(1)$=0.018 from [1, Eq.25] and from Equation (10) and Equation (8)

$$\Delta J_B^\infty = \beta(1)\frac{s\cdot d(r+x)^2\gamma_m^2}{5xkT} = \beta(1)\frac{9s}{5x}\gamma_m^2 J_{eN}^o \approx 0.11 J_{eN}^o \qquad (15)$$

which is indeed much smaller than the plateau compliance and cannot be detected by decomposition of the master curves.

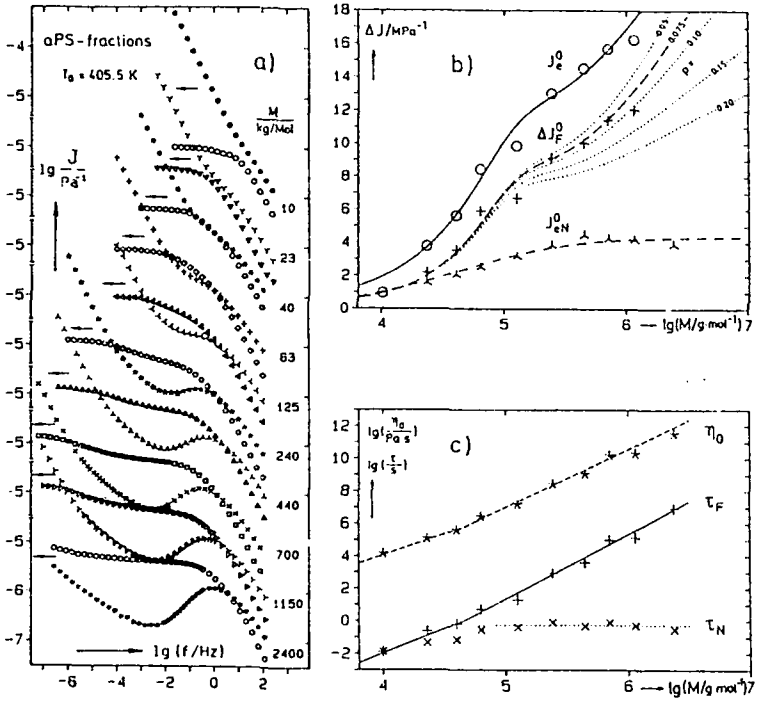

Fig. 10: (a) Compliance master curves of 10 aPS fractions in the melt.
(b) Relaxation strengths of the glass and flow processes (determined by curve decomposition) in dependence on M.
(c) Relaxation frequencies τ_g and τ_F and the zero-shear viscosity η_o (by the same analysis) in dependence on M.

To derive D_1 for chain reptation in the bulk in the frame of the meander model, one has to take into account that the chain folds are either sessile at the junctions (with probability 1-p) or fluctuating lengthwise (p) within the molecules (Fig.9). The latter motion doesn't contribute to an overall transport of the molecule's centre of mass (C.M.), if no diluent is present. Therefore the only segments to jump *independently* with frequency Γ_o are those at the ends of the molecule (outside the folds, Fig.9, fat drawn). Its average number per molecule is $l_o/p_f^o\lambda$, if λ denotes the length of the diffusing segment (in the meander model, the average length of the straight chain parts i.e. λ=2r). The C.M.-displacement resulting from an independent segmental jump of length l_o (monomer length) is $a=\pm l_o\lambda/L$, and the curvilinear diffusion constant D_1 becomes (with $L=nl_o$)

$$D_1 = \frac{1}{2}n^2\Gamma = \frac{1}{2}\left[\frac{l_o\lambda}{L}\right]^2\frac{l_o}{p_f^o\lambda}\Gamma_o = \frac{\lambda l_o^2}{2L}\frac{\Gamma_o}{np_f^o} \qquad (14)$$

(14) indicates two regimes of M-dependence of D_1: (i) For $np_f^o \le 1$ (molecules preferentially unfolded) np_f^o in (14) must be substituted by 1 and $D_1 \propto M^{-1}$. (ii) For $np_f^o > 1$, D_1 will be proportional to M^{-2}. So, $M_c = M_o/p_f^o$ signifies a critical molecular weight, which (using the p_f^o-data from [1]) comes close to the M_c-data from viscosity measurements [3]. Substitution of (14) into (13) reads

$$\tau_F = \left[\frac{L}{2}\right]^2\frac{L}{\lambda l_o^2}\frac{np_f^o}{\Gamma_o} = \frac{l_o np_f^o}{4\lambda\Gamma_o}n^3 = \frac{l_o}{4\lambda\Gamma_o}\left[\frac{M_c}{M_o}\right]^3\cdot\begin{cases}(M/M_c)^3 & \text{for } M\le M_c\\ (M/M_c)^4 & \text{for } M>M_c\end{cases} \qquad (13a)$$

In the last expression, np_f^o=1 and $p_f^o = M_o/M_c$ were used for $M\le M_c$ and $M>M_c$, respectively. Finally η_o can be calculated from (12), if ΔJ_f^o and its M-dependence is known (see below).

4. Viscoelasticity of polymer fractions and binary blends in the melt.

In Fig. 10a, shear compliance mastercurves for 10 aPS fractions of M_w/M_n<1.1 and with molecular weights beween 10^4 up to $2.4\cdot10^6$ g/mol are shown [1]. The reference temperature is T_o=405.5K in all cases and each pair of J',J"(f)-curves is shifted by one decade in the ordinate against the preceding one, starting at the bottom.
If one tries to analyze these curves by decomposing each pair into a few symmetric relaxation processes - characterized, e.g. by Cole-Cole distributions[3] - it turns out that a good fit can be achieved with two processes (glass relaxation and flow relaxation) and the viscous flow. This means that the shear band process between the glass and flow process is absent or lower in strength by at least a factor of 1/5 of the plateau compliance. Because all the chains in a fraction behave the same, it follows that Φ=1. One may also say ξ=1, because a rearrangement of strands is opposed to the chain reptation taking place within the bundles. Therefore, we have to apply Equation (10)

Since M_2/M_1 is about 11.3, the shorter chains can rearrange (dynamically fractionate by reptation) within the shearband, gaining back their free energy of rotation (cp. Fig.7c). Therefore, Equation (10) must be applied with $\Phi<1$. With a more sophisticated application of the formulae above and a proper averaging over all chain distributions, the strength and relaxation frequencies of all three processes and their dependences on mixing ratio can be understood. Postponing the theory to a subsequent paper it may only be mentioned here that a good fit to the M_w-dependence of the shearband relaxation strength is not achieved unless about 40 files of meander cubes operate in parallel.

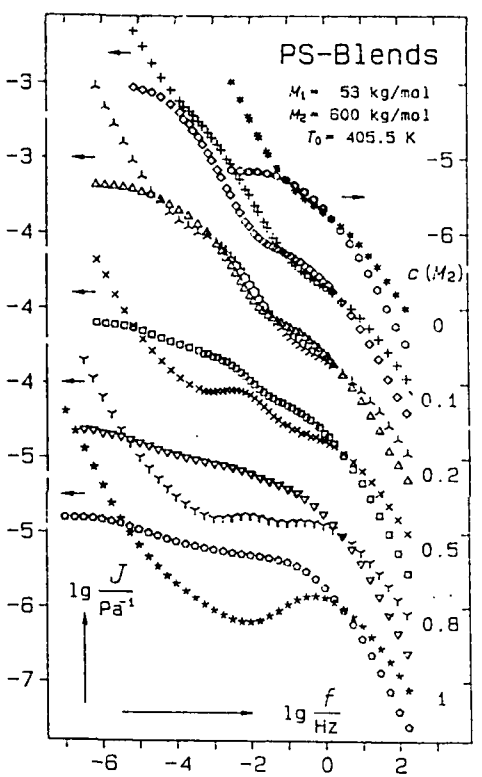

Fig. 11: Compliance master curves of 2 aFS fractions and 4 binary blends of them, the latter showing a rearranged shearband process in between the glass and flow relaxations.

5. The shear compliance of polymer networks in dependence on crosslink density.

The shear compliance of polymer networks is characterized by two relaxation processes: the glass process and a lower frequency relaxation which finally leads to the equilibrium compliance J_e. At low crosslinking, the low frequency process dominates in strength and is

For discussion of the glass and flow process, the respective relaxation strengths ΔJ^o_{gN} ($=J^o_{eN}$) and ΔJ^o_F are plotted (together with their *sum*, the steady state compliance J^o_e) versus lgM in Fig.10b and compared with the predictions of Equations (8) and (11), given by the dashed curves.

The agreement between theory and experiment is good within experimental error. The small value of 0.07 to 0.10 for the probability p in Equation (11) points out that most of the tight folds do not cross the junctions but prefer to stay near them. Because it is still in dispute whether the steady state compliance does level off at high M or continue to increase, one could think that it depends on the polymer and its probability p.

The decomposition of the master curves also yields the zero shear viscosity η_o and the relaxation times ($\tau_{N,F}=1/2\pi f_{N,F}$) and their M-dependence, plotted in Fig. 10c.

Whereas τ_N (the glass relaxation time for the compliance) stays constant for higher M (because $r=r_\infty$), τ_F shows the two regimes of M-dependence predicted in (13a). Approximately one can extract from Fig.10c

$$\tau_F/s \approx 0.65 \cdot \begin{cases} (M/M_c)^3 \\ (M/M_c)^4 \end{cases} \text{ for } \begin{matrix} M < \\ M > \end{matrix} M_c \approx 4\cdot 10^4 \text{g/mol} \qquad (16)$$

and, adapting a power law, from Fig.10b

$$\Delta J_F/\text{MPa}^{-1} \approx 3.5\ (M/M_c)^{0.5} \text{ for the whole M-range.} \qquad (17)$$

Inserting (16,17) into (12)[5] the zero shear rate viscosity becomes

$$\eta_o/\text{MPa}\cdot\text{s} \approx 0.37 \cdot \begin{cases} (M/M_c)^{2.5} \\ (M/M_c)^{3.5} \end{cases} \text{ for } \begin{matrix} M < \\ M > \end{matrix} M_c \qquad (18)$$

which nicely describes the experimental data (Fig.10c) and can also be considered as an experimental proof of the relation (12)[5].

For some polymers (e.g. polyisoprene, polysiloxane) the viscosity of molten fractions below M_c follows $\eta_o \sim M$. This is the consequence, via (12), of $\Delta J_F \sim M^2$, observed in this case.

To lead to polymer networks, the shear compliance master curves of which shall be discussed next, it is worthwhile asking the question of whether the shearband process can be observed in polymer melts at all. The answer is definitely yes, if one inspects the master curves in Fig.11 as the fingerprints of binary aPS blends of different mixing ratios.

---

5) To derive Equation (12), one may consider a flow element (serving one spreading junction) in Fig.8, and define a jump frequency Γ_F for flow. Then one has $\tau_F=1/2\Gamma_F$ ($\sigma\to 0$) and the two definitions $\sigma=\eta\dot\gamma$ and $\gamma=\Delta J_F\cdot\sigma$, with σ being that part of the shear stress inducing viscous flow. Accepting the plausible assumption $\dot\gamma=\gamma\Gamma_F$ for the shear rate, one gets by substitution the relation (12).

Figures 12a or 12b show master curves of cis-1,4-poly(isoprene)[6], crosslinked to various amounts by 2 MeV-electrons or by Dicumylperoxide (DCUP), respectively. Dropping a small flow component (for low crosslinking), most master curves could be perfectly decomposed into two relaxation processes, using Cole-Cole[3] distributions. The relaxation frequencies and relaxation strengths of these are plotted in Figures 13a,b and 14a,b, respectively.

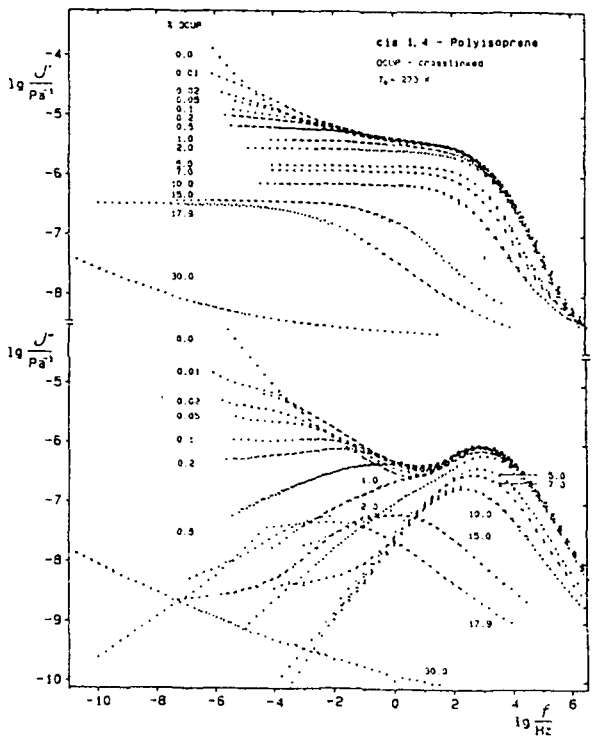

Fig. 12b: Compliance master curves of Dicumylperoxid (DCUP) crosslinked IR 305 samples. The phr of DCUP added to a sample before tempering it for 30min at 160°C is assigned to each curve.

---

6) Cariflex IR 305(Shell), $M_w = 2 \cdot 10^6$, $M_n = 2.5 \cdot 10^5$ g/mol, anionically polymerized with Butyl-Li-catalyst, 93% cis-1,4, 7% 1,2. All samples were kindly provided by Dr. U. Eisele, Bayer AG, Leverkusen.

well separated from the glass process. With higher crosslinking it strongly decreases and accelerates until it seems to merge below the glass relaxation. This behaviour is common to end-linked model networks [9] as well as to statistical networks [1,10,11] and will be discussed in the last part of this section.

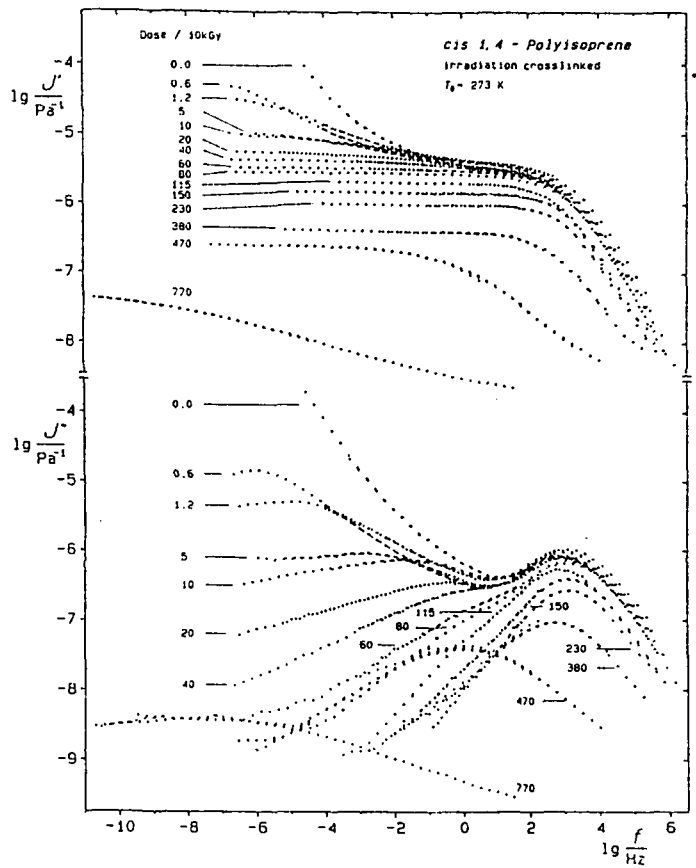

Fig. 12a: Compliance master curves of irradiation crosslinked IR 305 samples. The dose, in units of 10kGy, is assigned to each curve.

In the following we discuss these results (Fig.13a,b and 14a,b) separately for the glass relaxation and the shearband process.

The glass relaxation process

The glass relaxation frequency f_N (Fig.13) becomes influenced by crosslinking only at very high dose or DCUP addition (in the latter case, the cumenol formed during the reaction had been evaporated at 110°C, to avoid its swelling effect). This final influence probably can be understood by only statistical formation of adjacent crosslinks which strongly delay dislocation movement. The plateau compliance ΔJ_{eN} (Fig.14) starts to decrease very smoothly with crosslinking; its decay becomes very impressive if plotted semilogarithmically, as in Fig.15a,b. For its explanation one again must turn to the intrameander shear mode and its basic formula (8).

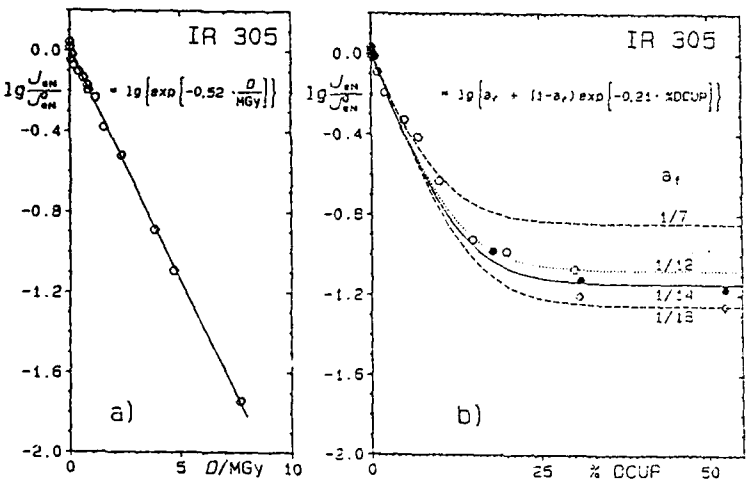

Fig. 15a,b: The reduced plateau compliance of IR-networks (plotted semilogarithmically) in dependence on the amount of crosslinking agent. (a) for radiation dose in MGy, (b) for DCUP in phr. For the meaning of the symbols cp. text.

If chemical crosslinks are present, say p_c per polymer segment, they will bridge adjacent layers of molecules in the meander cube and possibly hinder their relative displacements. But only a fraction p_c^* of the crosslinks present will effectively block the one d-displacement in the intrameander shear, as is illustrated in Fig.16 (for the cross-sectional shear): in the first two lines, uneffective crosslinks

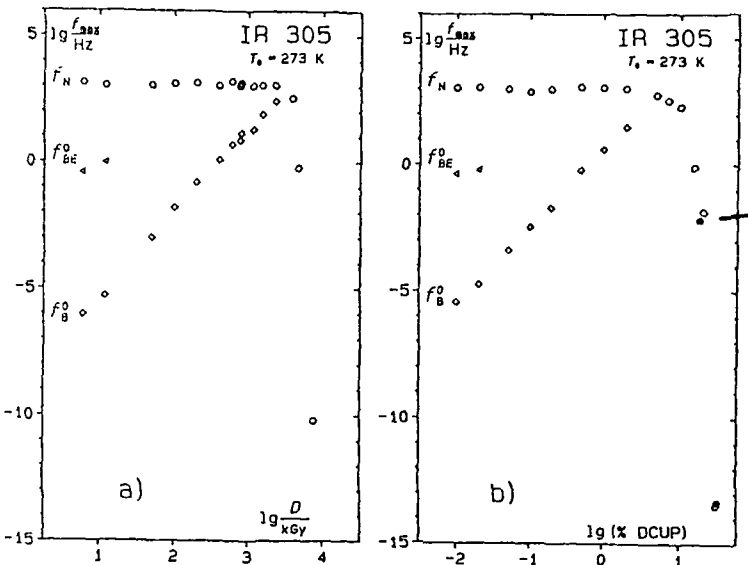

Fig. 13a,b: Relaxation frequencies from decomposition of the master curves in Fig.12 (f_N glass relaxation, f_B^o rearranged shearband process)

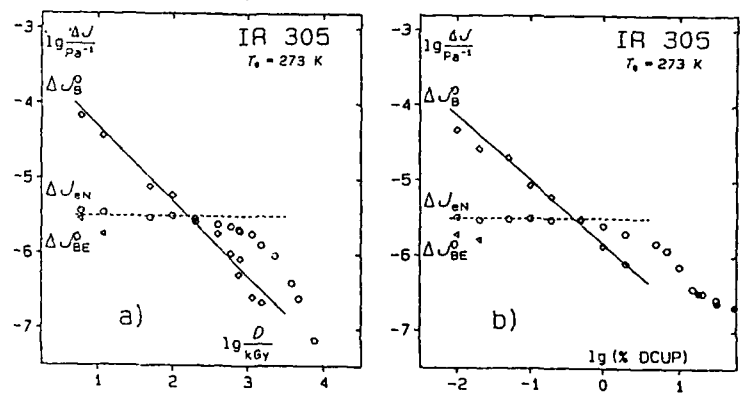

Fig. 14a,b: Relaxation strengths from decomposition of the master curves in Fig.12 (ΔJ_{eN} glass relaxation, ΔJ_B^o rearranged shearband process).

Whereas for irradiation crosslinking, Equation (20) with $p_c^* \propto D$ is valid at all doses examined, a saturation in J_{eN} is observed at higher DCUP-crosslinking. Only to a small amount, this may be due to inefficient crosslinking at high DCUP-content: The filled in hexagonal symbols, got from a two step crosslinking (after swelling a 5 p.c. sample with DCUP/hexane and drying at room temperature), are only a little lower (Fig.15b) as those for the samples (open hexagons) crosslinked as usual. A possible explanation for the obvious saturation effect in the frame of the meander model may be the lack of chemically induced effective crosslinks across the interfaces between meander cubes. This lack (or inefficiency) will be caused by larger shear fluctuations in these areas which increase the interchain distance across the interface and/or reduce the time of contact for the chemical agent. Quantitatively, the square-symbols (Fig.15b) indicate the reduction of the plateau compliance at 80°C, which levels off at a ratio $J_{eN}/J^o_{eN}=1/18$, that would correspond to a meander cube size $3r/d=18$, if all interfaces between the cubes are free of effective crosslinks. The hexagonal symbols refer to compliances from decomposition of the master curves (i.e. at 0°C). The top curve in Fig.15b, which best fits the ratios measured on medium crosslinked samples, levels off at $J_{eN}/J^o_{eN}=1/7$. This would correspond to a situation, where additionally all interfaces between the tight folded bundles within the cube are free of effective crosslinks (because of favoured shear fluctuation). It seems, that these interfaces of mostly parallel chains, become reduced in shear fluctuation with further crosslinking.

The saturation in J_{eN} with higher DCUP-addition does not indicate, however, a stagnation of further crosslinking. On the contrary, the glass relaxation starts to shift strongly to lower frequencies (Fig. 12b), very similar to that of the irradiated samples (Fig.12a).

But how could one explain this nonlinear frequency shift? Whereas single *ineffective* crosslinks (open symbols in Fig.16) are assumed to switch freely in intrameander shear, neither affecting dislocation movement nor increasing the free energy of formation ε_s of the segment dislocation, this obviously will change, if a segment is tied to two adjacent layers of molecules by two ineffective crosslinks. In this case of a double crosslink the local ε_s will be strongly increased (by additional intra- and intermolecular deformation energy). Since a dislocation wall contains many segment dislocations, the average ε_s will continously increase proportional to p_c^2, if the double crosslinks are formed statistically. In Figure 17a,b the activation curves for both crosslinking series are drawn according to formula (9), varying only the parameter ε_s. The fit to the experimental data looks very good and moreover $(\varepsilon_s-\varepsilon_{s0})$ turns out to change proportional to p_c^2, at least for $p_c<0.2$. A similar dependance should be valid for the glass temperature T_g. Further experiments on sulfur-crosslinked IR are expected to show $T_g \propto p_c$ [15] and will shine new light on the strong T_g-shift in the case of sulfur vulcanization.

(open symbols) are shown, which can always be formed and which do not block (21)- and (12)-shear deformation. The third type of crosslink (filled symbol) can only be formed in one position and will block subsequent shear deformation (otherwise it must be broken). From this scheme, one concludes a geometrical probability $p_c^*/p_c = 1/7$ for a given crosslink to be effective. But the realistic p_c^*/p_c will be smaller, because of different crosslinking reaction probabilities. These should be larger for the ineffective crosslinks (between chains remaining in contact during shear deformation) than for the effective crosslinks (between chains being in contact only for short times).

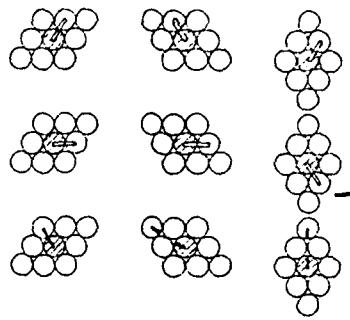

Fig.16: Ineffective (open) and effective (filled-in) crosslinks for cross-sectional shear.

Taking the ideal contact probability (without shear fluctuations) as a measure of efficiency, one gets as an upper limit

$$p_c^*/p_c \leq 1/7 \qquad (19)$$

To consider how effective chemical crosslinks influence plateau compliance, Equation (8) has to be applied, with P specified. It is reasonable that P, the probability of displaceable layers is equal to $P(p_c^*)$, the probability of finding no single effective crosslink between adjacent layers of molecules (consisting of $m=(r+x)^2/d\cdot s$ segments). Using Poisson distribution, one may write

$$P(p_c^*) = \exp(-mp_c^*). \qquad (20)$$

Evaluating Figures 15a,b, and assuming $3r/d=21$, $d=0.6$nm, $s=0.405$nm, i.e. $m=(3r)^2/d\cdot s\approx 650$, one concludes

a) for irradiated IR: $p_c^*=8.0\cdot10^{-4}$ D/MGy throughout,
b) for DCUP-crosslinked IR: $p_c^*=3.2\cdot10^{-4}$ DCUP/phr,

in the range up to 3 per cent of DCUP. The ratio of effective crosslink densities for these two crosslink agents is

$$\frac{p_c^*(\text{DCUP/phr})}{p_c^*(\text{Dose/MGy})} = 0.4\frac{\text{MGy}}{\text{phr}} \qquad (21)$$

To put it quantitatively, let us assume that only that part l of a tight fold length L* [8], which is "open", may contribute to the rearrangement and lose its orientation correlation (cf. Fig.18 ,inset). Then, ξ becomes approximately

$$\xi = 1 - \frac{l_o}{L^*} \int_0^{L^*/l_o} \exp\left\{-\frac{l}{l_o} p_c\right\} d\left(\frac{l}{l_o}\right) \qquad (22)$$

(l_o monomer length, L* average tight fold length[8], p_c total crosslinking probability per monomer (=segment in the case of IR), and $\exp(-p_c l/l_o)$ the Poisson probability for l being free of crosslinks). In Fig. 18 $\Delta J_B^o/\Delta J_B^\infty = 1/\xi$ is double - logarithmically plotted versus p_c for three L^*/l_o values. It can be quantitatively compared with Figs. 14a,b, assuming the parameters: s/d=4/6, r/d=7, d^3/kT_o=0.058 MPa^{-1}, γ_m=9, β=0.02 and therefore ΔJ_B^∞=0.40 MPa^{-1} according to Equation (10, with ϕ=1, ξ=1) and ΔJ_{eN}^o=2.9 MPa^{-1} according to Equ. (8, with P=1), if we also draw the ratio $\Delta J_{eN}^o/\Delta J_B^\infty$ into Fig. 18. Figs. 18 and 14 confirm that we have achieved a principal explanation of the relaxation strenghts versus crosslinking.

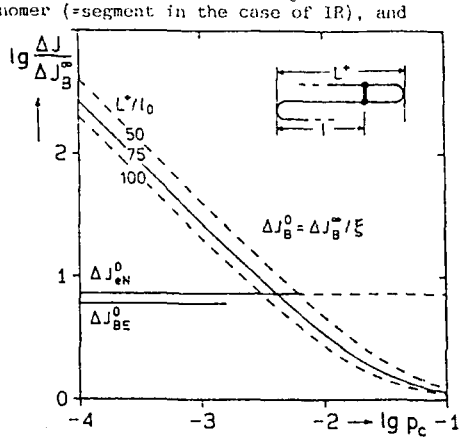

Fig. 18: Plot of the results of the model theory, to be compared with Fig.14a,b.

If we now compare e.g. the abscissa of the crossover point in Fig.18, say for the average tight fold lengths $1/p_f^o = L^*/l_o = 75$, i.e. $p_c = 4 \cdot 10^{-3}$, with those of the crossover points in Fig.14a,b, namely

a) $D_{crossover} \approx 0.166$ MGy
b) $DCUP_{crossover} \approx 0.41$ phr

we get the following relations between the total p_c and the amount of crosslinking agent

a) $p_c = 2.40 \cdot 10^{-2}$ D/MGy
b) $p_c = 0.97 \cdot 10^{-2}$ DCUP/phr

---

[8] "Tight fold length" L* is shorthand for the average chain length between tight folds.

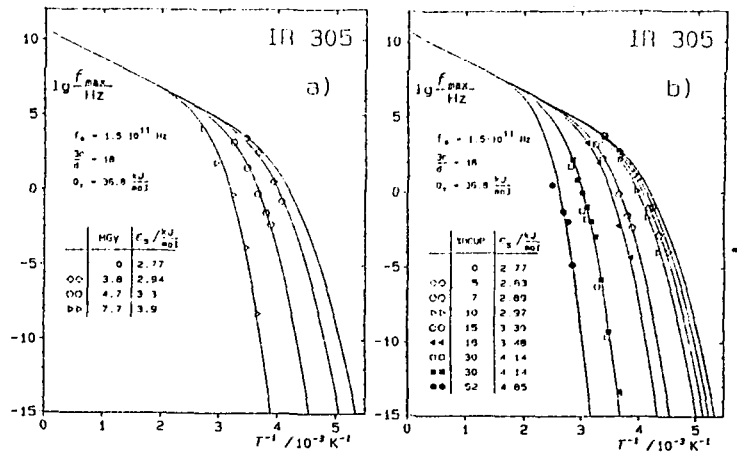

Fig. 17: Activation diagrams of two IR-series crosslinked (a) by radiation and (b) by DCUP.

The shearband process

The low frequency process is much more sensitive to crosslinking. We propose to attribute it to shearbands, if they are able to rearrange, thereby reducing their restoring forces [7]. The main experimental results are the dependences on the dose D or crosslinking density: $\Delta J_B^o \propto D^{-1}$, $f_B^o \propto D^{3.3}$, as is evident from Figures 14 and 13, respectively.

In the literature, the low frequency process is attributed to the slip of temporary entanglements and/or the onset of movement of pendant chains in the imperfect network [9-14]. Since, in the meander model of the bulk, the intrameander shear fluctuations determine the plateau compliance (no entanglements are needed), the low frequency relaxation can only be caused by dangling ends or mobile strands during shearband deformation: if a fraction (1-ξ) of polymer segments has lost its orientation correlation (x_2-x_1) within the shearband, its relaxation strength should be increased from ΔJ_B^∞ to $\Delta J_B^\infty/\xi$ according to Equation (10) with ϕ=1. Such rearrangement is envisaged in Figure 7b, which might suggest that it will be a cooperative process of local tight fold reptation, provided its motion is not hindered by crosslinks.

---

[7] At low crosslinking there is still another more rigid component ΔJ_{BE}^o, f_{BE}^o, which we attribute to the shearbands when the chain ends only have rearranged. It can be detected because it is much faster than the main component but still separated from the glass process.

The frequency of the glass relaxation stays about constant. The curve changes only little at low frequencies, i.e. at the onset of the flow region, where crosslinking would be strongly effective[10].
Therefore one has to conclude, that the filler particles - at least at low stress - do not primarily act as supercrosslinks, but shield part of the matrix from its normal deformation. To evaluate the measurements of Fig. 19, and those on slightly crosslinked samples[10], it is advantageous to plot the reduced compliance $J(\Phi_F)/J(0)$ versus filler content Φ_F (Fig.20).

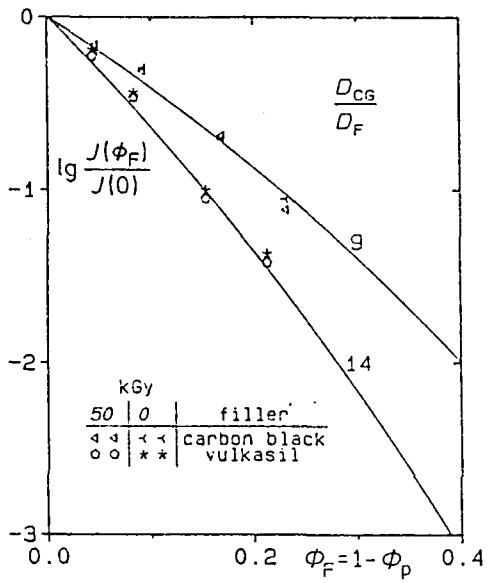

Fig. 20: The reduced shear compliance plotted versus the volume fraction of carbon black (D_F=30nm) and precipitated silicate (D_F=20nm)

Quantitatively, the filler effect on the zero shear compliance can be described on the level of the meander model and its coarse grain structure (Fig.21):
The paraelasticity of a file of meanders across one coarse grain of diameter D_{CG} is blocked up, if it contains at least a filler particle (of diameter D_F). This holds true for the intrameander shear (i.e. the plateau compliance) as well as for the shearband deformation.
According to this assumption shear deformation will only take place in those meander files not having embeded any filler particle, i.e. with the probability

$$J(\Phi_F)/J(0) = (1-\Phi_F)^{D_{CG}/D_F} \qquad (24)$$

---

9) Carbon black, Corax N220 (Degussa), particle density 1.8

10) Measurements on similar samples which were radiation crosslinked (50kGy) after preparation show the shearband process (as in Fig.12a), which does not change its shape and relaxation frequency with filler content.

A comparison of these p_c-relations with the previous ones (found from plateau compliance analysis for p_c^*) yields the same ratio as indicated in (21).

Moreover the ratio of effective crosslinks p_c^* for intrameander shear to the total crosslinking p_c turns out to be

$$p_c^*/p_c = 1/30 \qquad (23)$$

which is obout 1/4 of the value predicted by ideal contact probability consideration (19). p_c and therefore (23) rely on the model theory for ξ and the fold probability $p_f^o \approx 1/75$ assumed (from R_g-analysis [1]), and must be checked by equilibrium swelling. The appropriate theory in the frame of the meander model will be discussed in a subsequent paper.

6. The effect of filler on the dynamic shear compliance

In Fig.19 compliance master curves on uncrosslinked IR 305 rubber filled with different amounts (volume fraction Φ_F) of carbon black[9] are presented. Its main effect is a strong shift of the whole curve of the matrix towards lower compliance with increasing filler content.

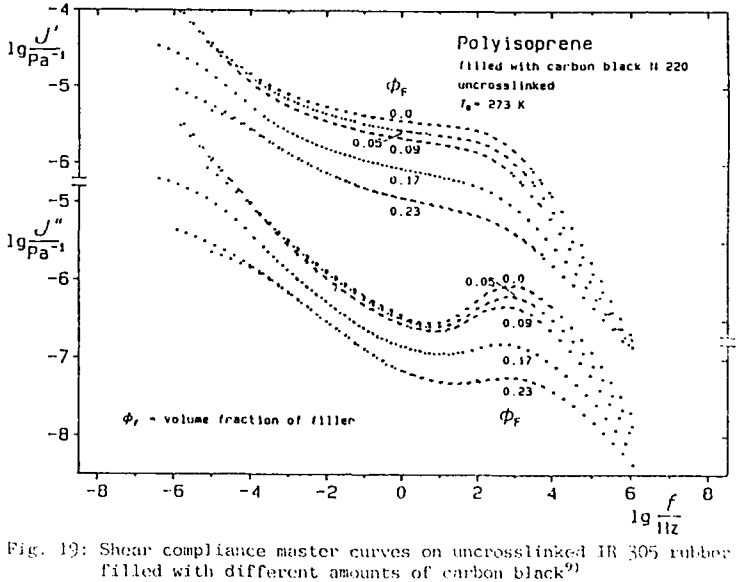

Fig. 19: Shear compliance master curves on uncrosslinked IR 305 rubber filled with different amounts of carbon black[9]

7. Conclusion

The study of the dynamic mechanical compliance of polymer melts and networks is very important to check molecular models in detail. This is a presupposition for its application to nonlinear phenomena, e.g. rheological properties or the stress-strain behaviour up to large strains in different deformation modes. The next step, which is under study, is that of the amplitude dependence of the relaxation strengths and frequencies and/or its dependence on superimposed stress, strain or shear rate.

Acknowledgement
The authors wish to thank Dr. U. Eisele for supplying the samples, the Deutsche Forschungsgemeinschaft (SFB 239) and the Fonds der Chemie for financial support, and Mrs. Auer-Oppitz and Mrs. Schiffner-Großmann for preparing the manuscript.

References

[1] Pechhold W, Böhm M, v.Soden W (1987) Coll&Polym Sci 75:23
[2] v.Soden W (1988) Thesis,Ulm
[3] Pechhold W, v.Soden W, Stoll B (1981) Macromol Chem 182:573
[4] Pechhold W (1984) Macromol Chem, Suppl 6:163
[5] Pechhold W, Gross T, Großmann HP (1982), Coll&Polym Sci 260:378
[6] Pechhold W, Großmann HP (1979) Faraday Discuss Chem Soc 68:58
[7] Pechhold W, Sautter E, v.Soden W, Stoll B, Großmann HP (1979) Macromol Chem, Suppl 3:247
[8] Pechhold W (1980) Coll&Polym Sci 258:269
[9] Havránek A, Ilavský M, Nedbal J, Böhm M, v.Soden W, Stoll B, (1987) Coll&Polym Sci 265:8
[10] Ferry JD (1980) Viscoelastic Properties of Polymers, 3rd ed., Wiley, New York
[11] Böhm M, v.Soden W, Heinrich W, and Yehia AA (1987) Coll&Polym Sci 265:295
[12] Valles EM, Macosko CM (1979) Macromolecules 12:673
[13] Havránek A (1982) Polym Bull 8:133
[14] Bibbo MA, Valles EM (1984) Macromolecules 17:360
[15] Heinze HD, Schmieder K, Schnell G, Wolf KA (1961) Kautschuk und Gummi 14:208 WT

The curves in Fig.20 were drawn according to the relation (24) with D_{CG}/D_F as a fit parameter. From the numbers found for best fit, one obtains for the average diameter of the coarse grains in isoprene rubber

$D_{CG} \approx 9D_F$ carbon black
$\approx 14D_F$ silicate
≈ 300 nm

because the diameters of the filler particles are roughly known to be 30 and 20nm, respectively.

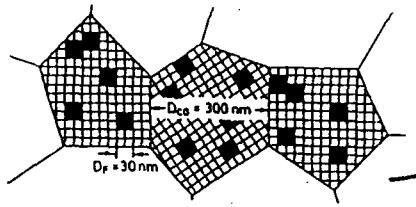

Fig. 21: The coarse grain structure of the polymer matrix with embeded filler particles blocking the shear deformation of several meander files within the grains.

The predicted particle size dependence of the zero shear compliance reduction (24) requires further check, if possible on a series of particles of similar nature but differing in diameter. The first step towards this aim is shown in Fig.22 on 3 60 phr carbon black filled samples, using N330, N220, N110 as filler. Their diameters are not yet known with sufficient accuracy to try a quantitative check of (24), but the compliance reduction is in the right direction.

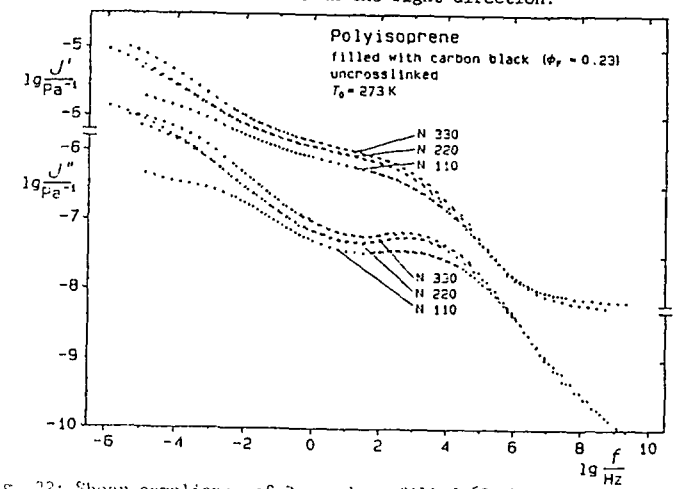

Fig. 22: Shear compliance of 3 samples, filled 60 phr with carbon black particles of different size (N330>N220>N110).

2. Paraelastic relaxation strength

To derive a formula for the relaxation strength of domains (kink-blocks, tilted chain-blocks), switching between two equivalent states (fig.1), one may simply consider the *free energy of shear deformation*,

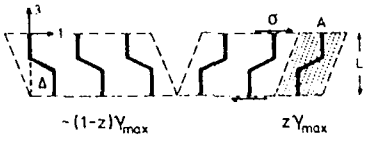

Fig. 1 Two-state model of kink-block orientation

$$\frac{\Delta g_{def}}{kT} = z\ln z + (1-z)\ln(1-z) + \frac{v\sigma}{kT}[\gamma-(2z-1)\gamma_{max}] \qquad (1)$$

asking for the equilibrium z (and hence γ) via minimization. The first two terms comprise the ideal mixing entropy of both states, the third term represents the necessary condition for the total shear γ, with vσ/kT as the Lagrangian multiplier. The latter relation follows from the definition $\partial(\Delta g/v)/\partial\gamma = \sigma$, v being the volume of the statistical element (e.g. a kink in a small kink-block). Minimization yields

$$\gamma = \gamma_{max}\cdot\tanh(v\sigma\gamma_{max}/kT) + v\sigma\gamma^2_{max}/kT \quad (\sigma\to 0) \qquad (2)$$

and the relaxation strength becomes (with $v = A\cdot L$, $\gamma_{max} = \Delta/L$)

$$2\Delta s_{1313} = \partial\gamma/\partial\sigma = \frac{v}{kT}\gamma^2_{max} = \frac{A\cdot L}{kT}\left(\frac{\Delta}{L}\right)^2 = \frac{N}{V}\frac{\Lambda^2\Lambda^2}{kT} \qquad (3)$$

where $1/v = N/V$ is the number of elements per unit volume.

PARAELASTICITY OF ORGANIC COLLOID SYSTEMS

W. PECHHOLD
Abteilung Angewandte Physik, Universität Ulm
Oberer Eselsberg
7900 Ulm, F.R.G.

ABSTRACT: The structure and the thermodynamic and electric properties of dense, organic colloid systems should be studied in conjunction with their mechanical properties to understand the role of interfaces and to have a further check on the structural models assumed. Such study can be carried out experimentally and by model theories. In this paper the dynamic shear compliance of two anisotropic colloids is reported (for a clay organic complex and an oriented stack of DPPC-lamellae) and interpreted by dislocation-mediated shear across the interfaces. An additional relaxation process in DPPC is attributed to a *switching of the tilted unit cells between equivalent states. Moreover*, the shear compliance in the "rotor phase" of the n-alkanes and the plateau-compliance of polymer melts can be described by the combined shear modes of cubic blocks, the size of which is determined by the molecule length (in the paraffins) or by the meander size (meande theory for polymer melts). It is worth mentioning that a single formula can explain to a first approximation all of the four examples reported.

1. Introduction

In dense colloid systems the interfaces between the particles (e.g. domains, grains, lamellae etc.) determine the mechanical properties. This is accomplished mainly in two ways: (i) The misfit between the particles allows the particles to deform or to interchange between equivalent states without increasing the energy. (ii) The interfaces *easily permit the creation and annihilation of dislocation loops*, mediating additional shear-defomation or even viscous flow between the particles.

In the following the paraelastic behaviour of two anisotropic colloids (a clay-organic mineral and an oriented stack of DPPC-lamellae) and two isotropic colloids (paraffin wax and polymer melt) will be discussed.

3. Clay organic complexes

Lagaly and *Weiss* have prepared n-alkylammonium-n-alkanol-beidellite- or vermiculite-complexes by cation exchange in Ca^{2+}-beidellite or vermiculite with n-alkylammonium, and subsequent drying and swelling in n-alkanol. They have described the organic bilayer-structures formed, and carefully measured their basal spacings from the melting point *of the n-alkanol to higher temperatures. In Fig.2 the preparation of* the model systems and the results got from the X-ray-diffraction are summarized as taken from [1,4]. With rising temperature the basal spacing decreases in distinct steps of 1.2 ± 0.1Å up to a transition temperature from the β into the α-phase (indicated by a larger step of 4-6 Å [2,3,4]).

Lagaly and *Weiss* explained these steps as the consequence of cooperatively formed kink-blocks [1,2,3,4] and *Pechhold et al* [5] confirmed this view by a statistical model theory applying Cluster-Entropy-Hypothesis (CEH). It should be kept in mind that there is a thermodynamic driving force towards kink-block formation in these clay organic complexes: the available *cross-section per all-trans chain is* 23-25 $Å^2$ (due to the pockets in the pseudohexagonal silicate layers) compared with that of the best intermolecular fit (18.2 $Å^2$ in PE).

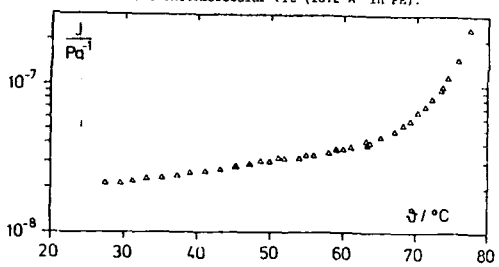

Fig. 3 Real part of the shear compliance of n-dodecylammonium-n-dodecanol-vermiculite at 12 kHz

Mechanically these clay organic complexes behave like wax parallel to the basal planes: at low frequencies they show a visco-plastic behaviour, but in the kHz-range they are elastic as reported in fig.3: the real part J' of the shear compliance (by a factor of 10 larger than the loss-compliance J") is smoothly depending on temperature with increasing slope only near to the β/α-transition. A first check of the kink-block *model discussed above requires a comparison of the* (nearly, i.e. within the present experimental error) missing J-steps (at 28° and 55°C) with the prediction from model theory. Applying formula (3)

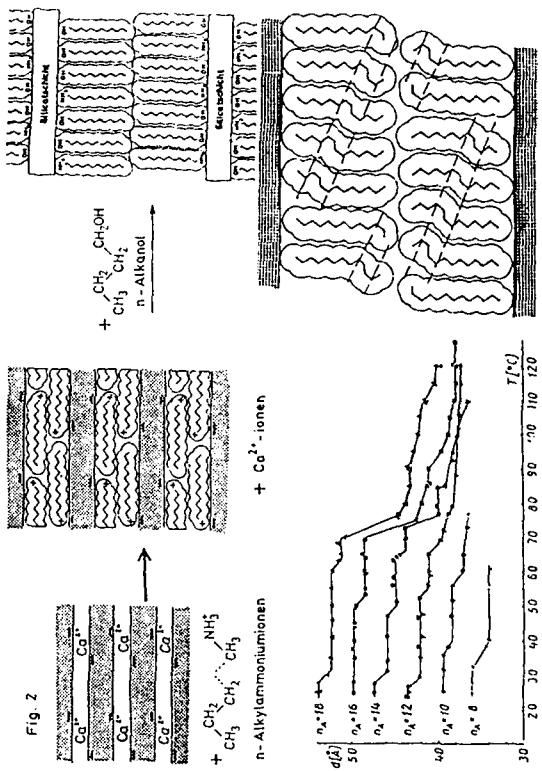

may assume average slip areas $A \approx (L/2)^2$ to exist in three states and produce local shears of d/L, 0, -d/L respectively. Then one can apply formula (3) (with an additional factor of 2/3 which follows from a similar derivation). Using the data

$\Delta \approx d = \sqrt{24.5}$ Å for the average chain distance

$A = (L/2)^2$, L = 43 Å and T = 320 K

one gets $J = 2\Delta s_{1313} = 4\cdot10^{-8}$ m²/N, a value not too far from the experimental result (but with a wrong dependence on temperature). The increasing slope of the compliance starting at 65°C indicates the onset of larger shear fluctuations which finally lead to tilted chain domains and a larger step in the basal spacing.

4. Oriented stacks of lipid lamellae

Dipalmitoyl-Phosphatidylcholine (DPPC) was incorporated with water at 90° to 120°C (i.e. in the LC-phase) in the vapour pressure of K-acetate/water solutions, pressed to about 0.2 mm thickness between silanated glass slides, and after 4 hours annealing slowly cooled to room temperature [7]. Fig.5 shows a freeze-fractured and Pt/C-shadowed electron-micrograph, almost perpendicular to the multilayers [7]. Such samples of different water content were glued in pairs into the double sandwich holder of the mechanical spectrometer and measured in the frequency range 10^{-4} to 200 Hz at different temperatures (30° to -30°C, i.e. in the $L_{\beta'}$ - or gel-phase). The water content was kept about constant by appropriate vapour pressure in the spectrometer cell. Quantitatively the water content was

Fig.5 Freeze-fracture electron-micrograph of oriented DPPC

with an additional factor of 1/2 (assuming half of the unit cells to contribute in one shear direction) one may use the following data

$\Delta^2 = (\delta_y^2+\delta_z^2) = 4.73$ Å² from ideal lateral kink displacements δ_y, δ_z [6]

T = 320 K,
A = 2·24.5 Å² (two pairs of molecules/unit cell), L = 43 Å,

and gets $\Delta J_1 = 2\Delta s_{1313} = 6.1\cdot10^{-10}$ m²/N for the single unit cell as the statistical element. More precise measurements of the shear compliance simultaneous with the sample thickness of perfectly swollen complexes will test this relaxation strength prediction. The view that the whole kink-blocks might act as statistical elements would lead to $\Delta J_b = \Delta J_1 \cdot L/2c = 5\cdot10^{-9}$ m²/N and can be excluded by the experimental result (fig.3), which therefore may be considered as a further proof of CEH.

The second question concerns the absolute value of the shear compliance and its smooth temperature dependence (fig.3). Since a shear compliance of $2...5\cdot10^{-6}$ m²/N cannot be explained by energy elasticity, it is supposed to be due to a paraelastic shear in the central interface of the bilayers. The model proposed here (fig.4) assumes creation and annihilation of dislocation loops across these interfaces. The loop density (or size) in equilibrium can be estimated by free energy consideration (applying CEH), thereby taking into account

Fig. 4

Dislocation-loop model to explain interface paraelasticity of less dense organic lamellar systems

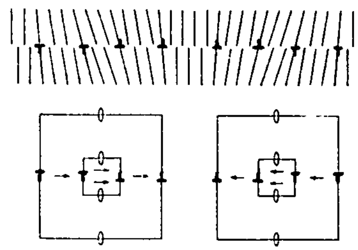

dislocation self-energy and interaction as well as the relation between the total shear and the dislocation density of both signs. This model theory which also explains the temperature dependence of the shear compliance will be published elsewhere. It is worth noting that the elastic modulus included in the dislocation energy is due to chain bending. This makes it clear why such interface paraelasticity can only occur in lamellae with less dense packing than in the ideal chain crystal. To have a rough estimation of the shear compliance here one

Fig. 7

Schematic drawing of the DPPC-bilayer with oppositely tilted domains

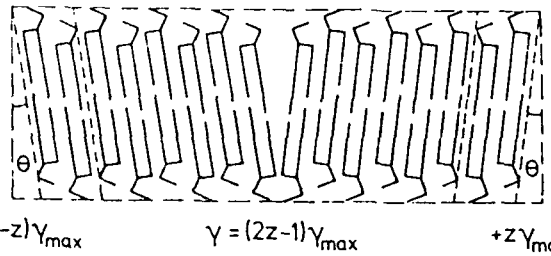

In fig.8a there are plottet the tilt angles $\Theta = \arctan \gamma_{max}$ calculated from the experimental relaxation strengths, using the data

$L = 57$ Å, $A = 4{\cdot}39$ Å^2 (4 pairs of molecules/unit cell), $T = 296$ K

This tilt-angle Θ includes the tilting of hydrocarbon chains Θ_h as well as the tilting of the polar heads Θ_p. In the gelphase ($L_{\beta'}$) $\Theta_h = 12\cdot\cdot13°$ obviously does not depend on water content [8,9,10]. Since the lamellar repeat L (fig.8b) stays about constant between the di- and tetrahydrate it must be assumed that Θ_p as well as Θ increases. The latter result is also shown by the tilt angles Θ deduced from the mechanical relaxation strengths via (3a).

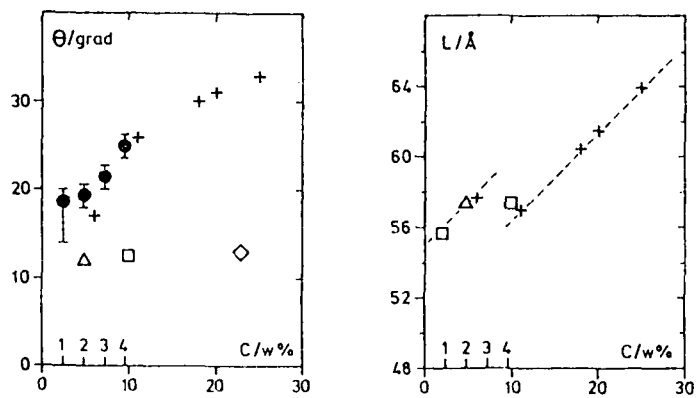

fig. 8 (a) tilt angle Θ_h of the hydrocarbon chains in DPPC, Δ[8], □[9], ◇[10]. Overall tilt angle Θ from X-ray and specific volume +[11] and from paraelastic relaxation strength •[this work]

(b) lamellar repeat L in DPPC in dependence on water content (from the same sources)

determined on excess samples before and after the measurement by coulombmetric titration using the Karl-Fischer-methode (Mitsubishi, moisture meter, model CA-02).

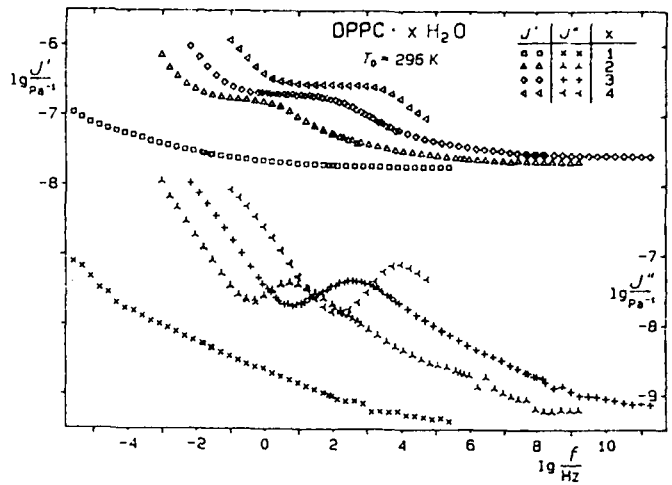

fig. 6 Shear compliance mastercurves of oriented DPPC in the $L_{\beta'}$-phase reduced to 296 K at different water contents

The frequeny-curves measured on each sample at different temperatures could be combined to give a mastercurve (T_0=296 K). Four of these are shown in fig.6 and will now be discusssed. (i) The high frequency plateau of J' is about $2{\cdot}10^{-8}$ m^2/N, a value similar to that of the clay organic complexes. Therefore its interpretation probably must be the same, i.e. a dislocation-loop mechanism within the hydrophobic interface of the lecithin-bilayer. (ii) At very low frequencies the onset of flow relaxation and viscous flow can nicely be seen. It seems to be characteristic for the waxy state as well as for the polymer melt, eventhough the retarding mechanisms will be different.
(iii) In the intermediate frequency range a strongly developed relaxation process takes place, which probably is due to a switching of the tilted unit cells between energetically equivalent states (in differently tilted domains).

Fig.7 gives a schematic drawing (according to the structure analysis in [8]) of two such domains tilted by an angle Θ. Applying formula (3) with an additional factor of 1/2 (assuming half of the unit cells to switch in one shear direction) one gets for the relaxation strength

$$\Delta J \equiv 2\Delta s_{1313} = \gamma_{max}^2 \cdot A \cdot L/2kT \qquad (3a')$$

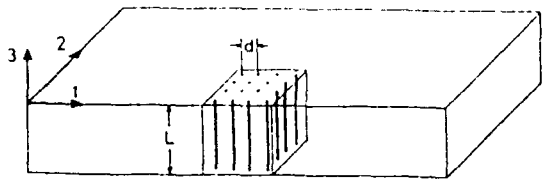

Fig. 10 A cubic block of chains as the statistical element for paraelastic shear in the "rotor phase" of n-alkanes

(i) Two contributions of interlamellar shear

$$2\Delta s^{(1)}_{1313} = 2\Delta s^{(1)}_{2323} = (d/2L)^2 \cdot L^3/kT \qquad (3b)$$

due to the dislocation loop mechanism, with two states of local shear (±d/2L) assumed, and

$$2\Delta s^{(2)}_{1313} = 2\Delta s^{(2)}_{2323} = (\tan\theta)^2 A \cdot L/2kT \qquad (3c)$$

due to the switching of tilted chains, assuming half of the unit cells to interchange in one shear direction.

(ii) a paraelastic shear of the cube in direction of the n-alkane chains, consisting of multiples of c/2 glide steps, which every row of molecules may undergo relativ to its neighbour

$$2\Delta s_{3131} = 2\Delta s_{3232} = \frac{1}{3} m(m+1)(c/2d_\perp)^2 d_\perp L^2/kT \qquad (3d)$$

This formula follows from a derivation similar to that of (3).
m, the maximum number of steps to each side, is restricted by one half of the overall thickness of the void layers between the lamellae. This has been determined with SAXS by *Strobl* [12] to be ~10/2 Å for $C_{33}H_{68}$. Therefore m=2 is most probable.
To calculate the isotropic shear compliance one favourably applies Reuss-averaging, which in this case reads

$$\Delta J_{iso} = \frac{1}{5}(\Delta s_{1313} + \Delta s_{2323} + \Delta s_{3131} + \Delta s_{3232}) \qquad (4)$$

Using the data [12]

A = 2·20.8 Å², d = 4.9 Å (chain distance), $d_\perp = d\sqrt{3}/2 = 4.25$
L/Å = 1.27 n (length of trans-chain, n number of C-atoms)
c = 2.54 Å (identity period), θ = 19.5° (tilt angle), m = 2,

the formulae (3b-d, 4)yield the isotropic shear compliances/moduli in dependence of the chain length which are listed in table 1. The respective temperatures were taken from fig.9.

5. The n-alkanes in the waxy state

The n-alkanes exhibit up to four (A-D) modifications below ultimate melting. A detailed description of the molecular packing (lateral and end-to-end) and motion in these phases has been given for $C_{33}H_{68}$ [12] mainly from X-ray, Raman, dielectric, NMR and INS analysis.

Dynamic mechanical measurements at 12 kHz [13] (cp. fig.9) show, that only the quasihexagonal modification (the so-called "rotor phase" below the melting point) exhibits strong paraelasticity (and waxy flow at low frequencies). Its interpretation in [13] - assuming switching of highly concentrated kink-blocks (without applying CEH at those days) - was disproofed by *Strobl's* finding [12] of only 0.4-0.7 kinks per chain in the D-phase. No further explanation for the paraelastic plateau in the kHz-range was put forward since that time.

Taking *Strobl's* analysis of the D-phase, the following model can now be suggested for its paraelasticity (fig.10): assuming a cubic block of chains as the statistical element for shear deformation of the lamellae, there will be three contributions of anisotropic relaxation strength.

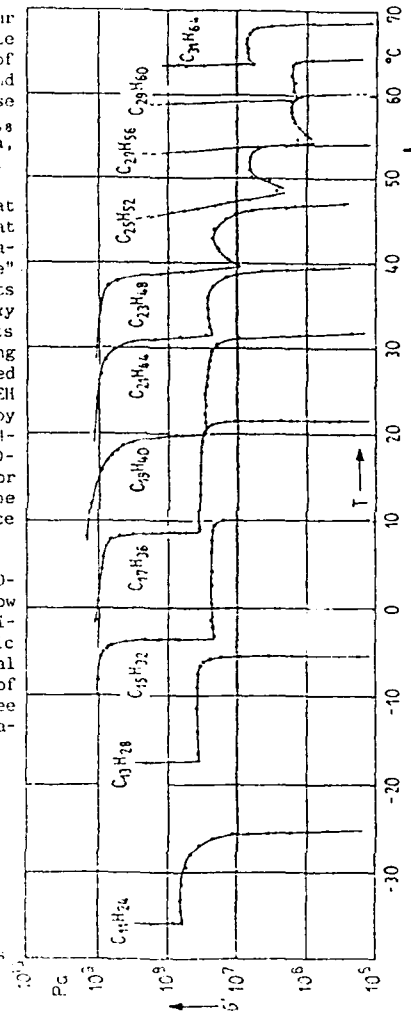

Fig. 9

The real part G' of the shear modulus at 12 kHz of isotropic n-alkanes near to the melting point. (G" is some 5 to 10 times smaller than G').

6. Polymer melts and networks in the rubbery state (plateau compliance)

The most remarkable property of polymer melts or networks is rubber elasticity, which can only be explained by assuming paraelastic segmental movement yielding entropic restoring forces. This can be nicely studied by analyzing dynamic shear compliances versus frequency. For melts and amorphous networks, the frequency/temperature superposition is valid, as a rule, yielding mastercurves (over more than 20 decades in frequency, fig.12) and the proper shift factors on both axes.

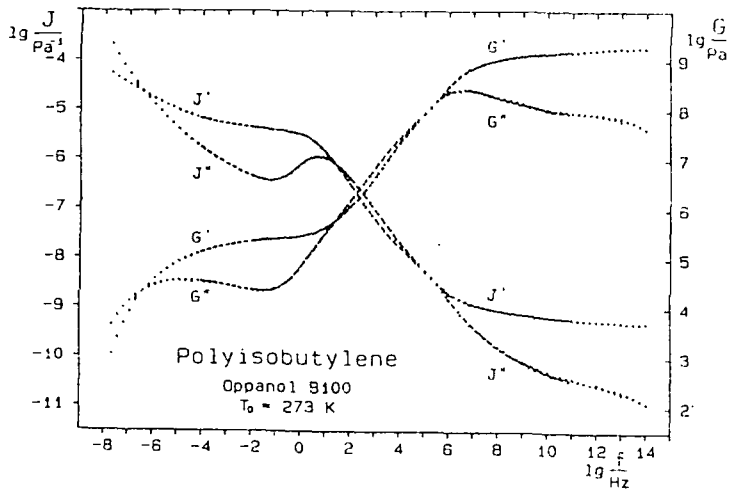

Fig. 12 Shear compliance - and shear modulus - mastercurves as deduced from measurements over 6 decades (10^{-4} ~ 200 Hz) at 6 temperatures

In the coil model, the plateau-compliance (also well defined in higher molecular weight polymer melts between the glass-relaxation and the flow region) is attributed to the number ν of network strands per unit volume between entanglements or crosslinks and reads in the simple case

$$J_{eN} = (R_0^2/R^2)/\nu kT \qquad (5)$$

In the meander model, the plateau compliance can be explained by the relaxation-strengths of intra-meander shear deformation modes (fig.13) applying Reuss-averaging. In the statistical derivation of the bulk anisotropic compliances, layers of molecules are allowed to be displaced by one chain distance d against each other. This theoretical model has been worked through in detail in preceding papers [14,15,16]

n-alkane	T_D/K	$2\Delta s^{(1)}_{3131}$	$2\Delta s^{(2)}_{3131}$	$2\Delta s_{3131}$	$\Delta J \cdot 10^7/\frac{m^2}{N}$	$\Delta G' \cdot 10^{-7}/\frac{N}{m^2}$
$C_{17}H_{24}$	240	0.253	0.110	0.447	0.162	6.17
$C_{15}H_{32}$	275	0.301	0.131	0.726	0.232	4.32
$C_{19}H_{40}$	300	0.350	0.152	1.067	0.314	3.19
$C_{23}H_{48}$	315	0.403	0.175	1.49	0.414	2.42
$C_{29}H_{60}$	335	0.478	0.208	2.23	0.583	1.72
$C_{33}H_{68}$	343	0.531	0.231	2.82	0.716	1.40

table 1: Paraelastic shear compliance/modulus relaxation strength in the "rotor phase" calculated from model theory in dependence on chain length (cp. text)

The agreement of theoretical prediction (table 1) and experiment (fig. 9) is quite good, including $C_{33}H_{68}$ which has been measured separately at 1.2 kHz (fig.11), therefore G" is much higher than at 12 kHz. A large deviation is observed in the chain length range $C_{25}\cdots C_{31}$ (fig. 9) which one might speculate may be due to m=4 c/2-glide steps in each chain direction, combined with a macroscopic orientation (the n-alkanes arranging parallel to the surface of the thin sample).

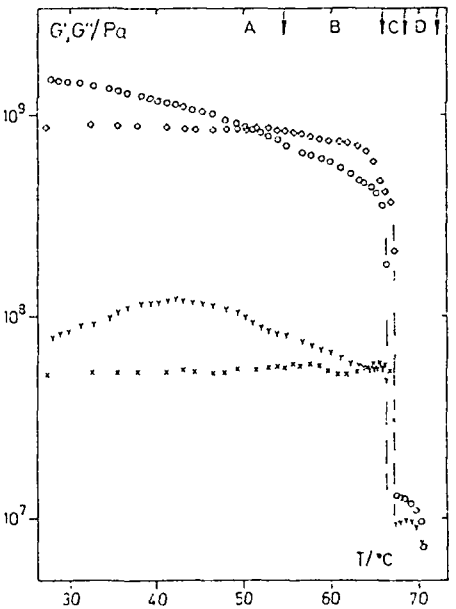

Fig. 11 Dynamic shear modulus of $C_{33}H_{68}$ measured at 1.2 kHz ◇× pressed powder, crystallized from petrol ether dilute solution : ○Y after heating into the waxy state

Conclusion

The study and interpretation of paraelastic properties of organic colloid systems is a powerful tool to understand the role of interfaces and to have a further check on the structural models assumed. The examples presented here shall be looked at as a first attempt towards this aim. The similarity in the approach to the "rotor phase" of the n-alkanes (though still crystalline) with that to the polymer melts and networks gives additional support to the meander model of amorphous polymers. (The rotation of the meander cubes across their space diagonals does not contribute to the plateau compliance.) The tilt-switch relaxation in the DPPC lamellae could be the important mechanism driving the gate-proteins in biological membranes. Further examples of paraelasticity to be dealt with in the future will include the deformation and swelling behaviour of biopolymers and biological structures e.g. the cornea and sclera of the eye.

Acknowledgement

The authors wish to thank the Deutsche Forschungsgemeinschaft and the Fonds der Chemie for financial support.

and yields, for the plateau compliance J^0_{eN} of an uncrosslinked polymer melt

$$J^0_{eN} = \frac{1}{5}\left\{ \begin{matrix} S_{1212} + S_{2121} \\ + S_{3131} + S_{3232} \end{matrix} \right\} = \frac{d(r+x)^2}{9kT} \qquad (6)$$

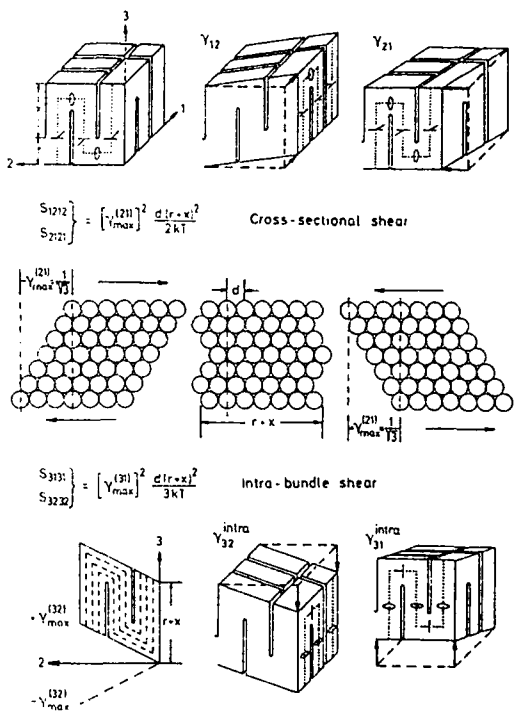

Fig. 13 The two main intra-meander shear modes demonstrated on single meander cubes with dislocations indicated on the surfaces

Taking J^0_{eN} from the decomposition of master curves of various polymer melts, equation (6) represents probably the best method to determine the cube side length r+x or the average number of quasiparallel stems (r+x)/d in a layer of molecules [17].

References

[1] Lagaly G., Fitz S., Weiss A. (1975) Prog.Coll.&Polym.Sci. 57:54

[2] Lagaly G., Fitz S., Weiss A. (1975) Clays and Clay Minerals 23:45

[3] Lagaly G. (1976) Angew. Chemie 88:628

[4] Lagaly G., Weiss A. (1971) Koll.Z.u.Z.Polymere 248:979

[5] Pechhold W., Liska E., Grossmann H.P., Hägele P.C. (1976) Pure & Appl.Chem. 46:127

[6] Pechhold W. (1968) Koll.Z.u.Z.Polymere 228:1

[7] Jürgens E. (1981) Thesis Universität Ulm

[8] Hauser H., Pascher I., Pearson R.H. and Sundell S. (1981) Biochim.Biophys.Acta 650:21

[9] Stamatoff J.B., Graddick F., Powers L. and Moncton D.E. (1979) Biophys.J. 25:253

[10] Hentschel M., Hosemann R. and Helfrich W. (1980) Z.Naturforschung 35a:643

[11] Tardieu A., Luzzati V. and Reman F.C. (1973) J.Mol.Biol. 75:711

[12] Ewen B., Strobl G.R., Richter D. (1980) Farad.Disc.Chem.Soc. 69:19

[13] Pechhold W., Dollhopf W. and Engel A. (1966) Acustica 17:61

[14] Pechhold W.R. (1980) Coll.& Polym.Sci. 258:269

[15] Pechhold W. (1984) Makromol.Chem., Suppl. 6:163

[16] Pechhold W., Böhm M. and v.Soden W. (1987) Progr.Coll.& Poly. Sci. 44:23

[17] Pechhold W., Sautter E., v.Soden W., Stoll B., Großmann H.P. (1979) Makromol.Chem., Suppl. 3:247

THE TIME-TEMPERATURE-TRANSFORMATION [TTT] DIAGRAM AS A BASIS FOR RELATING THE FORMATION AND PROPERTIES OF THERMOSETTING AND HIGH T_g SYSTEMS

JOHN K. GILLHAM
Polymer Materials Program
Department of Chemical Engineering
Princeton University
Princeton, New Jersey 08544, USA

ABSTRACT. A review of research in the author's laboratory is presented. Interrelationships between reaction conditions and material properties of thermosetting and high T_g polymers are discussed from the point of view of a generalized time-temperature-transformation (TTT) diagram. The TBA torsion pendulum is discussed as a technique for characterizing such polymeric systems.

Introduction

This review of reserch in the author's laboratory, which is set into a general context, pertains principally to the formation and properties of high T_g polymeric glasses which are made by the transformation of liquid to amorphous solid by chemical reaction. The area is of particular importance in the making of composites, coatings, and adhesives by thermosetting "cure" reactions in which multifunctional molecules of low molecular weight are converted into network macromolecules. An attempt has been made to produce a generalized model for the formation and properties of thermosetting systems which also incorporates linear systems: an example of the former is the cure of a neat epoxy resin; an example of the latter is the polymerization of neat styrene monomer below the glass transition of polystyrene. The review will therefore emphasize thermosetting systems with some reference to linear systems. The simplest model for chemical setting assumes a single reaction mechanism and no phase separation.

THE TIME-TEMPERATURE-TRANSFORMATION (TTT) ISOTHERMAL CURE DIAGRAM

A temperature vs. time transformation (TTT) isothermal cure diagram (Fig. 1) may be used to provide an intellectual framework for understanding and comparing the cure and physical properties of ther-

THE THERMOSETTING PROCESS:
TIME-TEMPERATURE-TRANSFORMATION CURE DIAGRAM

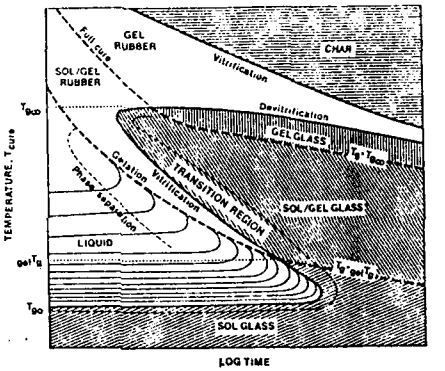

Figure 1. Schematic Time-temperature-transformation (TTT) isothermal cure diagram for a thermosetting system, showing three critical temperatures, i.e., $T_{g\infty}$, $_{gel}T_g$, T_{go}, and the distinct states of matter, i.e., liquid, sol/gel rubber, gel rubber (elastomer), gelled glass, ungelled (or sol) glass, and char. The full-cure line, i.e., $T_g = T_{g\infty}$, divides the gelled glass region into two parts: sol/gel glass and fully cured gel glass. Phase separation occurs prior to gelation. Successive isoviscous contours shown in the liquid region differ by a factor of ten. The vitrification process below $_{gel}T_g$ has been constructed to be an isoviscous one. The transition region approximates the half width of the glass transition.

mosetting systems (1,2). The main features of such a diagram can be obtained by measuring the times to events that occur during isothermal cure at different temperatures, T_{cure}. These events include the onset of phase separation, gelation, vitrification, full cure, and devitrification. Phase separation may occur, for example, by precipitation of rubber from solution in rubber-modified formulations, or by the formation of monomer-insoluble oligomeric species and by the formation of gel particles (and also by crystallization in crystallizable systems). Molecular gelation corresponds to the incipient formation of an infinite molecular network, which gives rise to macroscopic gelation behavior in the macroscopic fluid. Molecular gelation occurs at a definite conversion for a given system according to Flory's theory of gelation (3). After molecular gelation the material consists of normally miscible sol (finite molecular weight) and gel (infinite molecular weight) fractions, the ratio of the former to the latter decreasing with conversion. Molecular gelation does not correspond precisely to macroscopic gelation (see later). Vitrification occurs when the glass-transition temperature, T_g, rises to the temperature of cure. *The material is liquid or rubbery when* $T_{cure} > T_g$; it is glassy when $T_{cure} < T_g$. Devitrification occurs *when the glass-transition temperature decreases through the cure temperature*, as in thermal degradation. The diagram displays the distinct states encountered on cure due to chemical reactions. These states include liquid, sol/gel rubber, gel rubber (elastomer), ungelled (sol) glass, *gelled glass, and char. The gelled glass region in the TTT cure diagram is divided into two parts by the full-cure line*; in the absence of degradation (Fig. 1, devitrification and char), the top and lower parts can be designated fully cured gel glass and undercured sol/gel glass regions, respectively. The technological terms, A-, B- and C-stage resins correspond to sol glass, sol/gel glass, and fully cured gel glass, respectively. The illustration also displays the critical temperatures $T_{g\infty}$, $_{gel}T_g$, and T_{go}, which are the glass-transition temperature of the fully cured system, the temperature at which molecular gelation and vitrification occur simultaneously, and the glass-transition temperature of the reactants, respectively. The temperature at which macroscopic gelation and vitrification occur simultaneously is designated $_{gel}T_g$'.

Much of the behavior of thermosetting materials can be understood in terms of the TTT cure diagram through the influence of gelation, vitrification, and devitrification upon properties. Gelation retards macroscopic flow, and growth of a dispersed phase (eg, as in rubber-modified systems). Vitrification retards chemical conversion. Devitrification, due to thermal degradation, marks the lifetime for the material to support a substantial load.

The isothermal TTT cure diagram is more limited for the curing of linear rubber systems than for thermosetting systems because in practice only the region above $T_{g\infty}$ is relevant for the former. Gelation in the vulcanization of rubbers occurs at low conversions in comparison with typical thermosetting systems.

The ungelled glassy state is the basis of commercial molding materials since, upon heating, the ungelled (sol) material flows before gelling through further reaction. Formulations can be processed as solids (eg, molding compositions) when T_{go} > ambient temperature; they can be processed as liquids (eg, as casting fluids) *when* T_{go} < *ambient temperature*.

The glass transition temperature of the material at the composition corresponding to molecular gelation is $_{gel}T_g$, since molecular gelation occurs as the material vitrifies when the temperature of cure is $_{gel}T_g$ (4). The molecular gelation curve (Fig. 1) therefore corresponds to $T_g = {}_{gel}T_g$. *Temperature* $_{gel}T_g$ *is critical in determining the upper temperature for storing reactive materials to avoid* gelation (which relates to "pot life"). However, in practice, cure below $_{gel}T_g$ eventually leads to gelation.

The morphology developed in two-phase systems, for example, those in which rubber-rich domains nucleate and grow as a dispersed phase in a curing rubber-modified thermoset, depends on the temperature of cure. The reaction temperature determines the competition between thermodynamic and kinetic (ie, transport) factors which affects the amount, the composition, and the distribution of dimensions of the dispersed phase. As an example, reaction at intermediate temperatures can result in a maximum in the amount of precipitated phase which may accompany a minimum in the time to the onset of phase separation (as shown in Fig. 1). For optimum mechanical properties, a two-phase system is cured first at one temperature to provide a particular morphology, and subsequently at a higher temperature to complete the reactions of the matrix (5,6). The $T_{g\infty}$ and composition of the matrix will be determined by the extent of phase separation. A matrix parameter, the critical interparticle distance, has been reported (7) which determines the brittle to ductile transition in rubber-modified thermoplastics. For a given volume fraction of a dispersed low-modulus phase the critical interparticle distance is determined by the particle size. This concept should be applicable to rubber-modified thermosets where cure under different conditions affects both the amount of phase separation and the particle size distribution.

In composite systems, shrinkage stresses due to volume contraction of the resin on isothermal cure begin to develop with adhesion of the curing resin to a rigid inclusion or substrate. This occurs after gelation above $_{gel}T_g$ and before vitrification below $_{gel}T_g$. The tensile stresses in the resin and the corresponding compressive stresses on an inclusion and substrate affect composite behavior. One consequence is fiber-buckling in resin/fiber composites. A related consequence of the shrinkage due to cure and the different coefficients of expansion and contraction of the constituents in brittle resin/fiber composites is the formation of spiral and helical cracks in the resin around isolated filaments and yarns (8,9). Their large surface areas per unit volume of matrix may contribute to the toughening of fiber/resin composites.

Prolonged isothermal cure at temperature T_{cure} below $T_{g\infty}$ would lead to $T_g = T_{cure}$ if the reactions were quenched by the process of vitrification. In practice, T_g is higher than T_{cure} because it can increase during the heating scan employed for measurement. Although vitrification has been defined to occur when $T_g = T_{cure}$, T_g, as usually measured, does not correspond to the glassy state, but rather to a state approximately halfway between the rubbery and glassy states; therefore reactions at T_{cure} continue beyond the assigned time to vitrification, which also results in $T_g > T_{cure}$. Furthermore, the extents to which reactions proceed in the glassy state depend on the influence of the glassy state on the reaction mechanism. However, even the intramolecular reactions involved in the imidization of polyamic acids to polyimides are restricted by the vitrification process, leading again to T_g being controlled by the temperature and the time of cure (11). In practice, for epoxies and polyimides, T_g is greater than T_{cure} by about 30-50°C after "normal" isothermal cure below $T_{g\infty}$ (10,11,12,13). This corresponds approximately to the half-width of the glass transition temperature region since T_g (as measured) increases through the isothermal temperature T_{cure} to about T_{cure} + 30 to 50°C after which the reaction rate is controlled by the low physical relaxation rates of the glassy state. The half-width of the glass transition region which is qualitatively indicated in Figure 1 varies since the width of the glass transition depends on the value of T_g.

Correlations between macroscopic behavior and molecular structure of the reactants are most clearly defined in fully cured materials. Full cure is attained most readily by reaction above $T_{g\infty}$, and more slowly by curing below $T_{g\infty}$ to the full-cure line of the TTT cure diagram (12). The full cure line corresponds to $T_g = T_{g\infty}$.

In practice full cure is in general not a unique state because the state depends upon the time-temperature reaction path. In commonly used systems this is a consequence of competing chemical reactions with different activation energies. Furthermore, the time-temperature path of cooling after cure affects, for example, density and material behavior at room temperature.

At high temperatures, non-curing chemical reactions result in degradation. Thermal degradation can result in devitrification as the glass-transition temperature decreases through the isothermal temperature due to a reduction in cross-linking or formation of plasticizing material. Degradation can also result in vitrification, eg, char formation (Fig. 1), as the glass-transition temperature increases through the isothermal temperature because of an increase in cross-linking or volatilization of low molecular weight plasticizing materials (13). In high T_g systems, cure and thermal degradation reactions compete. There is a need to obtain high temperature polymers from low temperature processing.

The limiting viscosity in the fluid state is controlled by molecular gelation above ${}_{gel}T_g$, and by vitrification below ${}_{gel}T_g$. At gelation, the weight-average molecular weight and zero shear-rate viscosity become infinite, although the number-average molecular weight is very low. Viscosity prior to vitrification below ${}_{gel}T_g$ is described by the Williams-Landel-Ferry (WLF) equation (14,16).

The time to reach a specified viscosity (Fig. 1) is often used as a practical method for measuring gelation times. Although this macroscopic isoviscosity approach is inconsistent with the molecular isoconversion theory of gelation, above temperature ${}_{gel}T_g$ the apparent activation energies obtained from the temperature dependence of the time to reach a specified viscosity approach the true activation energy for the chemical reactions leading to molecular gelation with increase of the specified viscosity (1).

The time to molecular gelation can be computed from the reaction kinetics and the conversion at molecular gelation, which is constant according to Flory's theory of gelation. The time to vitrification can be computed from the reaction kinetics and the conversion at vitrification (15,16,17), which increases with T_{cure}. Since vitrification occurs when the glass-transition temperature reaches the temperature of cure, computation of the time to vitrify requires knowledge of the relationship between T_g and conversion. Figure 2 shows that T_g increases with conversion at an increasing rate. In the absence of diffusion control, the simplest kinetic equation describing the reaction is

$$dX/dt = [A\exp(-E_A/RT)]f(X)$$

where X is the extent of reaction, E_A the activation energy, and the other characters have their usual significance. The times to molecular gelation and to vitrification can be computed versus temperature using this equation when X_{gel} (for gelation), a relationship between X and T_g (for vitrification) (Fig. 2), and the reaction kinetics are known. The influence of diffusion control on the reaction rate can be deduced in principle from the differences between the experimentally measured and the computed gelation and vitrification curves.

The S-shaped vitrification curve obtained experimentally in the absence of thermal degradation has been matched by computation for one epoxy system from temperature T_{go} to temperature $T_{g\infty}$ (16).

The vitrification curve is generally S-shaped (17). At temperatures immediately above T_{go}, the time to vitrification passes through a maximum because of the opposing influences of the temperature dependences of the viscosity and the reaction rate constant. Immediately below $T_{g\infty}$, the time to vitrification passes through a minimum (18) because of the opposing influences of the temperature dependence of the reaction rate constant and the decreasing concentration of reactive sites at vitrification as $T_{g\infty}$ is approached. Knowledge of the minimum time and the corresponding temperature is useful in molding technology.

Cure of finite specimens at temperatures below that for the minimum time for vitrification (Fig. 1) can lead to the hotter

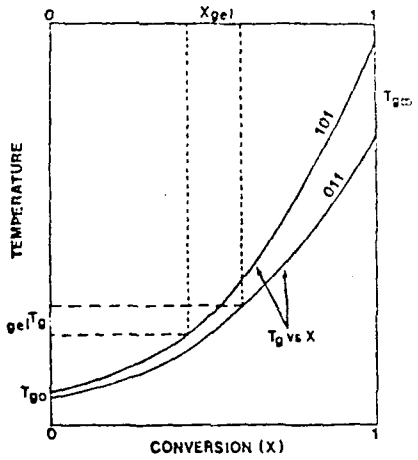

Figure 2. T_g vs. conversion at vitrification for reactants differing in functionality (101 > 011). The conversions at molecular gelation are also included. The diagram can be used to demonstrate the effect of increasing functionality of the reactants on molecular gelation, vitrification, and the temperatures $_{gel}T_g$, T_{go}, and $T_{g\infty}$.

inside vitrifying before the outside when the reaction is exothermic. Conversely, cure at higher temperatures can lead to the outside vitrifying before the inside: in this case internal stresses develop as the inside contracts relative to the vitrified outside due to the volume contraction of polymerization. The situation can be similar to the latter case when external heating causes the hotter outside to vitrify before the cooler inside. Similarly, cooling cured material from above $T_{g\infty}$ will lead to the outside vitrifying before the inside; internal stresses in this case will be minimized by cooling very slowly (i.e., annealing). These stresses, which are due to non-isothermal conditions in neat systems, are supplemented in composites by the differential shrinkage stresses which were referred to earlier in the article.

The conversion at vitrification can be computed in principle by relating the glass-transition temperature to contributions from the molecular weight and the cross-linking density, both of which vary with conversion (17). For polymerization prior to gelation (and for linear polymerization), the computation is simplified by the absence of cross-linking.

The fractional extent of reaction at vitrification (and therefore often the time to vitrify), like molecular gelation (3), decrease with increasing functionality of the reactants (13). The effect of increasing functionality on molecular gelation, vitrification, and the temperatures $_{gel}T_g$, T_{go}, and $T_{g\infty}$ can be understood by considering the X-vs-T_g and the X_{gel} relationships, such as those in Figure 2. For example, the figure shows how temperature $_{gel}T_g$ for the material of lower functionality can be higher than that of higher functionality.

Increasing reaction time at any temperature leads to increasing conversion, T_g, average molecular weight, and cross-linking density. The modulus and density at the curing temperature also increase. However, upon cooling intermittently from the curing temperature to a temperature well below T_g, eg, room temperature (RT) for high T_g materials, the modulus (e.g., see Figs. 9 and 10) and density can decrease, whereas equilibrium absorption of water can increase with increasing extent of cure. This anomaly can result, for example, in a net expansion at room temperature when a reactive material which has been set at RT is post-cured at elevated temperatures and cooled to RT. A common basis for these interrelated phenomena is the increasing free volume at room temperature with increasing extent of cure (19,20).

The room temperature density (ρ_{RT}) actually passes through a maximum value with increasing conversion. Figure 3, which was constructed from series of isothermal cures followed by cooling slowly to RT, includes a master curve of ρ_{RT} versus T_g - RT (20). (In the absence of vitrification, T_g is a measure of conversion.) Perturbations from the master curve are due to isothermal vitrification which prevents the density from decreasing to the level of the master curve with increasing conversion. (It is difficult experimen-

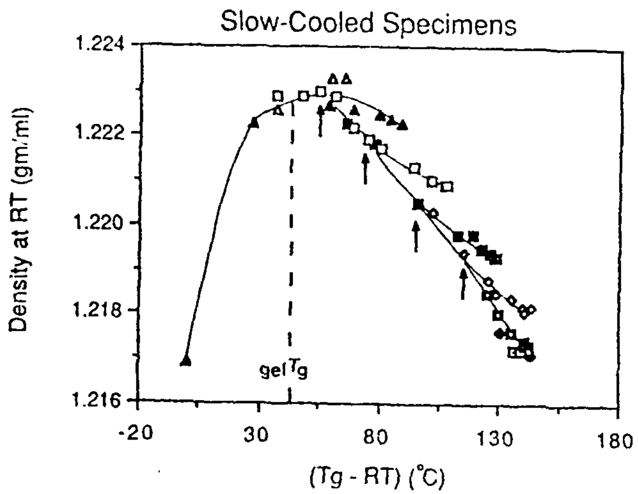

Figure 3. RT density of slow-cooled specimens vs. (T_g - RT) for different isothermal cure temperatures (20): ( ) 66.7°C; ( ) 80°C; ( ) 100°C; ( ) 120°C; ( ) 140°C; ( ) 165°C; ( ) 180°C, and ( ) 200°C. Arrows indicate vitrification where $T_g = T_{cure}$. *Temperature* $_{gel}T_g$ *(dashed line) is used as a demarcation between* ungelled and gelled specimens.

tally to obtain the complete master curve f... cure temperature
since the reaction rate is too high at high te ...atures of cure, and
vitrification limits the extent of reaction be temperature $T_{g\infty}$.)
Vitrification nullifies the unique relationshi ...tween ρ_{RT} and T_g.
The same value of T_g ...n then arise from diffe... r combinations of
conversion and exten... f physical annealing (a...)); for example, a
particular value of ... an be obtained at lowe... mperatures with
less conversion but n... physical annealing. limiting ρ_{RT} which
corresponds to the h... st T_g attained after ... times at each tem-
perature of cure depe... on T_{cure} and varies i... sely with T_{cure}
(when T_{cure} < $T_{g\infty}$). en T_g is high the lim... g ρ_{RT} will be
stable at room tem... re (if the cooling rat... very slow).
Although ρ_{RT} diff... which can be obtained ... curing to different
extents is only a... 5 percent, this corres... ds to differences of
about 20 percent free volume of the gla... It is not
surprising theref... bserve corresponding ...nges of 20 percent
in modul... and wa... rption at room temper... re. These concepts
are relevant to ... gn of plastics with t... imensional stability
needed f... the r... nt of metals by plast...

One factor co... ng to the maximum in ρ ... versus conversion
is summarized as ... (20). The value of ρ ... depends on the
contraction due ... cal reaction (cure) a... he subsequent
contraction ... ng from T_{cure}. The la... r involves contrac-
tion in the ... bb... state (from T_{cure} to T_g) a... contraction in the
glassy state (fr... to RT). With higher va... of T_g there is less
contraction ... since the coefficient o... ntraction of the
rubbery stat... than that of the glass... tate. Since T_g
rises non-li... ar ... increasing conversion ... g. 2), higher con-
versions ca... o less contraction on ... ling from T_{cure}.
The net sum... nkage and temperature ... inkage can therefore
change from ... negative with increasi... conversion. The
maximum in ... ated with gelation and ... erefore with the
glass trans... on ... ture $_{gel}T_g$ at the comp... tion corresponding
to gelation ... on-linearity in T_g ver... conversion rela-
tionship is ... the increase of cross... k density which
occurs prog... r gelation with incre... ng conversion.

Another f... to... uting to the ρ_{RT} decr... ing with
increasing c... ove... the increasing relaxa... n times: during
the tran... for... atio... of ... id or rubber to glas... his results, in
practice, in gla... ... *are progressively f*... her from
equilibrium. The ... T_g, the further from ... ilibrium a glass is
at RT.

The concept of t... cure diagram can be ... ended to non-
isothermal conditio... forming and annealin... olymeric materials.
For example, a cont... heating time-tempera... e-transformation
(CHT) diagram resul... *heating a reactive s... tem from (say) 25°*
to 300°C at a series o... fferent rates of incr... sing temperature
(T). The vitrificat... rve (i.e., T_g = T) w... be joined to a
devitrification curv... T_g = T) to form a... nvelope (21). This

devitrification is a consequence of the rising glass transition temperature eventually not increasing at the same rate as the rate of rise of temperature. Such a diagram is useful in molding technology for defining time-temperature cure paths in which vitrification does not occur, for example, so as to obtain full cure. Conversely vitrification can be an essential part of a cure cycle so as to control reaction rates which could run out of control because of the exothermic nature of a reaction. The polymerization of 250 gallons of epoxy to encapsulate a magnetic coil in Princeton University's experimental Tokomak nuclear fusion reactor is accomplished by heating at a very low rate of temperature increase; the reaction rate is controlled in the process by the T_g increasing in concert with the temperature until $T_{g\infty}$, i.e., full cure, is attained.

LINEAR POLYMERIZATION AND THE TTT DIAGRAM

This section attempts, in a general manner, to incorporate linear polymerization of neat systems into the concept of the TTT diagram.

Difunctional liquid monomers can be transformed into glassy linear polymeric materials by reaction below the maximum glass transition temperature of the polymer, $T_{g\infty}$. The time to vitrification curve for the isothermal free radical polymerization of neat styrene versus the isothermal temperature of reaction, T_{rx}, has been computed in the absence of diffusion control (22). The calculation involved using the well established chemical kinetics from zero conversion to the conversion corresponding to $T_g = T_{rx}$. Since the neat mixture at any time consists of monomer and polymer (neglecting initiator and active chain radicals), the proportion of polymer to monomer (i.e., the conversion) was calculated from the glass transition temperatures of the monomer (-100°C) and polymer (+100°C) and $T_g = T_{cure}$. The computed vitrification curves for the free-radical polymerization of styrene (and also for a linear-forming step-growth polymerization) were S-shaped.

Phase separation can occur in neat linear polymerization as a consequence of insolubility of oligomer or polymer. This has been a particularly important consideration in the synthesis by step-growth polymerization of high T_g linear polymers, which of necessity have relatively inflexible chain structures. Precipitation often effectively removes the growing species from the reaction medium, thereby limiting the molecular weight. Phase separation can be analogous to vitrification in limiting molecular weight and T_g. In the same type of polymerization the reaction temperature must be such that vitrification also does not occur (i.e. $T_{rx} > T_{g\infty}$). (Use of exotic solvents overcomes the problems of insolubility and vitrification in the synthesis of high T_g rigid molecules: however, these solvents must be subsequently removed, for example, by heating above $T_{g\infty}$.)

Although chemical gelation does not occur in linear polymerization, long range elasticity can develop in the polymerizing fluid as the consequence of entanglements between polymer molecules. These will occur at lower conversions for chain reactions where high molecular weight polymer forms throughout the reaction, than for step-growth polymerizations where high molecular weight polymer develops only late in polymerization.

The situation is more complex for the conversion of liquid monomers into polymers which can crystallize. Polymerization of neat monomer above $T_{g\infty}$ can lead to solidification because of crystallization. (The maximum melting temperature, $T_{m\infty}$, is greater than the maximum glass transition temperature, $T_{g\infty}$.) Polymerization below $T_{g\infty}$ can lead to solidification as the result of vitrification or crystallization. The melting temperature, as well as the glass transition temperature should be directly related to the temperature of reaction: it is well known that T_m of a linear polymer is directly related to the isothermal temperature of crystallization.

SOLVENT-BASED REACTIVE COATINGS AND THE TTT DIAGRAM

An important application of the transformation of reactive liquids to solids involves loss of solvent. In these vitrification can occur as the consequence of both solvent loss and chemical reaction (11). The following example demonstrates how the methodology of the TTT cure diagram has been used to characterize a particular solvent-based reactive coating (23). The summary isothermal TTT diagram is shown as Figure 4.

The particular system is reactive at reasonable rates only above $T_{g\infty}$ ($T_{g\infty} \approx 147$°C). Cure involves volatilization of both solvent (57.5 percent) and reaction by-products (4-6 percent). Although in practice vitrification is therefore not a consideration, complete characterization of a system would include it, as shown in Figure 4.

The progress of the changes which occur are summarized by iso-weight loss contours (obtained from crossplotting isothermal gravimetric analyses), iso-T_g contours (obtained from crossplotting isothermal changes of T_g and from analysis of T_{cure}, t_{cure} and T_g data) and contours corresponding to macroscopic gelation and to vitrification. Several data points for vitrification were obtained by direct measurement including T_{go} which was obtained by direct measurement on the unreacted formulation during a temperature scan. However, the vitrification contour was obtained for the most part by extrapolation techniques [a) extrapolating iso-T_g contours to $T_{cure} = T_g$; b) from analysis of T_{cure}, t_{cure} and T_g data; c) temperature $_{gel}T_g$' was obtained and defined by extrapolating the time to the macroscopic gelation contour such that the time to macroscopic gelation equals the time to vitrification].

The iso-weight loss contours in the TTT diagram indicate that solvent is essentially lost before macroscopic gelation occurs. (Retention of solvent beyond gelation is not generally desirable.) Subsequent loss of weight is attributed to the byproducts of the chemical reaction.

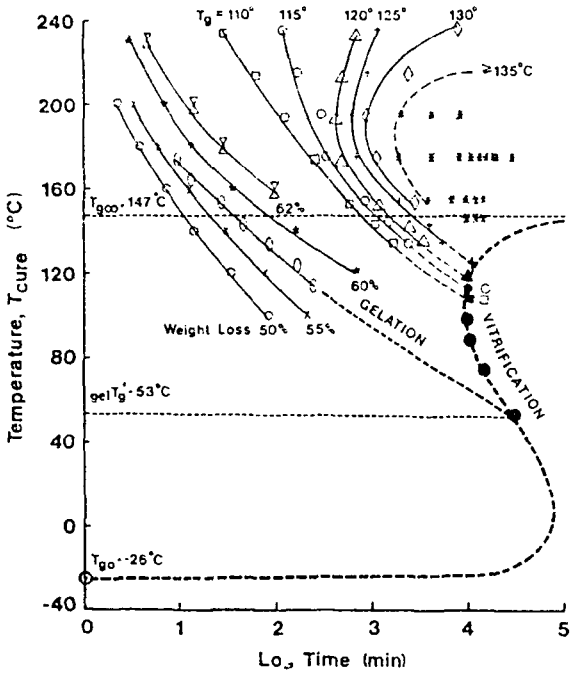

Figure 4. Summary Time-Temperature-Transformation (TTT) Diagram for a Solvent-Based Reactive Coating System. (Glass transition temperatures ≥ 135°C are bounded as marked.)

The iso-T_g contours would correspond to iso-conversion contours if T_g is a direct measure of conversion (Fig. 2). The conversion times to a fixed T_g would then be expected to decrease with increasing temperature in an Arrhenius fashion (see T_g = 110°C contour). However, at high temperatures of cure, thermal degradation is considered to compete with chemical cure to produce the minima in time to reach iso-T_g levels (e.g., see iso-T_g contour = 130°C). Competition between cure and thermal degradation therefore renders it difficult to evaluate $T_{g\infty}$, the maximum glass transition temperature due to only full cure. The maximum experimental value of T_g obtained (147°C) isothermally was taken to be the operational value of $T_{g\infty}$. Degradation is also held responsible for the maximum attainable value of T_g decreasing with increase of T_{cure} (e.g., see T_g = 135°C and T_g = 130°C contours).

TORSION PENDULUM (TP) AND TORSIONAL BRAID ANALYSIS (TBA): TECHNIQUES FOR CHARACTERIZING THERMOSETTING AND HIGH T_g SYSTEMS

Preamble: T_g as a Characterizing Parameter for Reactive Systems.

This section of the review deals with the principal technique -- TBA -- which has been developed and used in the author's laboratory to characterize the cure and properties of especially thermosetting and high T_g systems. The technique is especially useful in conveniently measuring glass transition temperatures including under conditions where the material is not self-supporting. The glass transition temperature is a) a measure of the state of cure (i.e., conversion), b) is used to define the vitrification contour, c) is in itself the characteristic softening temperature of amorphous materials and d) is a sensitive measure of cure since T_g changes by typically 200°C in the course of cure [and it is especially sensitive at high conversions due to the non-linear increase of T_g with conversion (Fig. 2)].

TP/TBA - Modes

The freely oscillating torsion pendulum can be used in two ways to characterize polymeric systems; these are the conventional torsion pendulum (TP) mode and the torsional braid analysis (TBA) mode, respectively (1). Geometrically simple specimens (e.g., films & filaments) are used in the TP mode to obtain quantitative values of the elastic and loss moduli. Impregnated braid specimens are used in the TBA mode to obtain transitions of polymers, to obtain a preliminary mechanical assessment of new polymers, and to characterize liquid to solid transformations (e.g. cure).

Instrumentation

A schematic diagram of the automated TBA torsion pendulum system which has been developed by the author is shown in Figure 5. The

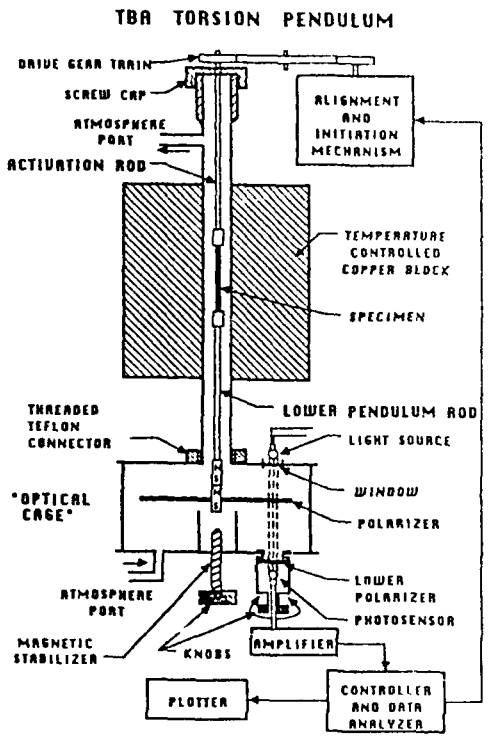

Figure 5 TBA Torsion Pendulum.

system is available from Plastics Analysis Instruments, Inc., Princeton, NJ 08540. The activation rod is held vertically in alignment with a bushing and is rigidly attached to a horizontal gear which intermittently initiates free oscillations through computer-controlled angular displacement of the gear (by the slow stretching and step-releasing of a spring). The lower pendulum rod hangs freely and is magnetically coupled to a polaroid disc at its lower end.

The pendulum is enclosed in an air-tight cylindrical chamber (0.5" diameter), the atmosphere of which is closely controlled and monitored: inert, water-doped, and reactive gases have been used. There are no electronic devices within the specimen chamber. Dry helium, rather than nitrogen, is usually used as an inert atmosphere because of its higher thermal conductivity at cryogenic temperatures. An on-line electronic hygrometer is used to continuously monitor the water vapor content of atmospheres from < 20 to 20,000 ppm H_2O. A cylindrical copper block, wound around with cooling coils for liquid nitrogen and with band heaters, surrounds the specimen. Excellent temperature control is achieved by virtue of the large thermal mass of the copper block, with a temperature spread of <1°C over a 2" specimen. A temperature programmer/controller system permits experiments to be performed in isothermal (±0.1°C above 30°C) and dynamic modes from -190 to 400°C; in the dynamic mode the temperature may be increased or decreased linearly at controlled rates of 0.05 to 5°C/min. Cooling is achieved by controlling the flow of liquid nitrogen from a pressurized container. Routine temperature scans are made at rates of change of temperature of ± 2°C/minute. Measurements have been made as low as 4°K and as high as 700°C in modified apparatus.

A key factor in the instrumentation is the non-drag optical transducer which produces an electrical response that varies linearly with angular displacement. A polarizing disc is used as part of the inertial member of the pendulum, and a stationary second polarizer is positioned in front of a linearly-responding photocell. An analog electrical signal is obtained from a light beam passing through the pair of polarizers (Fig. 5).

The clamps on the pendulum allow a variety of specimens to be used: film, fiber, or coating on glass braid or foil substrate. Depending on the specimen, the system can be used as a conventional torsion pendulum or in the supported TBA mode. The substrate generally used in a TBA experiment is a loose, heat-cleaned glass braid containing about 3600 filaments. The specimen is prepared by simply dipping the braid into the neat liquid or into a solution of the material of interest dissolved in a solvent.

Quantitative values of the shear and loss moduli of polymer films are obtained from the natural frequency (~ 1 Hz) and damping of the induced oscillations of the torsion pendulum. Some advantages of using the automated torsion pendulum system for the dynamic mechanical thermal analysis of polymers are its fundamental simplicity and ruggedness, its cost (less than $50,000), its utilization of

the pendulum's resonance frequency (which means that the measurement is always made at the maximum sensitivity, since the specimen is a primary component of the pendulum), its use of a non-drag optical transducer (i.e., the pair of polarizers) which permits the use of small specimens (< 20 mg), and its free movement (because the pendulum is fixed only at one end, no adjustments for thermal expansion or contraction are required). In the torsional braid analysis (TBA) mode a glass braid (or other substrate) is impregnated with a polymer solution or polymer "melt", and measurements are made on the composite specimen. Although the specimen's relative rigidity is obtained instead of its shear modulus, the transition temperatures can readily be identified. The advantages of the TBA technique include ease of specimen fabrication, vertical self-alignment (by gravity), and the capability of monitoring the physical properties of a specimen from the liquid to the solid state (as in the cure by chemical reaction of a thermosetting resin or on cooling through the glass transition region of a thermoplastic system).

The pendulum is intermittently set into oscillation to generate a series of damped waves as the material properties of the specimen change with temperature and/or time. The damped oscillations are converted to electrical analog signals by the optical transducer.

The shear modulus, G', is given by

$$G' = KI(2\pi f)^2 \left[1 + \left(\frac{\Delta}{2\pi}\right)\right] \tag{1}$$

where f is the frequency (Hz) of the oscillation, I is the moment of inertia, Δ is the logarithmic decrement [$\Delta = \ln(A_i/A_{i+1})$, A_i is the amplitude of the ith oscillation], and K is a geometric constant. Equation 1 is usually approximated by

$$G' \approx KI(2\pi f)^2 \tag{2}$$

when $\Delta/2\pi < 0.1$. The loss modulus, G", is

$$G'' = \frac{KI\Delta}{\pi}(2\pi f)^2 \tag{3}$$

The loss tangent, tan δ, is a characteristic measure of the ratio of the energy dissipated per cycle to the maximum potential energy stored during a cycle:

$$\frac{G''}{G'} = \tan\delta = \frac{\Delta}{\pi} = \frac{\alpha}{\pi f} \tag{4}$$

where α is the damping coefficient. During a dynamic mechanical thermal analysis experiment, the moduli can be monitored by observing the changes in the frequency and logarithmic decrement (Δ) of the oscillations. In a torsion pendulum experiment, where the geometric constants are known, the absolute moduli are obtained: [e.g., for a rectangular film,

$$G' = \frac{(2\pi f)^2 IL}{N}\left[1 + \left(\frac{\Delta}{2\pi}\right)^2\right] - \frac{mgb^2}{12N} \tag{5}$$

in which the form factor, N, is

$$N = \frac{a^3 b}{3}\left(1 - 0.63\,\frac{a}{b}\right) \tag{6}$$

where a, b, and L are the thickness, width (a < b/3), and length respectively of the film, g is the gravitational constant, and m is the mass. I can be obtained in a calibration experiment using a wire of known modulus and dimensions]. Although the geometric constants are not known in a TBA experiment, the frequency can be used to calculate a relative modulus, since $G' \propto f^2$. The TBA plots display the relative rigidity as $1/P^2$ where P is the natural period of the oscillations.

The natural frequency of the oscillations generally ranges from 0.01 Hz (for a liquid) to 10 Hz (for a solid), and the logarithmic decrement generally ranges from 0.001 to 3.0.

The data acquisition system (24) consists of a desktop computer (with printer, plotter, and disc drives), multiplexed switch, and a digital voltmeter, as shown in Figure 6. The computer monitors the temperature and torsion pendulum oscillation signals, controls the initiation of the oscillations, and derives the frequency and logarithmic decrement of the oscillations from the raw data. The reduced data are stored and are available for plotting and/or printing or further massaging.

The computer controls the pendulum in a repetitive sequence, as shown in Figure 7: after monitoring the wave until it has damped out, the computer aligns the pendulum for a linear response by rotating one of the polarizers and then initiates a new oscillation by cocking the pendulum against a spring (via a gear train), again monitoring the wave until the oscillations have decayed, and then

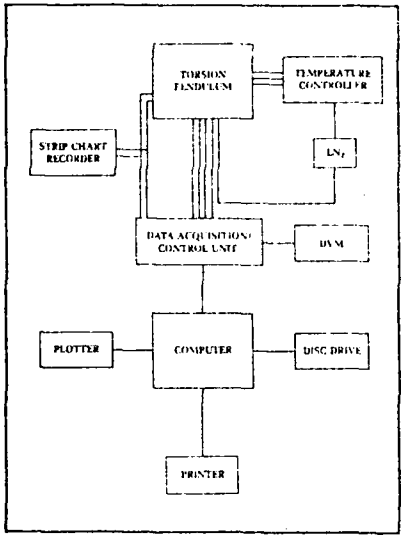

Figure 6. System Diagram

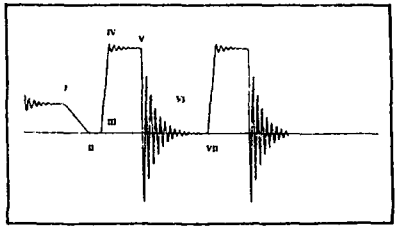

Figure 7. Theory of Operation. An analog electrical signal is obtained from a light beam passing through a pair of polarizers, one of which oscillates with the specimen. The pendulum is aligned for linear response and oscillations are initiated by the computer which also processes the damped waves to provide the dynamic mechanical spectrum. Automated torsion pendulum: control sequence. Key: I, previous wave decays, drift detected and correction begins; II, reference level of polarizer pair reached; III, wave initiating sequence begins. IV, decay of transients; V, free oscillations begin; VI, data collected; and VII, control sequence repeated.

releasing it so that the oscillations are centered about the center of the linear region. The wave is digitized and stored until the oscillations have decayed. The frequency and logarithmic decrement are extracted from the digitized wave by, for example, a non-linear least squares fit to the solution of the differential equation of motion:

$$\theta = \theta_o e^{-\alpha t}\cos(2\pi f t + \phi) + Bt + C \qquad (7)$$

where θ is the angular deformation of the pendulum as a function of time t, θ_o is the initial deformation, ϕ is the phase angle, B is the drift coefficient, and C is the offset.

Applications

Much of the text of this review can be obtained by of analysis of TBA data. This includes the TTT cure diagram itself (Fig. 1 and Fig. 4), and the T_g versus conversion relationship, in conjunction with calorimetric data (Fig. 2). Typical TBA plots for a) the isothermal cure of a liquid epoxy and b) the temperature dependent behavior of a cured rubber-modified epoxy are included in Figures 8 and 9, respectively. Transition times (e.g., vitrification and macroscopic gelation) and transition temperatures (e.g., T_g) are located by maxima in the mechanical damping (logarithmic decrement) curves. A typical TP plot displaying quantitative data for an epoxy film is shown in Figure 10. A review of the technique and its application to polymers in general has been published (1,24).

Acknowledgements

Financial support has been provided by the Office of Naval Research.

References

1. J. K. Gillham in J. V. Dawkins, ed., Developments in Polymer Characterisation, Vol. 3, Applied Science Publishers, Ltd., London, 1982, Chapt. 5, pp. 159-227.
2. J. K. Gillham, Encyclopedia of Polymer Science and Engineering, Second Edition, 4, 519 (1986).
3. P. J. Flory, Principles of Polymer Chemistry, Cornell University Press, Ithaca, N.Y., 1953.
4. P. G. Babayevsky and J. K. Gillham, J. Appl. Polym. Sci. 17, 2067 (1973).
5. L. C. Chan, J. K. Gillham, A. J. Kinloch, and S. J. Shaw, Adv. Chem. Ser. 208, 235 (1984).
6. Ibid., 261 (1984).

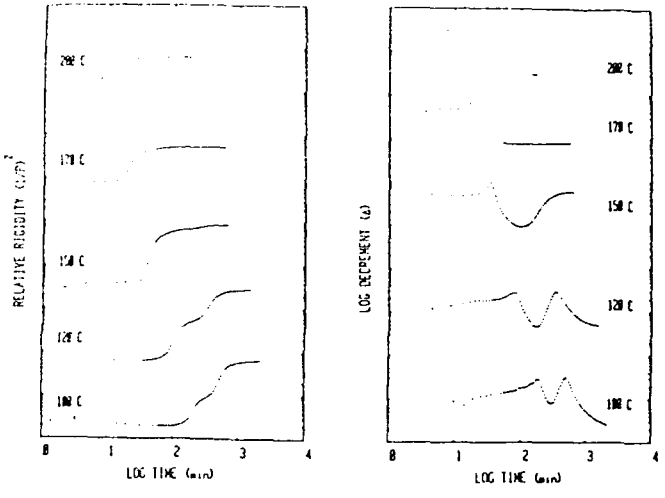

Figure 8. Representative TBA Isothermal (100 to 200°C) Cure Spectra of a Rubber-Modified Epoxy System (13). Relative Rigidity (Left) and Logarithmic Decrement (Right) versus Log_{10} Time.

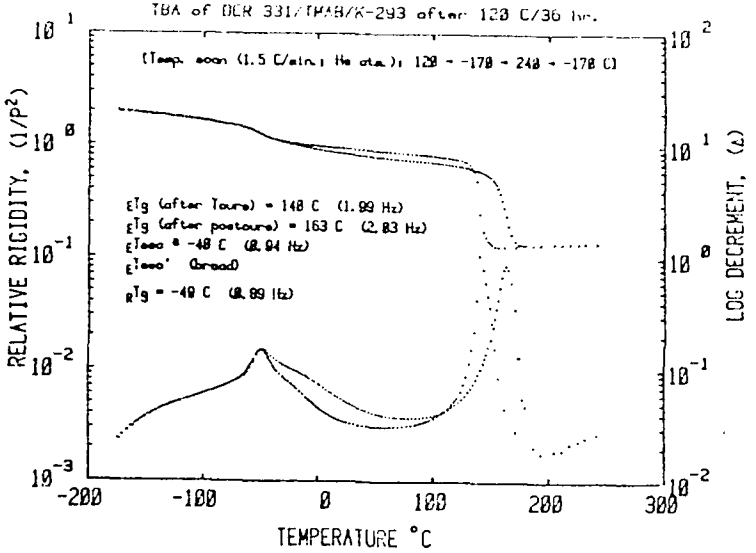

Figure 9. Sequential TBA Temperature Scans after Isothermal Cure (120°C/36 hr) of a Rubber-Modified Epoxy system (13). Temperature scan: 120 to -170 to 240 to -170°C at 1.5°C/min in dry helium atmosphere. Transition temperatures (°C) and frequencies (Hz) are marked.

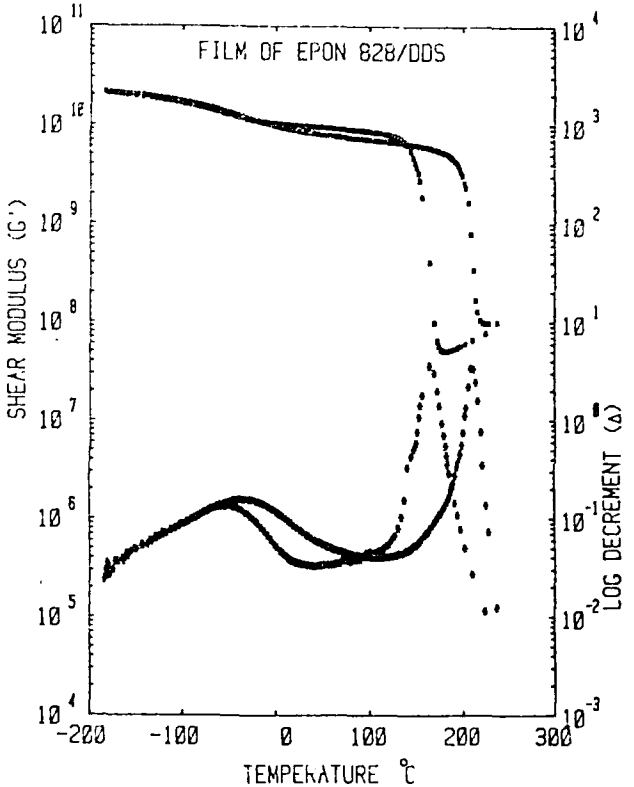

Figure 10. Sequential TP Temperature Scans of an Epoxy Film. Temperature scan 120 to -180 to 240 to -180°C at 1.5°C/min in dry helium atmosphere. Note that postcure during the heating scan results in a higher T_g but in a lower modulus at RT.

7. S. Wu, Polymer 26, 1855 (1985).
8. J. K. Gillham, P. N. Reitz and M. J. Doyle, Polym. Eng. Sci. 8, 227 (1968).
9. M. B. Roller, Polym. Eng. Sci. 10, 692 (1979).
10. J. B. Enns and J. K. Gillham, Adv. Chem. Ser. 203, 27 (1983).
11. G. Palmese and J. K. Gillham, J. Appl. Polym. Sci. 34, 1925 (1987).
12. X. Peng and J. K. Gillham, J. Appl. Polym. Sci. 30, 4685 (1985).
13. L. C. Chan, H. N. Naé, and J. K. Gillham, Polym. Prepr. Am. Chem. Soc. Div. Org. Coat. Plast. Chem. 48, 566 (1983); J. Appl. Polym. Sci. 29, 3307 (1984).
14. J. D. Ferry, Viscoelastic Properties of Polymers, 3rd ed., John Wiley & Sons, Inc., New York, 1980.
15. H. E. Adabbo and R. J. J. Williams, J. Appl. Polym. Sci. 27, 1327 (1982).
16. J. B. Enns and J. K. Gillham, J. Appl. Polym. Sci. 28, 2567 (1983).
17. M. T. Aronhime and J. K. Gillham, J. Coat. Technol. 56(718), 35 (1984).
18. J. K. Gillham, J. A. Benci and A. Noshay, J. Appl. Polym. Sci. 18, 951 (1974).
19. M. T. Aronhime, X. Peng, J. K. Gillham and R. D. Small, J. Appl. Polym. Sci., 32, 3589 (1986).
20. K. P. Pang and J. K. Gillham, J. Appl. Polym. Sci. In Press (1988).
21. A. F. Lewis, M. J. Doyle and J. K. Gillham, Polym. Eng. Sci. 10, 683 (1979).
22. M. T. Aronhime and J. K. Gillham, J. Appl. Polym. Sci. 29, 2017 (1984).
23. S. Gan, J. K. Gillhan and R. B. Prime, J. Appl. Polym. Sci. In press (1988).
24. J. B. Enns and J. K. Gillham, in T. Provder, ed., Computer Applications in Applied Polymer Science, Am. Chem. Soc., Symposium Series, No. 197, 329 (1982).

HIGH ENERGY RADIATION- AND UV LIGHT-INDUCED CROSSLINKING AND CHAIN SCISSION

WOLFRAM SCHNABEL

HAHN-MEITNER-INSTITUT, BEREICH S
GLIENICKER STR.100
D-1000 BERLIN 39
Federal Republic of Germany

ABSTRACT. The 1st part of this chapter deals with fundamental aspects concerning (a) the absorption of UV and high energy radiation by matter, (b) the detection of crosslinks and scissions in linear polymers and (c) mechanistic aspects regarding crosslinking and main-chain scission. The 2nd part concerns some recent results regarding ion beam- and soft X-ray-induced radiation effects in linear polymers

1. Introduction

1.1 IMPORTANCE OF RADIATION-INDUCED CROSSLINKING AND MAIN-CHAIN SCISSION IN LINEAR POLYMERS

There are various modes of inducing crosslinking (XL) and chain scission (CS) in polymers, the most important ones concern thermal, mechanical, biological, chemical, radiation chemical and photochemical processes.
Characteristic for the radiation-induced modes is the following:
XL and/or CS can be initiated at low temperatures by simply placing polymer specimen into the radiation field. Moreover, XL and/or CS occur spontaneously without the aid of added low molar mass additives.
Notably, radiation is a convenient tool to alter physical properties of polymers, *since XL and/or CS cause alterations in the average molar* mass and many practically important physical properties depend on the molar mass. In this connection it should be pointed out that XL commonly exerts beneficial effects on mechanical properties up to a certain absorbed radiation dose, i.e. up to a certain degree of crosslinking, whereas CS leads to severe property deteriorations right after the irradiation has started. Irradiation of polymers to high absorbed doses is always harmful: it causes embrittlement and color changes. This applies both to treatment with high energy radiation and UV light. Since the sunlight penetrating the earth's atmosphere contains a portion of UV light, photodegradation of polymers caused by XL and/or CS is of enormous practical and economical importance with respect to commercial polymers. Notably, polymer degradation is frequently significantly enhanced by oxidative processes which are initiated by radiation and perform in many cases kinetically as "chain reactions", i.e. as auto-oxidative processes involving CS. To overcome this problem stabilizers are added quite frequently to commercial polymers. Stabilizers are low molar mass compounds which protect the polymer with respect to XL and CS against the action of UV light.
Apart from the detrimental effects of radiation-induced XL and CS, there are various quite useful applications. Typical examples for the beneficial effects of XL and CS in polymers apply to photolithographic techniques which are used to manufacture integrated circuits, compact discs, cathode ray tubes and printed circuit boards. Moreover, high energy induced XL is applied in the production of *shrinkable polyethylene tubes and foils, and to improve thermal and* mechanical properties of insulations of high voltage cables.
The main intention of this paper is to give a brief introduction into the field of radiation and photochemistry of polymers as far as XL and CS are concerned. For this purpose types of radiation of interest, radiation sources and the absorption of radiation by matter will be treated in the next sections. Furtheron, the detection of XL and CS and the determination of XL and CS yields will be dealt with in a concise form. At the end of the chapter some recent results obtained in the author's laboratory will be presented

1.2. TYPES OF RADIATION AND RADIATION SOURCES.

The types of radiation concerned in this article are listed in Tables 1 and 2. Electromagnetic radiations are to be discriminated from particle radiations. Commercially available lamps such as deuterium,xenon or mercury lamps serve as sources for visible and UV light. In addition, powerful lasers emitting monochromatic and coherent light are used nowadays in research work and practical applications. Quite popular are solid state lasers such as ruby and Nd-YAG systems and gas lasers producing light of wavelengths covering the range from UV to IR. X-rays can be produced by commercially available tubes. Very powerful X-ray sources are electron synchrotrons which are now operated in various countries.
Apart from the classical particle radiations, α- and β-rays, electrons as well as *light and heavy ions of energies ranging up to several* hundred eV can be produced nowadays by particle accelerators, and neutrons are generated in nuclear reactors.

1.3. ABSORPTION OF RADIATION

The absorption of electromagnetic radiation of wavelengths corresponding to infrared (IR), visible and ultraviolet (UV) light is

determined by the availability of appropriate energetic levels E_2 and E_1 ($E_2 > E_1$ and $E_2 - E_1 = h\nu$) in a molecule or in a "chromophoric" group of a molecule. The absorption of light of wavelength λ by chromophoric groups at the concentration c (in mol/l) in a system of optical path length d (in cm) is described by the Lambert-Beer law

$$I = I_0 10^{-\epsilon_\lambda c d} \qquad (1)$$

I_0: intensity of incident light, ϵ_λ: decadic molar extinction coefficient (in l/mol cm).
Typical absorption spectra of polymers are shown in Fig.1.

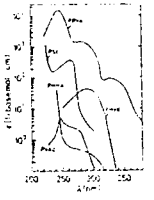

Fig.1. Optical absorption spectra of several polymers recorded in dioxane solution.
PMMA: poly(methyl methacrylate)
PVAc: polyvinylacetate
PSt: polystyrene
PMVK: poly(methyl vinyl ketone)
PPVK: poly(phenyl vinyl ketone)

Only a small number of practically important polymers is capable of absorbing solar radiation. However, quite frequently commercial polymers contain impurities capable of absorbing sunlight. This explains, in most cases, the instability of polymers which, according to their chemical constitution, should be resistant to solar radiation.The probability that an absorbed photon induces a chemical change in a molecule depends on the importance of competing photophysical processes (radiationless transitions, luminescence, see Scheme 1) following the absorption act.
Contrary to UV and visible light, high energy radiation is absorbed non-specifically. i.e., there are no chromophores for γ-rays, fast electrons etc.. The absorption of high energy electromagnetic radiation and of fast particles by matter occurs via interactions with both the nuclei of the atoms and the clouds of electrons surrounding them. Interactions with atomic nuclei can be neglected if the energy of the photon or the particle is lower than about 10 MeV and if the irradiated material consists only of light nuclei (C,O,H,N,S,P), which applies to organic polymers.

Table 1. Types of Electromagnetic Radiation

Type of Radiation	λ (nm)	E_{Photon} (eV/photon)	E_{Photon} (kJ/mol)
Visible Light	800	1.55	149.6
	400	3.10	299.2
Ultraviolet Light	100	12.4	1194
X-Rays	10	124	1.19×10^4
	0.01	1.24×10^5	1.19×10^7
γ-Rays	≤ 0.001	$\geq 1.24 \times 10^6$	$\geq 1.19 \times 10^8$

Table 2. Types of Particle Radiation

Type of Radiation	Source
Neutrons	Nuclear Reactors
β-particles (electrons)	Radioactive Decay (Accelerators)
α-particles ($^4_2He^{2+}$)	Radioactive Decay
H^+, D^+, $^4_2He^{2+}$ and heavy ions: e.g. $^{16}_8O^{4+}$, $^{20}_{10}Ne^{7+}$, $^{40}_{18}Ar^{8+}$ etc.	Accelerators (van de Graaff, Linear Accelerators, Cyclotrons etc.)

Reaction (2) describes a primary ionization event and reactions (3a) and (3b) represent the interaction of secondary electrons with intact molecules. Notably, reactions (3a) and (3b) also apply for the absorption of corpuscular radiation, i.e. fast electrons and ions (protons, α-particle etc.) as far as the fraction of energy lost by inelastic collisions is concerned. The ionization of a molecule M by a fast electron is described by reaction (4):

$$\underset{\text{primary electron}}{e^-_{fast}} + M \longrightarrow \underset{\text{radical cation}}{M^{+\cdot}} + \underset{\text{secondary electron}}{e^-_{kin}} + \underset{\text{primary electron}}{e^-_{fast}} \qquad (4)$$

$$(E_{kin}) \qquad\qquad (E''_{kin}) \qquad (E'_{kin})$$

$$(E'_{kin} < E_{kin})$$

E''_{kin} of most secondary electrons is less than 100 eV. Therefore, a large fraction of energy is deposited in close proximity to the place of original ionization. On the other hand, a fast electron of e.g. E_{kin} = 1 MeV, passes many molecules without interaction. Consequently, energy absorption occurs rather heterogeneously. According to radiation chemists' terminology a "track" of a fast electron consists of a series of "spurs" having an average distance of several hundred nm. The distribution of spurs is subject to the linear energy transfer, LET, of a particle traversing matter, i.e. the amount of energy dissipated per unit path length , - dE/dx. Concerning interactions of particles of energy E_{kin} and mass M with electron clouds of atoms of atomic number Z the LET is given by the Bethe equation:

$$-\frac{dE}{dx} = \frac{2\pi e^4 z^2 MZN}{E_{kin}{}^m} \ln\frac{4E_{kin}{}^m}{I_m M} \qquad (5)$$

e: elementary charge, m: mass of electron, z: number of charges per particle, N: number of atoms/cm^3, I_m: average ionization potential. At a given particle energy E_{kin}, - dE/dx increases according to eq.(5) if Z and z increase. It must be pointed out that the average distance between spurs is reduced if the LET increases. Actually, overlapping of spurs leads to almost "cylindrical" tracks "filled" with ionizations and excitations. This applies to the absorption of particle radiations (protons, α-particles etc.). Pronounced differences in initial local concentrations of reactive intermediates are the basis of theories explaining the differences in XL and CS yields found on irradiating polymers with radiations of low and high LET.

Scheme 1. Important photophysical processes. (The superscripts 1,2 and 3 denote singlet, doublet and triplet states; asterisks denote excited states.)

Photon Absorption:

$^1M + h\nu \longrightarrow {}^1M^*$	(1st excited singlet state)
$^1M + h\nu \longrightarrow {}^1M^{**}$	(higher excited singlet state)
$^1M + h\nu \longrightarrow {}^2M^{+\cdot} + e^-$	(photoionization)

Radiationless Transitions:

$^1M^* \longrightarrow {}^1M + \text{energy}$	(internal conversion)
$^1M^* \longrightarrow {}^3M + \text{energy}$	(intersystem crossing)
$^1M^{**} \longrightarrow {}^1M^* + \text{energy}$	(internal conversion)
$^3M^{**} \longrightarrow {}^3M + \text{energy}$	(internal conversion)

Radiative Transitions (Luminescence):

$^1M^* \longrightarrow {}^1M + h\nu$	(fluorescence)
$^3M^* \longrightarrow {}^1M + h\nu$	(phosphorescence)

Regarding the interaction of γ- or X-rays with matter, three processes are to be considered: photoelectric effect, Compton effect and pair formation. The relative importance of these processes depends on the photon energy and the atomic number of the nuclei as well as on the electron density of the irradiated system. In all three cases secondary electrons are ejected from the atoms involved, most of them possessing kinetic energies sufficiently large to induce additional ionizations or electronic excitations in surrounding molecules:

$$M \xrightarrow{\text{high energy photon}} \underset{\text{radical cation}}{M^{+\cdot}} + \underset{\text{secondary electron}}{e^-_{kin}} \qquad (2)$$

$$M \xrightarrow{e^-_{kin}} \begin{cases} M^{+\cdot} + e^-_{kin} & (3a) \\ M^* & (3b) \end{cases}$$

electronically excited molecule

With respect to chemical alterations caused by the absorption of high energy radiation in organic polymers, the elementary reactions listed in Scheme 2 have to be considered.
The formation of a stable product in a simple decay process as described by reaction (e) in Scheme 2 is a very rare event. The overwhelming portion of final products is formed via radical-radical or ion-ion (neutralization) processes.

Scheme 2. Interaction of high energy radiation with organic compounds. Generation and decay of intermediates.

Primary radiolytic act	$M \longrightarrow M^{+\cdot} + e^-_{kin}$	(a)
Capture of thermalized electron by positive ion	$M^{+\cdot} + e^-_{th} \longrightarrow M^*$	(b)
Capture of thermalized electron by neutral molecule	$M + e^-_{th} \longrightarrow M^{-\cdot}$	(c)
Bond breaking reactions:		
Decomposition of excited molecule (radical formation)	$M^* \longrightarrow R_1^\cdot + R_2^\cdot$	(d)
Decomposition of excited molecule (formation of stable products)	$M^* \longrightarrow A + B$	(e)
Decomposition of positive radical ion	$M^{+\cdot} \longrightarrow R^\cdot + C^+$	(f)
Decomposition of negative radical ion	$M^{-\cdot} \longrightarrow R^\cdot + D^-$	(g)
Side reactions:		
Charge transfer	$M^{+\cdot} + S \longrightarrow M + S^{+\cdot}$	(h)
	$M^{-\cdot} + S \longrightarrow M + S^{-\cdot}$	(i)
Energy transfer	$M^* + S \longrightarrow M + S^*$	(j)

2. General Aspects Concerning XL and CS in Linear Polymers

2.1. RANDOM AND SPECIFIC SITE ATTACKS

Regarding homopolymers consisting of identical structural repeating units, the initiation of XL and CS under the influence of UV light or high energy radiation can be considered as random processes. This concerns the fact that all repeating units are equally likely to be affected during radiation absorption. A typical example of such a random process is the photolytical CS of ketone polymers, e.g. that of poly(phenylvinyl ketone) by a Norrish type II process:

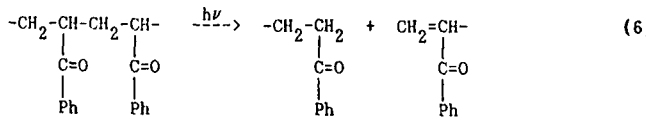

(6)

Upon irradiation with light of wavelength 300-370 nm, the carbonyl groups act as chromophores and, provided the polymer sample is thin enough to permit homogeneous distribution of absorption acts, CS occurs at random.
The occurrence of non-random processes can be visualized, for example, in the case of block copolymers of the type $-(A)_n-(B)-(A)_n-$ consisting of long blocks of repeating units A and short sequences of repeating units B, with the latter being attacked exclusively. Such a situation applies, however, straightaway, only to photochemical initiation, where energy absorption is limited to chromophores. As far as high energy radiation is concerned principally all repeating units can be involved in absorption processes. The ensuing intermediates, e.g. free radicals might vary, however, in reactivity with the result that XL and/or CS are not distributed statistically over the chains of the block copolymer.
It should be pointed out that randomness of absorption events does not necessarily imply randomness of formation of reaction products. In heterogeneous systems, such as in partially crystalline polymers, products can be distributed also heterogeneously, if the product yields depend on the physical state of the system at the time of irradiation. This applies, e.g. to the γ-irradiation of polyethylene, where crosslinks are formed preferentially in the amorphous regions.

2.2. DETECTION OF XL AND CS

Both processes XL and CS alter the average molar mass (MM), and often also the molar mass distribution (MMD) of polymers. Therefore, all means of MM determination are applicable to evidence XL and CS provided the polymer sample is soluble in an appropriate solvent. In this case,

crosslinking, if $G(S) < 4G(X)$, or $\phi(S) < 4\phi(X)$.
$\phi(S)$ and $\phi(X)$, and $G(S)$ and $G(X)$ can be obtained separately if M_n and M_w are measured as a function of the absorbed dose. From eqs.(7) and (8) it results:

$$\frac{\phi(S)}{\phi(X)} = \frac{4k_n - k_w}{k_n - k_w} \qquad (11)$$

with $k_n = \phi(S) - \phi(X)$ and $k_w = \phi(S)/2 - 2\phi(X)$.

Analogously, G(S) and G(X) can be obtained with the aid of eq.(12), derived from eqs. (9) and (10) :

$$\frac{G(S)}{G(X)} = \frac{4k'_n - k'_w}{k'_n - k'_w} \qquad (12)$$

with $k'_n = G(S) - G(X)$ and $k'_w = G(S)/2 - 2G(X)$.

If crosslinking predominates, the polymer becomes insoluble at absorbed doses exceeding the gel dose, D_{gel}. In this case, $\phi(S)$ and $\phi(X)$, and G(S) and G(X) can be determined with the aid of the Charlesby-Pinner method according to eq.(13) or (14):

PHOTOLYSIS:

$$s + s^{1/2} = \frac{\phi(S)}{2\phi(x)} + \frac{N_A}{M_w \phi(X) D} \qquad (13)$$

RADIOLYSIS:

$$s + s^{1/2} = \frac{G(S)}{2G(X)} + \frac{100\ N_A}{M_w G(X) D} \qquad (14)$$

Here, s denotes the soluble fraction of the irradiated polymer sample. Eqs.(13) and (14) hold for simultaneous random XL and CS and for a random initial MMD.

average molar mass determinations can be carried out with the light scattering method which yields the weight average molar mass, M_w, and with osmotic methods (vapor pressure, membrane osmometry) which yield the number average molar mass, M_n. MMD's are determined by gel permeation chromatography which affords, however, calibration by an absolute molar mass determination method.

2.3. SIMULTANEOUS XL AND CS

Apart from a few cases, where main-chain scission occurs exclusively, linear polymers undergo both XL and CS upon exposure to UV light or high energy radiation. Then, the dependence of M_n and M_w on the absorbed dose D is given by the following equations:

PHOTOLYSIS:

$$\frac{M_{n,o}}{M_{n,D}} = 1 + \left(\phi(S) - \phi(X)\right)\frac{D}{N_A} \qquad (7)$$

$$\frac{M_{w,o}}{M_{w,D}} = 1 + \left(\phi(S)/2 - 2\phi(X)\right)\frac{D}{N_A} \qquad (8)$$

D: absorbed dose in photons/g; N_A: Avogadro's number,

$\phi(S)$ and $\phi(X)$: quantum yields, i.e. number of scissions and crosslinks, respectively, per photon

RADIOLYSIS:

$$\frac{M_{n,o}}{M_{n,D}} = 1 + \left(G(S) - G(X)\right)\frac{D}{100\ N_A} \qquad (9)$$

$$\frac{M_{w,o}}{M_{w,D}} = 1 + \left(G(S)/2 - 2G(X)\right)\frac{D}{100\ N_A} \qquad (10)$$

D: absorbed dose in eV/g; N_A: Avogadro's number, G(S) and G(X): number of scissions and crosslinks, respectively, per 100 eV.
Whereas eqs. (7) and (9) hold for any initial MMD, eq.(8) and (10) hold only for an initially random MMD. From eqs.(8) and (10) it can be seen, that M_w does not change if $G(S) = 4G(X)$ or $\phi(S) = 4\phi(X)$. If $G(S) > 4G(X)$, or $\phi(S) > 4\phi(X)$, the polymer degrades predominantly, i.e. M_w decreases with increasing absorbed dose. On the other hand, a three-dimensional, insoluble network is formed due to predominant

2.4. MECHANISMS

Generally, alterations in the molar mass of polymers induced by UV light are easier to understand than those induced by high energy radiation. In the photolysis of polymers mostly only one kind of chromophore giving rise to a certain reaction mechanism is involved whereas high energy radiation generates simultaneously various kinds of intermediates which initiate different reaction routes. Principally, reaction mechanisms are quite specific and depend strongly on the chemical nature of the polymer. Some generalizations can be made, however, with respect to polymers containing carbonyl groups. Reaction (6) describes the light-induced chain cleavage of poly(phenyl vinyl ketone). In this case the excited carbonyl group abstracts a hydrogen from a carbon in γ-position. The biradical generated this way is short-lived and rearranges to the final products as described in reaction (6). Excitation of carbonyl groups might also induce α-scission, a process commonly referred to as Norrish type I reaction. Provided the carbonyl group is located in the chain, main-chain scission results from this reaction:

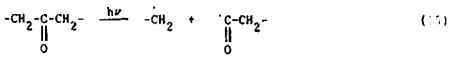

(7)

If the carbonyl groups are located in side chains, such as in the cases of poly(methyl acrylate), PMA, and poly(methyl methacrylate), PMMA, side groups are split off and lateral macroradicals are formed by the Norrish type I reaction. This was inferred from the fact that, upon UV irradiation, in both cases the same low molar mass products, especially $HCOOCH_3$, CH_3OH, CO_2 and CO are formed. That PMMA undergoes predominantly main-chain scission, whereas PMA crosslinks predominantly, is explained in terms of differences in the stability of the macroradicals generated by side group cleavage: $-CH_2-\dot{C}H-CH_2-$ is more stable than $-CH_2\dot{C}(CH_3)-CH_2-$. The mechanism is illustrated in Scheme 3.

Scheme 3. Photolysis of poly(methyl acrylate) and poly(methyl methacrylate)

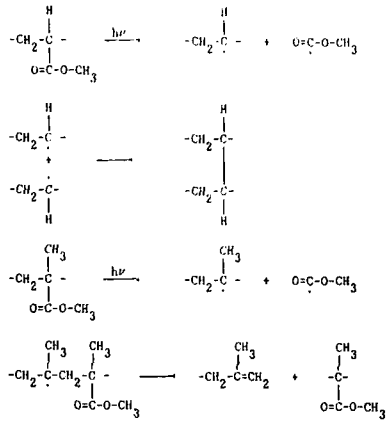

An example applying to crosslinking refers to the photolysis of poly-p-chloromethylstyrene, which was investigated in our laboratory (Zhu and Schnabel (1988)). In this case, a major light-induced reaction is the scission of the C-Cl bond in chloromethyl groups. The resulting chlorine radicals are reactive and abstract to a great extent hydrogens from carbons in the main chain. Macroradicals produced by both reactions form crosslinks by combination. This mechanism is illustrated in Scheme 4.

with intermediates, i.e. ions, excited molecules, free radicals. Because of the high local initial concentration of intermediates it is feasible to assume that radiation effects should differ qualitatively and quantitatively if polymers are subjected to radiations of different LET (-dE/dx). Actually, LET effects have been detected during the last decades. For example, G(S) was found to decrease with increasing LET in the case of poly(methyl methacrylate) (Zverev et al.(1969), Schnabel et al. (1984)) and G(X) was reported to be independent of LET in the cases of poly(vinyl chloride) (Makhlis (1975)) and polyethylene (Shinohara et al. (1958); Lavrentovich et al. (1969)). Polystyrene was reported to be crosslinked more efficiently by heavy ion radiation than by sparsely ionizing radiation (Parkinson et al. (1965); Zverev et al. (1969)).

Regarding the determination of G-values for high LET radiation various obstacles have to be overcome:
1) It is rather difficult to irradiate polymer samples homogeneously with heavy ion beams because of the small beam diameter (only a few mm). Moreover, the range of heavy particles is generally very short.
2) The LET is a function of the particle energy. Fig.2 shows a graph depicting -dE/dx= f(E) for α-particles.

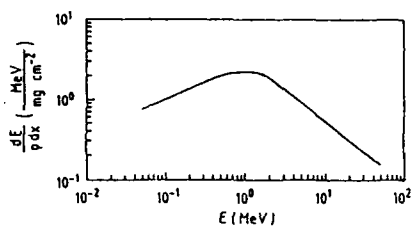

Fig.2. Stopping power - dE/dx vs. particle energy E. Absorption of α-particles in poly(methyl methacrylate)

Notably, -dE/dx increases and passes through a maximum with increasing E.
In a theoretical treatment by Chatterjee and Magee (1987) the track structure is characterized by two parameters, the "core radius" r_c and the" penumbra radius" r_p with $r_p > r_c$. $r_p - r_c$ is attributed to the volume surrounding the inner part of the track in which secondary electrons of relatively high energy, originating from the inner part, dissipate their energy. The inner part of the track is characterized by r_c. As has been outlined by Chatterjee and Magee (1987), the track structure varies with E. A typical calculation yielded that r_c and r_p vary with E in the following way: when E/nucleon decreases from 14 to 0.01 MeV/u, r_c decreases by at least one order of magnitude and r_p by at least three orders of magnitude. Consequently, the local density of primary acts and the local density of reactive intermediates should differ significantly, if identical particles differing in E but not in dE/dx are compared. With respect to Fig.2 this implies that differences in the nature of chemical products and/or differences in product yields might be observable if a polymer is irradiated with the same particle radiation (differing in E_o) at equal stopping power (corresponding to points at the curve on both sides of the maximum). In praxi, heavy particles are totally absorbed in the polymer specimen and the track structure will be subject to alterations up to the track end. Therefore, track structure effects can only be evidenced experimentally, if the thickness of the polymer film traversed by the ion beam is much smaller than the particle range. Up to now experiments covering the energy range on both sides of the maximum of the curve in Fig.2 have not been carried out systematically.
3) A very high fraction of the absorbed dose is converted into heat (more than 90 %), i.e., only a small fraction of the particle energy serves to initiate chemical reactions. This implies, that the local temperature can increases drastically, if the short range of the particles is taken into account. Therefore, due to the low heat conductivity of organic polymers, the sample temperature is not easily controllable during irradiation.

In the following some results obtained recently in the author's laboratory are reported (Klaumünzer and Schnabel (1988)). Thin films of three polymers (d: 20-35 μm) were irradiated with 275 MeV $^{20}_{10}Ne^{7+}$ and 180 MeV $^{40}_{18}Ar^{8+}$ ions: poly(2-chloroethyl methacrylate),PMCMA, polymethacrylonitrile, PMCN, and polystyrene, PSt. The influence of temperature increase on the radiation chemical behavior could be studied best with PMCMA. This polymer crosslinks when heated in vacuo to temperatures above 220°C. Upon irradiating PMCMA with 180 MeV Ar ions at absorbed doses exceeding 1.2×10^{21} eV/g an insoluble gel was formed indicating the occurrence of intermolecular crosslinking. However, upon irradiating PMCMA films coated on one side with a 0.25 μm thick gold layer, the films remained soluble and the average molar mass decreased with increasing absorbed dose. Obviously, the gold layer provided for a fast transport of heat. The scission yield could not be determined in this case because a GPC calibration curve was not available for this polymer. - G(S) was determined, however, in the case of PMCN. Values are presented in Table 3:

Table 3. Main-chain scission of polymethacrylonitrile induced by radiation of different stopping power (LET).

Radiation	-dE/dx (MeV/μm)	G(S)	References
^{60}Co-γ-rays	2×10^{-4}	3.3	Helbert et al.(1980)
X-rays (λ≈ 1 nm)	2×10^{-4}	3.6	Sotobayashi et al. (1984)
$^{20}_{10}Ne^{7+}$ (E_o = 275 MeV)	0.43	0.5	Klaumünzer, Schnabel (1988)
$^{40}_{18}Ar^{8+}$ (E_o = 180 MeV)	2.5	0.4	Klaumünzer, Schnabel (1988)

Table 3 shows that G(S) decreases with increasing stopping power.

Notably, in the case of PSt the 100 eV yield of crosslinking was found to be almost independent of LET. This can be seen from Table 4.

Table 4. Crosslinking of polystyrene induced by radiations of different stopping power (LET)

Radiation	-dE/dx (MeV/μm)	G(X)	References
^{60}Co-γ-rays	2×10^{-4}	0.05	O'Donnell et al.(1979)
$^{20}_{10}Ne^{7+}$ (E_o = 275 MeV)	0.37	0.05	Klaumünzer, Schnabel (1988)
$^{40}_{18}Ar^{8+}$ (E_o = 180 MeV)	2.26	0.03	Klaumünzer, Schnabel (1988)

In this connection it is notable that Calcagno et al.(1987) reported G(X)= 0.3 for irradiation of PSt with 100 keV He, 200 keV Ne and 400 keV Ar ions covering the LET range from 0.21 MeV/μm to 0.85 MeV/μm. It should be pointed out that the total stopping power, dE/dx, is 0.37 MeV/μm both for 275 MeV and 200 keV neon ions and that, therefore, the differences in G(X) found by the two groups could reflect a strong track structure effect, as discussed before. A strong dependence of G(X) on E was also reported recently by Aoki et al. (1988) for the irradiation of PSt with H^+ and He^+ ions. Also these authors interpret their results partly on the basis of a track structure effect. Actually, the beam intensity in the experiments with ions of relatively low energy was very high. Therefore, the possibility of a strong temperature increase in the polystyrene films during irradiation cannot be excluded. One should be careful, therefore, in arriving at final conclusions with respect to the track structure effect in this case.

4.X-RAY-INDUCED RADIATION EFFECTS IN LINEAR POLYMERS

A fascinating application regarding XL and CS applies to lithographic techniques for the production of microchips. Actually, polymers play a rather clandestine role here, since the final product does not contain polymer. Polymers are used, however, for protection of part of the wafer during processing. One of the important requirements on the polymer applies to (plasma) etch resistance , i.e. the polymer must be resistant against etching agents that are used to pattern the surface of the wafer. Therefore, appropriate polymers are denoted as "polymer resists". Lithographic techniques have to be rather sophisticated insofar as fine line structures of line width $\leq$ 0.3 μm must be generated in thin polymer films in order to produce 4 or 16 Mbit chips. To obtain fine line patterns of these dimensions, even deep UV radiation is insufficient. Quite appropriate are, however, electron beam radiation, generated by accelerators, and soft X-rays, provided by electron synchrotrons. For industrial large scale production only X-rays are applicable. In this case silicon wafers coated with a thin polymer film , about 1 μm thick, are irradiated through a finely structured mask. This way, the mask pattern is replicated in the polymer film. At present, liquid processing serves to develop the latent fine line pattern in the film.
In principle, positively working polymer resists are distinguished from negatively working ones depending on whether the exposed areas of the polymer film are rendered in the developer more soluble or less soluble than the unexposed areas. For many resist systems investigated during the last years crosslinking or main-chain scission were the essential radiation-induced chemical reactions giving rise to a decrease or increase in solubility, respectively. A major problem regarding the selection of appropriate polymers concerns the difficulty to combine high radiation sensitivity with high (plasma) etch resistance. One of the important criteria concerning the radiation sensitivity applies, of course, to the radiation chemical yields G(S) and G(X).
Investigations carried out in our laboratory with a positively working resist, polymethacrylonitrile , PMCN,

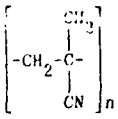

yielded that, apart from a high G(S) value, also the selection of appropriate development conditions is of great importance with respect to an improvement in the radiation sensitivity (Schlegel and Schnabel (1988)). The latter is defined here as the minimum exposure dose necessary to achieve full development of the latent line pattern in the polymer film. G(S)= 3.3 was found both for irradiations with ^{60}Co-γ-rays and soft X-rays ($\lambda_{inc} \approx 0.1$-$1.0$ nm), respectively.

In the case of positively working resists, the molar mass of the polymer should be reduced significantly, say, by a factor of 5, to attain a sufficiently large difference in solubility between irradiated and unirradiated areas of the polymer film. From eq.(10) it follows that the absorbed dose D_5, resulting in $(M_{w,o}/M_{w,D})= 5$, is

$$D_5 = \frac{800\ N_A}{G(S)\ M_{w.o}} \qquad (16)$$

According to eq.(16) D_5 is inversely proportional to the initial molar mass $M_{w,o}$ which implies that $M_{w,o}$ should be as high as the limitations, set by the processibility in spin-coating, allow.

In the case of PMCN it turned out, however, that the initial molar mass did not affect the radiation sensitivity to the extent expected from eq.(16). Much more important than the employment of a polymer sample of high initial molar mass was the selection of solvents capable of dissolving the irradiated polymer portions without swelling the unirradiated ones

Regarding the dissolution of amorphous polymers at temperatures below the glass transition ($T<T_g$) the following steps have to be discriminated:

(a) Solvation: penetration of solvent molecules into the pores of the rigid matrix.
(b) Relaxation: transition of the polymer from the glassy to the equilibrated state
(c) Reptation: disentanglement and diffusion of macromolecules towards regions of low polymer concentration
(d) Convection: transport of the macromolecules by the flowing solvent.

In order to generate fine line patterns of high quality the insoluble portions should remain in the glassy state during the development. The contrast between exposed and unexposed areas is determined by the ratio of the solvation rates $v_{s,D}/v_{s,o}$. This ratio is the higher the weaker the interaction is between polymer and solvent. Here, the Hansen parameter of solvents served as a measure for the strength of interaction during the selection of appropriate liquids. This way, cyclohexanone, acetophenone, benzonitrile and cyclopentanone were selected and it was found that the surface of PMCN films did not swell during development with these solvents. Solvation was the rate determining step. This explains, why, in the case of PMCN, the radiation sensitivity is only to some extent affected by the radiation-induced decrease in average molar mass. Actually, it is assumed that differences in the dissolution rates referring to irradiated and unirradiated areas are essentially due to an increase in the free volume of the glassy polymer which could be a consequence of the formation of micromolecular gaseous degradation products. This assumption was substantiated by the fact that the dissolution rate was proportional to the exposure dose.

Although high quality fine line patterns could be replicated with the aid of the solvents mentioned above, obstacles still existed with respect to rather long times of development combined with a partial dissolution of unexposed areas of the polymer film. These difficulties were overcome by selective pre-swelling of the unirradiated areas. For this purpose liquids were used that interact only very weakly with PMCM, for example methylpropylketone or diethylketone. These liquids are incapable of dissolving PMCN but are capable of penetrating into the film and transforming it thereby from the glassy to the relaxed state. Consequently, the subsequent development is significantly accelerated. In typical experiments, in which high quality fine line patterns of 0.3 μm line were obtained at an exposure dose of about 200 mJ/cm^2, the pre-swollen polymer films were developed for 2 minutes in a mixture of cyclohexanone/o-xylene/water at a weight ratio of 65/34/1.

From the results obtained in this work it can be concluded that, although the importance of a high yield of main-chain scission should not be neglected, the employment of proper development conditions is crucial for the generation of fine line patterns in polymers at relatively low exposure doses.

REFERENCES

Polymer Degradation

- B. Dolezel, " Die Beständigkeit von Kunststoffen und Gummi", Hanser, München (1978)
- W.Schnabel,"Polymer Degradation, Principles and Practical Applications", Hanser, München (1981)
- H.H.G.Jellinek, ed., Aspects of Degradation and Stabilization of Polymers", Elsevier, Amsterdam (1978)
- T.Kelen, "Polymer Degradation", Van Nostrand Reinhold Co., New York (1983)
- L.Reich and S.S.Stivala, "Elements of Polymer Degradation", McGraw-Hill, New York (1971)
- N.Grassie and G.Scott, "Polymer Degradation and Stabilization",Cambridge University Press, Cambridge (1985)

Photochemistry of Polymers

- W.Schnabel and J.Kiwi, Photodegradation", in H.H.G.Jellinek, ed., "Aspects of Degradation and Stabilization of Polymers", Elsevier,Amsterdam (1978)
- G.Geuskens, "Photo-degradation of Polymers", in C.H.Bamford and C.F.H.Tipper, eds., Elsevier (1975)
- J.F.McKellar and N.S.Allen, "Photochemistry of Man-Made Polymers", Applied Science Publ., London (1979)
- N.S.Allen, ed., "Developments in Polymer Photochemistry", Vol.1-3, Applied Science Publ., London (1980-1982)
- V.A.Shlyapintokh, "Photochemical Conversion and Stabilization of Polymers", Hanser, München (1984)
- J.Guillet, "Polymer Photophysics and Photochemistry" Cambridge University Press, Cambridge (1985)
- J..G.Eloosterboer, "Network Formation by Chain Crosslinking. Photopolymerization and its Applications in Electronics", Adv.Polym.Sci 84, 1 (1988)

Radiation Chemistry of Polymers

- W.Schnabel,"Degradation by High Energy Radiation", in H.H.G.Jellinek, ed., "Aspects of Degradation and Stabilization of Polymers", Elsevier, Amsterdam (1978)
- A.Makhlis, "Radiation Physics and Chemistry of Polymers", J.Wiley & Sons, New York (1975)
- M.Dole, ed., "The Radiation Chemistry of Macromolecules", Academic Press, New York (1972)
- A.Charlesby, "Atomic Radiation and Polymers", Pergamon Press, Oxford (1960)
- A.Chapiro, "Radiation Chemistry of Polymeric Systems", Interscience, New York (1962)

Reaction Mechanisms

- Q.Q.Zhu and W.Schnabel, Polym.Degrad.Stab. in print
- I.Popovic and W.Schnabel, Eur.Polym.J. submitted

LET Effects

- Y.Aoki, N.Kouchi, H.Shibata, S.Tagawa and Y.Tabata Nucl.Instr.Meth.Phys.Res. B33, 799 (1988)
- A. Chatterjee and J.L.Magee, in Farhataziz and M.A.J.Rodgers, eds., "Radiation Chemistry, Principles and Applications", *VHC Publ., Weinheim (1987), Chapters 1,5 and 6*
- L.Calcagno, G.Foti, A.Licciardello and O.Puglisi, Appl.Phys.Lett. 5,907 (1987).
- N.Helbert, G.Iafrate, C.U.Pittman and J.H.Lai, Polym.Eng.Sci.20, 1077 (1980)
- F.A.Makhlis, "Radiation Physics and Chemistry of Polymers", J.Wiley, New York (1975)
- J.H.O'Donnell, N.P.Rahman, C.A.Smith and D.J.Winzor, J.Polym.Sci., Polym.Chem.Ed. 17, 4081 (1979)
- W.W.Parkinson, C.D.Bopp and D.Binder, J.Phys.Chem. 69, 604 (1965)
- W.Schnabel, S.Klaumünzer, H.Sotobayashi, F.Asmussen and Y.Tabata, Macromolecules 17, 2108 (1984)
- W.Schnabel and S.Klaumünzer, Rad.Phys.Chem, in print
- K.Shinohara, A.Amemiya and A.Danno, J.Phys.Soc.Japan, 13, 604 (1958)
- H.Sotobayashi, F.Asmussen, Gunawan M.Angga, N.Abou-Samra, W.Schnabel and F.P.Wolf, BESSY, Anual Report, p.190 (1984)
- A.B.Zverev, Ya. Lavrentovich and A.M.Kabakhi, Khim.Vys.Energ. 3,453 (1969)

Lithography

- F.A.Vollenbroek, "Photoresist Systems for Microlithography", Adv.Polym.Sci. 84, 85 (1988)
- W.S.DeForest, "Photoresist, Material and Processes", McGraw-Hill, New York (1975)
- L.F.Thompson, C.G.Willson and M.J.Bowden, eds., "Introduction to Microlithography", ACS Symposium Series 219, Washington (1983)
- L.Schlegel and W.Schnabel, J.Vac.Sci.Techn.B 6, 82 (1988)
- L.Schlegel, " Zur Optimierung von Polymerresists für die Röntgenlithographie - Untersuchungen über Entwicklersysteme und Prozeßführung bei der Naßentwicklung", Dissertation, Technische Universität Berlin (1988)
- C.M.Hansen, "Three dimensional solubility paramater and solvent diffusion coefficient", Dänische Technische Presse, Kopenhagen (1967); J.Paint Technol. 39, 104 (1967); 39, 505 (1967)
- A.E.Novembre, L.M.Masakowski and M.A.Hartney, Proceed. Conf. on Photopolymers: Principles,Processes and Materials, Ellenville, October (1985)

DETERMINATION OF CROSS-LINK DENSITY IN AMORPHOUS NETWORKS BY STRESS-STRAIN-SWELLING EXPERIMENTS

Burak Erman
Polymer Research Center
Boğaziçi University
Bebek, 80815
İstanbul, Turkey

ABSTRACT. The degree of cross-linking in an amorphous elastomeric network is related to the shear modulus which may be determined either by stress-strain experiments or by equilibrium swelling measurements in a solvent. The value of the cross-link density determined in this manner depends on the molecular model used. In the present paper, the molecular constitution of affine and phantom models is reviewed in detail, followed by a discussion of the constrained junction model of real networks. Results of experiments are compared with predictions of the theory and an improved method of determining cross-link density is discussed.

1. INTRODUCTION

The determination of cross-link density by stress-strain experiments or by equilibrium swelling measurements is well-known and has been discussed in various books (1-3). The value of the cross-link density calculated in this manner depends on the molecular model chosen. The simplest and most commonly used molecular models are the affine network model of Wall and Flory (4), and the phantom network model of James and Guth (5,6). Experimental work on various aspects of rubbers since the dawn of these two theories has shown, however, that a network tested in the dry state conforms neither to the phantom nor to the affine model. Experiments in simple tension, in particular, show that the modulus of a network is closer to that of the affine model for small deformations, and approach to that of the phantom model with increasing strain. Similarly, the modulus of a network tested in the swollen state is not equal to that of the dry network, the former being significantly less than that of the latter.

Various improvements in the theory for understanding the strain dependence of the modulus of a network have been proposed after 1975. The original idea describing the decrease of the modulus upon stretching is given by Ronca and Allegra (7). According to the theory proposed by these authors, the constraints affecting the fluctuations of junctions are more effective at smaller strains and become progressively less important as extension increases. In a different approach, Deam and Edwards (8) have introduced the effect of topological entanglements into network behavior. The theory based on this paper was later presented in terms of the slip-link model (9,10) according to which the strength of entanglements surrounding a given network chain depends on the imposed macroscopic strain. According to this treatment, the small strain modulus shows contributions from entanglements trapped permanently into the network structure by cross-linking. Such effects are modelled by links joining different chains. At higher deformations, contributions from such entanglements vanish and the modulus becomes proportional to the number of chemical cross-links. The ideas proposed by Ronca and Allegra (7) have been put into a mathematically and physically more rigorous form by Flory (11). According to this model, which has subsequently been termed as the 'constrained junction model', the intermolecular constraints or entanglements acting at all points along the chains are assumed to be concentrated at the junctions. These constraints depend on strain and swelling. Their effects diminish with increasing strain and swelling, leading to a substantial decrease in the modulus at high extensions and/or swelling. Unlike the model presented by Edwards, trapped entanglements do not contribute to the small strain modulus in the constrained junction model (see sequel). The constrained junction model has later been improved (12,13) and quantitative agreement has been obtained between the predictions of the theory and results of stress-strain experiments on various elastomeric networks.

The molecular models cited in the preceding paragraph, as well as various extensions of these by various authors have been reviewed by Eichinger (14) without going into mathematical details. Discussion of various elasticity theories may also be found in the monograph by Mark and Erman (3).

All of the modern theories cited above indicate that a state of phantom-like network behavior is obtained at high degrees of extension and swelling. The phantom network model thus constitutes a convenient reference structure on which the behavior of real networks may be superposed.

In the present paper, the molecular constitution of a network is defined, followed by a discussion of the affine, phantom and constrained junction models. Predictions of the moduli of networks based on these models are compared with results of experiments and a method of estimating the correct cross-link density is suggested.

2. MOLECULAR CONSTITUTION OF A NETWORK

An amorphous elastomeric network consists of long flexible chains joined together to form a three dimensional solid structure. The chains are joined together by permanent chemical bonds either randomly located along their lengths or at specific locations. This method of joining the chains together is called cross-linking. Alternatively, the chains may be joined together only at their ends, called end-linking. The numbers of chains and junctions in the network are denoted by ν and μ, respectively. The functionality ϕ of a junction is defined as the number

of chains meeting at that junction. Some of the chains may be attached to only one junction. Such chains are called dangling chains and do not contribute to the elastic activity of the network. Similarly, a loop which is a chain starting and terminating at the same junction does not contribute to elastic activity of a network. A junction of functionality 2 does not contribute to the elastic activity of the network but causes only chain extension. A network in which there are no loops, dangling chains and $\phi \geq 3$ for all junctions is called a perfect network. The cycle rank ξ of a network is defined as the number of independent circuits, or the number of cuts required to reduce the connected structure to a tree. The cycle rank is a measure of the connectivity of a perfect as well as an imperfect network. The structure of networks is discussed in detail by Flory (15). For a perfect network, the parameters μ, ν, ϕ and ξ are related by two equations,

$$\mu = 2\nu/\phi$$
$$\xi = (1 - 2/\phi)\nu \qquad (1)$$

Denoting the average molecular weight of chains between junctions in a network by M_c, another expression may be written as

$$\xi/V_o = (1 - 2/\phi)\rho N_A/M_c \qquad (2)$$

where V_o is the volume of network during formation, ρ is the corresponding density and N_A is the Avogadro number. Modification of eqs 1 and 2 for imperfect networks requires further discussion which will not be undertaken in the present review. The reader may refer to references 1 and 3 and papers by Scanlan (16), Case (17) and Flory (18) for imperfect network.

As will be shown below, contributions to the modulus of a real network do not contain effects from dangling chains and loops. The experimentally obtained modulus is a direct measure of the cycle rank or of connectivity. Stress-strain-swelling experiments thus lead to information on the values of μ and ν of the perfect network only. Without further information from an independent source, stoichiometry for example, the numbers of inactive chains that do not participate in the elastic activity of the network cannot be estimated.

3. MACROSCOPIC DEFORMATION

The molecular theory of rubber elasticity requires proper use of the measure of macroscopic deformation. In this section the state of macroscopic deformation is outlined for the two widely employed experiments, i. the uniaxial (or simple) tension and ii. homogeneous swelling.

i. Simple Tension. Dimensions of a test specimen in the reference and deformed states are shown in Figure 1. L_o in Figure 1a indicates the length of the specimen in the reference state which may conveniently be taken as the state of formation of the network. In the case of network

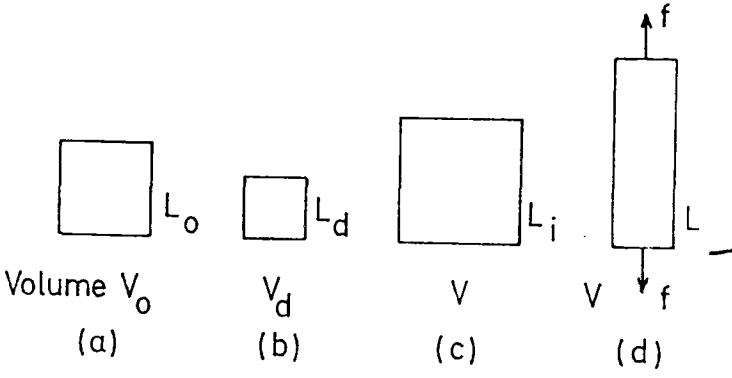

Figure 1. Dimensions of a test specimen in simple (uniaxial) tension. (a) The specimen in the state of formation, which may be taken as reference stress-free state. L_o and V_o are the reference length and volume, respectively. (b) The dry state of the network, L_d and V_d denoting the dry length and volume, respectively. (c) The initial swollen state of the network. For experiments in the swollen state, the network is swollen with a sufficiently nonvolatile solvent and stretched in air. V is the volume of network at the start of the experiment, which is assumed to be constant during stretching. L_i is the initial swollen but undistorted length. (d) The length L obtained under the uniaxial force f.

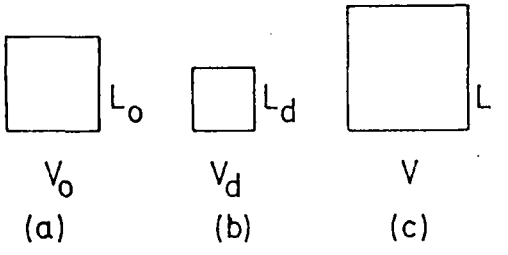

Figure 2. Dimension of the network in swelling experiments. (a) The state of the network during formation. V_o is the stress-free reference volume. (b) The dry state, represented by the volume V_d of the dry bulk network. (c) The final swollen volume V.

formation in the presence of a solvent, the total volume V_o of the network is comprised of the volumes V_s of solvent and V_d of the dry polymer. Figure 1b shows the length L_d of the dry network of volume V_d. Figure 1c depicts the dimensions of the network which has subsequently been swollen with a suitable (sufficiently nonvolatile) solvent. In this case the length has changed to L_i. This is the state of the network at the start of the experiment. The subscript i refers to the initial state where the volume is V. The change of dimensions from Figure 1a to 1b to 1c are isotropic. If the simple tension experiment is to be performed in the unswollen state, then $L_i = L_d$. Figure 1d depicts the final shape with length L obtained under a force f along the x-direction. The experiment is performed in air or preferably in an inert atmosphere. The volume change is negligibly small during stretching. The final volume in the stretched state may therefore be identified with the volume V of the swollen undistorted state. The volume fraction v_{2o} of polymer during the formation of network is defined as

$$v_{2o} = V_d/V_o = (L_d/L_o)^3 \tag{3}$$

Once the network is formed, v_{2o} is fixed. The volume fraction of polymer v_2 during the experiment is defined as

$$v_2 = V_d/V = (L_d/L_i)^3 \tag{4}$$

v_2 may be changed by removing or adding solvent into the network prior to extension. Constant v_2 data for the stress-strain relations requires the use of a sufficiently nonvolatile solvent. Homogeneous diffusion of the solvent into the network before the stress-strain experiment is required.

The deformation gradient tensor $\underset{\sim}{\lambda}$ for the simple tension shown in Figure 1d is given by

$$\underset{\sim}{\lambda} = \begin{vmatrix} \lambda_x & & \\ & \lambda_y & \\ & & \lambda_z \end{vmatrix} = \begin{vmatrix} L_x/L_{ox} & & \\ & L_y/L_{oy} & \\ & & L_z/L_{oz} \end{vmatrix} \tag{5}$$

where L_x, L_y and L_z are the dimensions of the sample in the deformed state along the x, y and z directions, respectively. L_{ox}, L_{oy} and L_{oz} are the corresponding components in the reference state. Components of the deformation gradient tensor defined in this manner thus relate the final dimensions of the sample to its dimensions in the state of formation. Another measure of deformation, the extension $\underset{\sim}{\alpha}$, is defined as

$$\underset{\sim}{\alpha} = \begin{vmatrix} \alpha_x & & \\ & \alpha_y & \\ & & \alpha_z \end{vmatrix} = \begin{vmatrix} L_x/L_{ix} & & \\ & L_y/L_{iy} & \\ & & L_z/L_{iz} \end{vmatrix} \tag{6}$$

where L_{ix}, L_{iy} and L_{iz} are the dimensions in the swollen but undistorted state of the network. Experimental data are reported, in general, in terms of the components of $\underset{\sim}{\alpha}$. Using eqs 3 and 4, the i th component λ_i may be related to α_i as

$$\lambda_i = (v_{2o}/v_2)^{1/3}\alpha_i \tag{7}$$

Using the definitons for $\underset{\sim}{\lambda}$ and $\underset{\sim}{\alpha}$, the following identities are obtained

$$\begin{aligned} \lambda_x\lambda_y\lambda_z &= V/V_o = (v_{2o}/v_2) \\ \alpha_x\alpha_y\alpha_z &= 1 \end{aligned} \tag{8}$$

For uniaxial tension along the x direction, letting $\lambda_x = \lambda$ and $\alpha_x = \alpha$, one obtains

$$\underset{\sim}{\lambda} = \begin{vmatrix} \lambda & & \\ & (v_{2o}/v_2)^{1/2}\lambda^{-1/2} & \\ & & (v_{2o}/v_2)^{1/2}\lambda^{-1/2} \end{vmatrix} \tag{9}$$

$$= (v_{2o}/v_2)^{1/3} \begin{vmatrix} \alpha & & \\ & \alpha^{-1/2} & \\ & & \alpha^{-1/2} \end{vmatrix}$$

ii. Swelling. The dimensions of a sample during formation and in the swollen state are shown in Figure 2. Figure 2a depicts the volume V_o during formation. Figure 2b is the dry state and Figure 2c corresponds to the final swollen state of volume V. Inasmuch as isotropic swelling does not produce distortion of the sample, components of $\underset{\sim}{\alpha}$ equate to unity by definition and one obtains from eq 9,

$$\underset{\sim}{\lambda} = \begin{vmatrix} (v_{2o}/v_2)^{1/3} & & \\ & (v_{2o}/v_2)^{1/3} & \\ & & (v_{2o}/v_2)^{1/3} \end{vmatrix} \tag{10}$$

4. MICROSCOPIC DEFORMATION

The state of macroscopic deformation in a homogeneously deformed network may be determined unambiguously by measuring the macroscopic dimensions before and after the application of the strain. The microscopic state of deformation, on the other hand, requires averaging over all the chains of the network before and after deformation. The mean-

squared end-to-end chain length $\langle r^2\rangle_o$ between junctions averaged over all chains of the network in the reference state denoted by the subscript zero is assumed to be equal to the mean squared end-to-end distance of a single chain in the unperturbed state. Inasmuch as network formation is carried out in the isotropic state, the x, y and z components of $\langle r^2\rangle_o$ are equal and

$$\langle x^2\rangle_o = \langle y^2\rangle_o = \langle z^2\rangle_o = \langle r^2\rangle_o/3 \tag{11}$$

In the deformed state, the components $\langle x^2\rangle$, $\langle y^2\rangle$ and $\langle z^2\rangle$ change anisotropically, and the microscopic state of deformation may be defined in the mean-squared sense by the diagonal tensor

$$\underset{\sim}{\Lambda}^2 = \begin{vmatrix} \Lambda_x^2 & & \\ & \Lambda_y^2 & \\ & & \Lambda_z^2 \end{vmatrix} = \begin{vmatrix} \langle x^2\rangle/\langle x^2\rangle_o & & \\ & \langle y^2\rangle/\langle y^2\rangle_o & \\ & & \langle z^2\rangle/\langle z^2\rangle_o \end{vmatrix} \tag{12}$$

The relationship of the components of microscopic deformation tensor to the components of the macroscopic deformation requires a molecular model as will be described below.

5. THE ELASTIC FREE ENERGY OF THE SINGLE CHAIN AND THE NETWORK

The length of chains between cross-links in a typical network are sufficiently long to be considered Gaussian. Calculations by the rotational isomeric state sheme (19) indicate that the end-to-end chain vector distribution becomes approximately Gaussian for sufficiently flexible chains with more than 40-60 repeat units. Inasmuch as chains in a typical network are longer, they may satisfactorily be represented by the Gaussian distribution

$$W(r) = (3/2\pi\langle r^2\rangle_o)^{3/2}\exp(-3r^2/2\langle r^2\rangle_o) \tag{13}$$

where $W(r)$ is the distribution of the end-to-end vector, $\underset{\sim}{r}$, and $\langle r^2\rangle_o$ is the mean-squared unperturbed value for the same chain. The elastic free energy A_{el} of the single chain whose ends are kept at a fixed distance r is given as (19)

$$\begin{aligned} A_{el} &= -kT\ \ln W(r) \\ &= C(T) + (3kT/2\langle r^2\rangle_o)r^2 \end{aligned} \tag{14}$$

where k is the Boltzmann constant, T is the temperature and the second line is obtained by substitution from eq 13. $C(T)$ is a function of temperature. The average force f required to keep the chain ends at the fixed separation r is obtained from thermodynamics as

$$\begin{aligned} f &= \partial A_{el}/\partial r \\ &= (3kT/\langle r^2\rangle_o)r \end{aligned} \tag{15}$$

where the second line is obtained by substituting from eq 14. The term in parenthesis in eq 15 may be interpreted as a spring constant. Thus eq 15 shows that a Gaussian chain behaves as a linear spring.

The fundamental assumption of both the affine and phantom network models is that the total elastic free energy of a network is equal to the simple sum of the free energies of the constituent chains. Thus the elastic free energy ΔA_{el} of the network relative to the reference state is obtained by summing the free energies of the single chains as

$$\begin{aligned} \Delta A_{el} &= \sum_\nu (3kT/2\langle r^2\rangle_o)r^2 - (A_{el})_o \\ &= \frac{3\nu kT}{2}\left(\frac{\langle r^2\rangle}{\langle r^2\rangle_o} - 1\right) \\ &= \frac{\nu kT}{2}\left(\frac{\langle x^2\rangle}{\langle x^2\rangle_o} + \frac{\langle y^2\rangle}{\langle y^2\rangle_o} + \frac{\langle z^2\rangle}{\langle z^2\rangle_o} - 3\right) \end{aligned} \tag{16}$$

Equation 16 is the starting point of the phantom and affine models. The third of eq 16 represents the elastic free energy of the network in terms of the components of the molecular deformation tensor $\underset{\sim}{\Lambda}^2$ defined by eq 12. For the complete formulation of the problem, the relationship of the components of $\underset{\sim}{\Lambda}^2$ to the macroscopic state of deformation has to be known. The form of this relationship depends on the molecular model chosen. The affine and the phantom models to be treated below are the two models that lead to simple expressions for ΔA_{el}.

6. THE AFFINE NETWORK MODEL

The affine network model assumes that the junction points are rigidly embedded in the medium, thus performing affine displacements with macroscopic strain. The components $\langle x^2\rangle$, $\langle y^2\rangle$ and $\langle z^2\rangle$ in the deformed state are related to those in the undeformed state as

$$\langle x^2\rangle = \lambda_x^2\langle x^2\rangle_o\ ,\ \langle y^2\rangle = \lambda_y^2\langle y^2\rangle_o\ ,\ \langle z^2\rangle = \lambda_z^2\langle z^2\rangle_o \tag{17}$$

Substituting these expressions into eq 16 then leads to the elastic free energy of the network as

$$\Delta A_{el} = \frac{\nu kT}{2}(\lambda_x^2 + \lambda_y^2 + \lambda_z^2 - 3) \tag{18}$$

A more general derivation of the affine network elastic energy by Flory (1) contains an additional logarithmic term that results from the distribution of cross-links over the sample volume. Thus the more complete elastic energy reads as

$$\Delta A_{el} = \frac{\nu kT}{2}(\lambda_x^2 + \lambda_y^2 + \lambda_z^2 - 3) - \mu kT \ln(V/V_o) \qquad (19)$$

The last term vanishes for a network whose final volume equals to that of the reference state.

7. THE PHANTOM NETWORK MODEL

In the phantom network model picture of James and Guth (5,6), the instantaneous values of end-to-end vectors for each chain may be written as the sum of a mean chain vector and fluctuation from it as

$$\begin{aligned} x_i &= \bar{x}_i + \Delta x_i \\ y_i &= \bar{y}_i + \Delta y_i \\ z_i &= \bar{z}_i + \Delta z_i \end{aligned} \qquad (20)$$

Here, the subscript i denotes the i th chain and x_i, y_i, z_i are the three components for the i th chain $\bar{x}_i$, $\bar{y}_i$, $\bar{z}_i$ and Δx_i, Δy_i, Δz_i denote the mean values and fluctuations from these means, respectively.

According to the phantom network model, mean chain vectors transform affinely with macroscopic deformation. The fluctuations, however, are not affected by macroscopic deformation. Thus eq 20 may be written in terms of undeformed values as

$$\begin{aligned} x_i &= \lambda_x \bar{x}_{i,o} + \Delta x_{i,o} \\ y_i &= \lambda_y \bar{y}_{i,o} + \Delta y_{i,o} \\ z_i &= \lambda_z \bar{z}_{i,o} + \Delta z_{i,o} \end{aligned} \qquad (21)$$

The subscript zero in eq 21 denotes the undeformed state. Squaring both sides of eqs 21 and taking the ensemble average, one obtains

$$\begin{aligned} \langle x^2 \rangle &= \lambda_x^2 \langle \bar{x}^2 \rangle + \langle (\Delta x)^2 \rangle \\ \langle y^2 \rangle &= \lambda_y^2 \langle \bar{y}^2 \rangle + \langle (\Delta y)^2 \rangle \\ \langle z^2 \rangle &= \lambda_z^2 \langle \bar{z}^2 \rangle + \langle (\Delta z)^2 \rangle \end{aligned} \qquad (22)$$

where the angular brackets denote an average over all the chains. The mean-squared values $\langle \bar{x}^2 \rangle$, etc. and fluctuations $\langle (\Delta x)^2 \rangle$, etc. are related to the chain vector components, $\langle x^2 \rangle$, etc. by the following relations (see, for example, reference 3 and the further reference cited therein)

$$\begin{aligned} \langle \bar{x}^2 \rangle_o &= (1 - 2/\phi)\langle x^2 \rangle_o \\ \langle \bar{y}^2 \rangle_o &= (1 - 2/\phi)\langle y^2 \rangle_o \\ \langle \bar{z}^2 \rangle_o &= (1 - 2/\phi)\langle z^2 \rangle_o \end{aligned} \qquad (23)$$

$$\begin{aligned} \langle (\Delta x)^2 \rangle_o &= (2/\phi)\langle x^2 \rangle_o \\ \langle (\Delta y)^2 \rangle_o &= (2/\phi)\langle y^2 \rangle_o \\ \langle (\Delta z)^2 \rangle_o &= (2/\phi)\langle z^2 \rangle_o \end{aligned} \qquad (24)$$

Substituting eqs 23 and 24 into eq 22 leads to the components of molecular deformation tensor as

$$\begin{aligned} \Lambda_x^2 &= \langle x^2 \rangle / \langle x^2 \rangle_o = (1 - 2/\phi)\lambda_x^2 + 2/\phi \\ \Lambda_y^2 &= \langle y^2 \rangle / \langle y^2 \rangle_o = (1 - 2/\phi)\lambda_y^2 + 2/\phi \\ \Lambda_z^2 &= \langle z^2 \rangle / \langle z^2 \rangle_o = (1 - 2/\phi)\lambda_z^2 + 2/\phi \end{aligned} \qquad (25)$$

Substituting eq 25 into eq 16 then leads to the elastic free energy of the phantom network as

$$\begin{aligned} \Delta A_{el} &= \frac{\nu kT}{2}(1 - 2/\phi)(\lambda_x^2 + \lambda_y^2 + \lambda_z^2 - 3) \\ &= \frac{\xi kT}{2}(\lambda_x^2 + \lambda_y^2 + \lambda_z^2 - 3) \end{aligned} \qquad (26)$$

The last of eq 26 is obtained by substituting for the cycle rank from eq 1.

8. STRESS-STRAIN RELATIONS FOR THE PHANTOM AND AFFINE NETWORK MODELS IN SIMPLE TENSION

Equations 18 and 26 may be written in compact form as

$$\Delta A_{el} = F kT(\lambda_x^2 + \lambda_y^2 + \lambda_z^2 - 3) \qquad (27)$$

where F equates to $\nu/2$ for the affine network model and to $\xi/2$ for the phantom network model. For uniaxial tension, eq 27 takes the following form

$$\Delta A_{el} = F kT(v_{2o}/v_2)^{2/3}(\alpha^2 + 2\alpha^{-1} - 3) \qquad (28)$$

The relationship of the force f along the x direction to ΔA_{el} is given (1) by thermodynamics as

$$\begin{aligned} f &= \partial \Delta A_{el}/\partial L \\ &= \partial \Delta A_{el}/L_{x,i}\partial\alpha \end{aligned} \qquad (29)$$

where $L_{x,i}$ denotes the length of the test specimen in the initial state. Using eq 28 in eq 29 leads to

$$f = 2\left(\frac{\mathcal{F}kT}{L_{x,i}}\right)(v_{20}/v_2)^{2/3}(\alpha - \alpha^{-2}) \qquad (30)$$

Experimental data is in general given in terms of the reduced force $[f^*]$ defined as

$$[f^*] = f\, v_2^{1/3}/A_d(\alpha - \alpha^{-2}) \qquad (31)$$

Here, A_d represents the dry cross-sectional area of the network. Defined in this manner, the reduced force equates to the shear modulus of the dry network for small strains. Substituting eq 30 into 31 leads to

$$[f^*] = 2\left(\frac{\mathcal{F}kT}{V_d}\right)v_{20}^{2/3} \qquad (32)$$

According to eq 32, the reduced force is independent of the degree of deformation. In Figure 3, the reduced force for the phantom and affine networks are shown by the lower and the upper horizontal dashed lines respectively. The points denote results on natural rubber networks (20) tested in tension at various degrees of swelling. The reduced force is clearly seen to decrease with swelling. It is also seen that the reduced force becomes, for this network, to be independent of deformation at a v_2 value of 0.24. The dependence of the natural rubber network on swelling as depicted in Figure 3 is in fact a universal phenomenon for amorphous networks in general (3). The reduced force becomes less dependent on strain upon swelling and becomes approximately independent of swelling at high degrees of dilution. The value of the reduced force at such high dilution equates to that of the phantom network as shown by the lowermost dashed line in Figure 3. The validity of this statement have now been shown by several experimental data on model networks of well known structure (3). At this limit, the reduced force is obtained from eq 32 with $\mathcal{F} = \xi/2$ as

$$[f^*] = (\xi kT/V_d)v_{20}^{2/3} \qquad (33)$$

Determination of $[f^*]$ from experimental data thus establishes the value of the cycle rank ξ for the network, which is also related to cross-link density μ/V_d and to molecular weight M_c of chains between cross-links as (3)

$$[f^*] = (\phi/2 - 1)\frac{\mu}{V_d}kT\, v_{20}^{2/3} = (1 - 2/\phi)\frac{\rho RT}{M_c} \qquad (34)$$

Here, ρ is the density of the bulk polymer and R is the gas constant.

The above discussion illustrates the determination of cross-link density from mechanical data on highly swollen networks. Equations 34

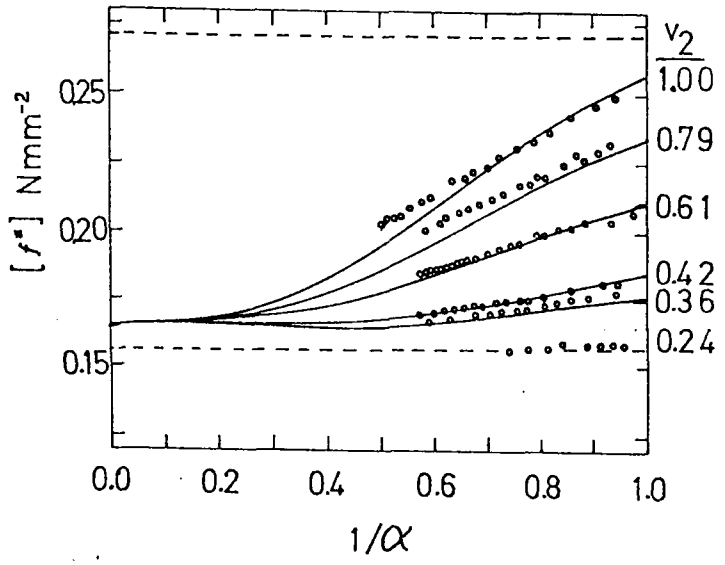

Figure 3. Results of simple tension experiments on natural rubber, from Reference 20. The ordinate represents the reduced force and the abscissa is the reciprocal extension, α^{-1}. The points represent experimental data. Curves are obtained by the constrained junction theory (From Reference 13). Data points are obtained at various degrees of swelling v_2 shown on the right ordinate for each curve. The upper and lower dashed horizontal lines represent the affine and phantom network behavior. The value of the κ parameter used in obtaining the theoretical curves was 8.

are valid for perfect networks only. Their extension to imperfect networks is discussed in some detail in Reference 3.

The curves indicated by solid lines in Figure 3 are obtained by the constrained junction theory (11-13) described in more detail in the following section.

9. THE CONSTRAINED JUNCTION THEORY OF NETWORKS

Experimental data shown in Figure 3 for the dry state and also for smaller degrees of swelling indicate significant departures from the phantom network behavior shown by the lowest horizontal line. One universal nature of these curves is that their extrapolation to $\alpha^{-1} = 0$ leads, approximately, to the phantom network modulus. Thus, performing stress-strain experiments in the dry state and extrapolating $[f^*]$ values to $\alpha^{-1} = 0$ by a straight line is another way of determining the degree of cross-linking. This technique corresponds to determination of cross-link density by the use of the Mooney-Rivlin plot which is discussed in large detail in Reference 21. The relationship of the small-strain modulus to network constitution is not understood well, however. We may conclude for the time being that the determination of cross-link density by measuring the phantom network modulus described above is the only established technique.

The theory based on the constrained junction model of networks by Flory is helpful in describing the behavior of networks in the dry state at all levels of deformation. According to this model, the junctions in a real network do not fluctuate freely as they do in the phantom network because of the effect of entanglements present in the real network. The strength of constraints limiting the fluctuations of junctions in real networks is described by a parameter, designated as κ by Flory (11). If there are no constraints, $\kappa = 0$ and the phantom network is obtained. The value of κ increases with increasing degree of constraints. At the other extreme, if the constraints are infinitely strong, the fluctuations of junctions are totally supressed and κ equates to infinity. In this limit the junctions are rigidly embedded in the network, corresponding to the affine network model. Calculations of the reduced force based on this model agree well with experimental data as shown in Figure 3. The constrained junction model thus describes the source of the deviations of real network behavior from that of the phantom networks model. The solid curves that pass through experimental points in Figure 3 are obtained by the constrained junction theory. The value of the κ parameter is chosen as 8 for best fit to all sets of data points at different swelling degrees (A second less important parameter of the theory, ζ, is chosen as 0.12 in the curve fitting. This parameter is not essential for the theory but is introduced to obtaind quantitative agreement with experimental data. The reader is referred to reference 12 and 13 for a detailed discussion of the complete theory).

The constrained junction theory thus completes the gap between the affine and the phantom network formulations. Inasmuch as real networks exhibit properties between affine and phantom networks, the constrained junction model seems to be a satisfactory description.

10. DETERMINATION OF THE DEGREE OF CROSS-LINKING BY EQUILIBRIUM SWELLING MEASUREMENTS

When a network is exposed to the continuous action of a solvent, it swells until equilibrium is reached between the swelling action of the solvent and the elasticity of the network. The volume fraction of polymer in the network swollen to equilibrium is designated by v_{2m}. The phenomenon of swelling of networks immersed in solvents is discussed in the book of Flory (1). However, the formulation there is based on the affine network model. The shortcomings of the affine network model have since been well established (3). The network behaves very close to the phantom network, especially at the high degrees of dilution obtained in the swelling experiment. The formulation based on the affine network model has therefore to be modified to that of the phantom model. The condition that determines the equilibrium degree of swelling of the network is that the chemical potential of the solvent in the network should equate to that in the surrounding pure solvent. This condition leads to the following expression for the phantom network:

$$\Delta\mu_1/RT = \ln(1 - v_{2m}) + \chi v_{2m}^2 + v_{2m} + (V_1/RT)(\xi kT/V_o)(v_{2m}/v_{20})^{1/3} = 0 \qquad (35)$$

Here, $\Delta\mu_1$ is the solvent chemical potential, χ is the Flory-Huggings interaction parameter, V_1 is the molar volume of solvent and V_o is the volume of network in the state of cross-linking. Measurement of v_{2m} in an equilibrium swelling experiment for known values of χ, V_1, T, and v_{20} thus leads to the evaluation of the cycle rank density ξ/V_o from eq 35. This value of ξ/V_o may then be used to estimate the degree of cross-linking of the network. Values of cross-link density obtained from swelling data based on the phantom network model are in general less than those obtained from the affine model. Values of ξ/V_o obtained from equilibrium swelling measurements are in general in good agreement with those obtained by mechanical experiments discussed in the preceding sections.

11. NUMERICAL EXAMPLE OF CROSS-LINK DENSITY CALCULATION

In this section, a numerical example for determining the cross-link density from stress-strain-swelling data will be worked out using the data given in Figure 3 for natural rubber.

The lower horizontal dashed line, representing the phantom network behavior, has an $[f^*]$ intercept of 0.155 N mm^{-2}. The natural rubber networks of this example were cross-linked in the dry state, and had a functionality of 4. Thus the $[f^*]$ intercept may be related to μ and M_c by the expressions

$$[f^*] = 0.155 \text{ N mm}^{-2}$$

$$= (\mu/V_d)kT \qquad (36)$$

$$= \rho RT/2M_c$$

Taking k as 1.381×10^{-20} N mmK^{-1} and T as 300 K, the cross-link density may be obtained from the first and second lines of eq 36 as

$$\mu/V_d = 1.12 \times 10^{19} \text{ cross-links/mm}^3$$

$$= 6.31 \times 10^{-8} \text{ mols of chains/mm}^{-3}$$

Taking $\rho = 0.97$ g cm^{-3}, the average molecular weight M_c between cross-links follows from the first and third lines of eq 36 as

$$M_c = 7800 \text{ g mol}^{-1}$$

The values of μ/V_d and M_c would also follow by extrapolating the data points for $[f^*]$ for the dry network to $\alpha^{-1} = 0$ by a straight line. This operation leads to an $[f^*]$ intercept of 0.15 N mm^{-2}. This value is only 3% less than that obtained from the highly swollen data points.

The value of M_c may also be obtained by equilibrium swelling measurements, by solving eq 35 for M_c as

$$M_c = -\frac{\rho(1 - 2/\phi)V_1 v_{2c}^{2/3} v_{2m}^{1/3}}{\ln(1 - v_{2m}) + \chi v_{2m}^2 + v_{2m}} \qquad (37)$$

Assuming that the solvent in which the network was swollen to equilibrium is benzene with $V_1 = 88$ cm^{3}mol^{-1} and $\chi = 0.44$, a value of $v_{2m} = 0.157$ would lead to $M_c = 7800$ g mol^{-1}.

12. DEVIATIONS FROM IDEAL NETWORK BEHAVIOR

The network model presented in this brief review is based on Gaussian chains. The value of the phantom modulus obtained as $\xi kT/V_o$ thus reflects the properties of networks comprised of such chains. In technological applications, however, behavior of networks deviates from the ideal phantom like behavior in many respects. The most important contribution to modulus in actual networks is due to the presence of fillers such as carbon black, silica, etc. Presently there is no study that relates the amount of fillers to deviations from phantom modulus. Presence of crystallites is a second source of contribution to the modulus. Performing the readings before reaching equilibrium conditions also leads to values of moduli higher than those obtained from equilibrium measurements. Measurements performed at temperatures close to the glass transition temperature of the network lead to significantly higher moduli values if performed relatively rapidly. Finally, the presence of very short chains in the network leads to a large modulus due to the effect of finite chain extensibility. This effect is not taken into consideration neither in the phantom nor the constrained junction models.

The magnitude of deviations from phantom-like behavior cited in the above paragraph are often very important and may be several times that of the phantom network itself. For this reason, the constitution and the state of the networks should be carefully specified as to the presence of fillers, crystallites, short chains, etc., and care should be exercised in performing the experiments at equilibrium conditions.

13. CONCLUSIONS AND DISCUSSION

The present study emphasizes that the behavior of networks in the highly swollen state resembles that of a phantom network model. The latter model is well understood. Identifying the highly swollen network by the phantom network thus establishes the degree of cross-linking in a straight forward manner. Alternatively, experiments performed on dry networks require extrapolation of data to high extension ratios, where the mechanical modulus becomes close to that of the phantom network model.

The small strain modulus of dry networks does not relate to the degree of cross-linking and should not be adopted for a measure of cross-link density.

Equilibrium swelling measurements lead to cross-link values close to those obtained by mechanical data. However, care should be taken to use eq 35 for this purpose. This equation is based on the phantom network model rather than the incorrect affine network model of previous treatments.

Resemblance of real network behavior to that of the phantom network model in the highly swollen state is established also by neutron scattering experiments. According to these experiments, the directly observed chain dimensions in the swollen deformed network transform close to that calculated from the phantom network model (22). This important observation makes the identification of the swollen network behavior with that of the phantom network more plausible.

REFERENCES

1. Flory, P.J. *"Principles of Polymer Chemistry"*, Cornell University Press, Ithaca, New York, 1953.

2. Treloar, L.R.G. *"The Physics of Rubber Elasticity"*, 3rd ed., Clarendon Press, Oxford, 1975.

3. Mark, J.E. and Erman, B. *"Rubberlike Elasticity: A Molecular Primer"* Wiley, New York, 1988.

4. Wall, F.T. and Flory, P.J. *J. Chem. Phys., 19*, 1435 (1951).

5. James, H.M. *J. Chem. Phys., 15*, 651 (1947).

6. James, H.M. and Guth, E. *J. Chem. Phys., 15*, 669 (1947).

7. Ronca, G. and Allegra, C. *J. Chem. Phys., 63*, 4990 (1975).

8. Deam, R.T. and Edwards, S.F. *Philos. Trans. R. Soc. London, 280*, 317 (1976).

9. Ball, R.C., Doi, M., Edwards, S.F. and Warner, M. *Polymer, 22*, 1010 (1981).

10. Edwards, S.F. and Vilgis, T. *Polymer, 27*, 483 (1986).

11. Flory, P.J. *J. Chem. Phys., 66*, 5720 (1977).

12. Flory, P.J. and Erman, B. *Macromolecules, 15*, 800 (1982).

13. Erman, B. and Flory, P.J. *Macromolecules, 15*, 806 (1982).

14. Eichinger, B.E. *Annu. Rev. Phys. Chem., 34*, 359 (1983).

15. Flory, P.J. *Proc. R. Soc. Lond. A., 351*, 351 (1976).

16. Scanlan, J. *J. Polym. Sci., 43*, 501 (1960).

17. Case, L.C. *J. Polym. Sci., 45*, 397 (1960).

18. Flory, P.J. *Macromolecules, 15*, 99 (1982).

19. Flory, P.J. *"Statistical Mechanics of Chain Molecules"*, Wiley-Interscience, New York, 1969.

20. Allen, G., Kirkham, M.J., Padget, J., and Price, C. *Trans. Faraday Soc., 67*, 1278 (1971).

21. Mark, J.E. *Rubber Chem. Technol., 48*, 495 (1975).

22. Bastide, J., Duplessix, R., Picot, C., and Candau, S. *Macromolecules, 17*, 83 (1984).

THERMALLY STIMULATED DISCHARGE AND DIELECTRIC MEASUREMENTS OF CURE IN RESINS AND GELLED MATERIALS

RICHARD A. PETHRICK
Department of Pure and Applied Chemistry
University of Strathclyde
Cathedral Street,
Glasgow G1 1XL

INTRODUCTION

Network formation leads to a modification of both the short and long range relaxation properties of the matrix. Dipole relaxation will be dominated by the reorientational relaxation of polar elements of the polymer network structure. In a small molecule, dipole reorientation occurs at high frequency and is associated with the structural relaxation process of the fluid. In theory, the randomization of the dipole should occur via all angles, however, even in the case of small molecules, the interactions with neighbouring molecules restrict this process. In a low molecular weight polymeric species, the relaxation of the dipole can occur via a process which is analogous to that observed in small molecules and involves overall rotation of the whole molecule. As the molecular mass is increased to the local viscosity of the fluid rises and the net result is a slowing down of the rotational motion. The process observed in the low molecular species is similar to the first normal mode relaxation process, discussed in the chapter on ultrasonics and viscoelastics. The relaxation time is directly related to the end to end distance and hence to the root of the molecular mass. Increase of the molecular weight causes a decrease of the relaxation frequency. The dipole relaxation leads to a frequency dependence of the complex permittivity of the media * which can be written as

$$(\epsilon)^* = (\epsilon)' + i(\epsilon)'' \qquad (1)$$

where (ϵ)' and (ϵ)'' are respectively the real and imaginary parts of the permittivity and are often referred to as the dielectric constant and loss. The width of the loss peak is a measure of the correlation of the relaxation of one dipole with another. A highly correlated process will exhibit a broad relaxation feature, whereas an weakly correlated dipolar relaxation process will approximate to the ideal Debye process. Alternatively, the occurance of several relaxation processes which have slightly different activation energies or pre-exponential factors can also lead to the observation of a broad relaxation process. The analysis of the curves in terms of distribution parameters has been made by Cole and Cole, Cole and Davidson and Havryliak and Negami.

The former of the three types of equation are presented below:

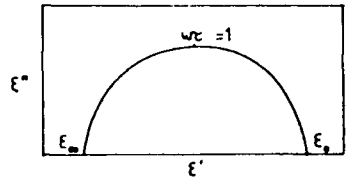

The Cole-Cole equation introduces a constant α.

$$\epsilon^*(\omega) = \epsilon_\infty + (\Delta E)/(1+(i\omega\tau)^\alpha)$$

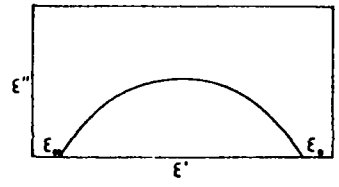

The Cole-Davidson equation introduces a constant β.

$$\epsilon^*(\omega) = \epsilon_\infty + (\Delta E)/(1+i\omega\tau)^\beta$$

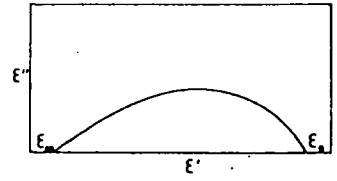

The Havriliak-Negami equation combines these two equations.

$$\epsilon^*(\omega) = \epsilon_\infty + (\Delta E)/(1+(i\omega\tau)^\alpha)^\beta$$

An alternative approach has been proposed by Williams based on the concept of correlation theory and this leads to the conclusion that the relaxation spectrum is a composite of self and auto correlation functions. The self correlation function is the mathematical representation of the memory of a dipole of its original position $\mu(1).\mu(1)$, whereas the auto correlation function is a correlation of the dipole with that of its neighbours,$\mu(i).\mu(j)$. It is not appropriate to develop the theory of dielectric relaxation in this article, however like ultrasonics and viscoelastics it is sensitive to both local and longer range dipolar motions.

Molecular Weight Effects If we compare the relaxation frequencies of narrow molecular weight samples of polyethyleneoxide, we observe for low molecular weight materials a very fast relaxation which is dependent on the end-to-end distance of the polymer coil, figure (2). As the molecular weight is increased the frequency decreases until above a certain molecular weight it becomes independent of molecular weight.

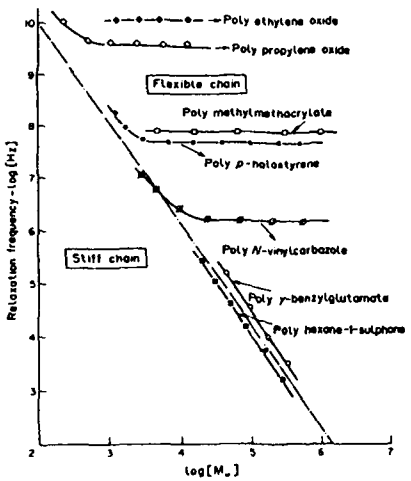

Figure(2) Variation of the dielectric relaxation frequency with molecular weight for polymers of different flexibility

A comparison of the data for the polymer indicates that in the molecular weight dependent region the dominant process is overall rotation of the polymer whereas in the molecular weight independent region it is reorientation of small segments of the backbone which leads to dipolar relaxation. Matsoui and Stockmayer have observed that two processes can be observed, one due to the local motion of the dipole-segmental reorientation and the other due to co-operative motion of large elements of the chain and having a frequency which is close to that for normal mode relaxation. Whereas in the case of viscoelastic or mechanical relaxation, the co-operative motion is dominant, in the case of dielectric relaxation it is local motion of the chain which dominates. Figure (2) does however illustrate the point that the relative importance of each of these processes depends on the stiffness of the polymer backbone. In a chain, such as polyethylene oxide, the molecular weight independent region starts at approximately 10^3, whereas in the case of polystyrene it is 10^4 and in the case of polyvinyl carbazole 10^5-10^6.

INFLUENCE OF GELATION OF POLAR MEDIA

To illustrate the way in which dipolar relaxation is influenced by the process of gelation, we will initially consider the case of a crosslinked polyester coating. Observation of the dielectric relaxation at a frequencey of 1KHz as a function of cure time provides information on the way in which the local mobility changes with network formation. Initially the dipolar relaxation occurs at high frequency and hence the loss is quite low. As the cure proceeds the molecular weight of the chains will increase and this will lead to a slowing down of the dipolar relaxation process, observed as an increase in the loss. However, as the molecular weight increases further we know that the longer range motions will be inhibited and the dipolar process will be dominated by local relaxation processes. As the network formation increases so the chain-chain interactions increase and the mobility of the dipole decreases. The result of this and also the reduction in free volume associated with the glass transition temperature leads to a reduction in the dipolar loss. The observation of the dielectric loss at 1 kHz is therefore an indication of the extent to which the chains in the syste are being constrained by the formation of the matrix structure.

The thermally stimulated current method is also a useful method for the examination of the properties of a curing system. It is observed that in a simple epoxy resin with the exact stoichiometric ratio the TSD curves are composed of a single glass transition peak and a higher temperature space charge peak. The latter is associated with the motion of charge carriers through the matrix and are not associated with individual dipoles. However slight changes in the cure conditions and also the introduction of filler particles into the matrix lead to a multiple glass transition peak being observed, figure (3). The peaks correspond to regions of greater or less mobility. The observation of multiple glass transition peaks can be associated with regions which have a greater or lesser degree of crosslinking than the average value for the matrix. In the case of a filled system, it is easy to undersand, that if there are significant interactions between the resin and the surface then there is the possibility of an immobilized region of polymer in the interfacial region which will have a higher T_g than that of the bulk polymer. Similarly, if the filler reduces the overall density of the matrix material then there are likely to be regions which are more open than the average. It is however surprising that these regions are infact as large as they appear to be.

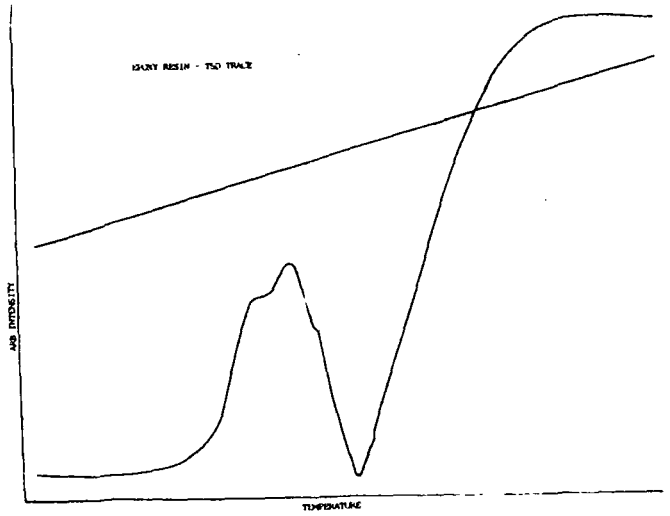

Figure (3) Multiple peaks observed in the TSD traces of an epoxy resin matrix containing a filler system

The technique allows one to observe the change in the position of the glass transition peak as a function of the extent of cure and hence to allow correlation with the degree of reaction, figure (5).

INTERFACIAL REGIONS IN COPOLYMER SYSTEMS

Polyurethanes are widely studied elastomers in which the crosslinks may either be generated by use of a tri functional rreactive unit or as a result of the phase segregation of the copolymer and the subsequent hydrogen bonding. The dielectric studies of this system have revealed a number of interesting features.
To illustrate this type of system we shall consider the case of the MDI-polyethyleneadipate-MDI prepolymer chain extended with either 1,4 or 1,3 butanediol. In the case of the 1,4 butandiol the copolymer will tend to form well defined hard blocks which are fairly well phase separated. The addition of 1,3 butanediol causes a disruption of the hard block structure and as a consequence a greater intermixing of the soft and hard blocks with a consequent increase in the interactions and consequently the glass transition temperature. These trends are clearly illustrated in the case of mechanical studies of the copolymers figure (4). It is also possible to use the modulus to derive the effective crosslink density. The values correlate relatively well with those obtained from the swelling data and indicate that the crosslinking

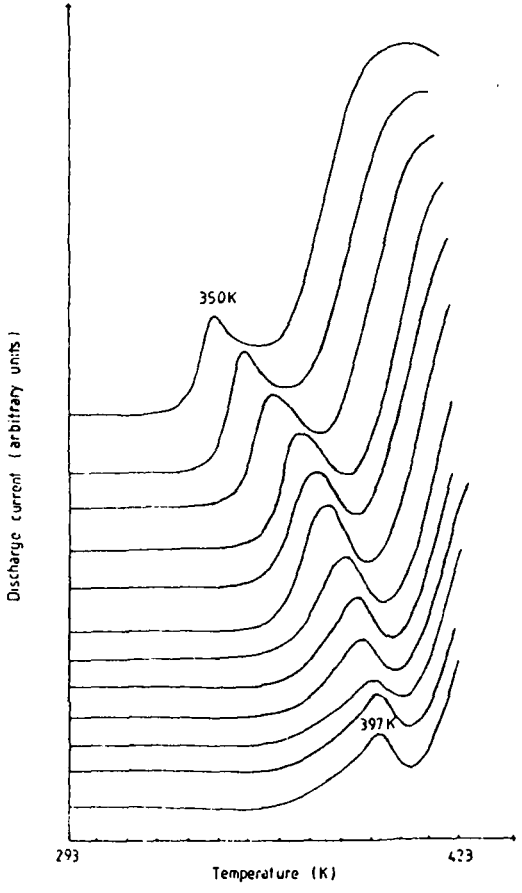

Figure (4) TSD traces illustrating the shift in the glass transition peak as a result of cure of the resin

which can be associated with the elastomeric properties is associated with a combination of urethane and chain entanglement interactions. A detailed study of the dielectric measurements on these systems also indicates that it is possible to observe two relaxation processes with slightly different activation energies. A detailed analysis of these

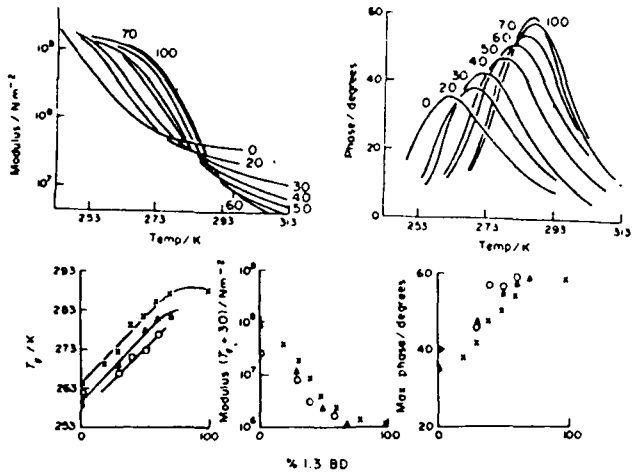

Figure (5) Mechanical relaxation spectra and analysis for the effects of the variation of 1,3 to 1,4 butanediol ratio on the properties of segmented polyurethane elastomers.

systems indicates that the two processes can be associated with relaxation of the dipoles in the completely phase separated region of the polymer and also in the interfacial region, figure (6).

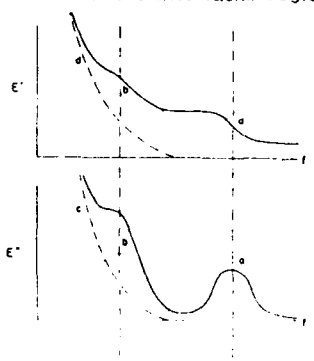

Figure (6) Dielectric relaxation curves for segmented polyurethanes.

The typical elastomer may therefore be modelled in the following way, figure (7).

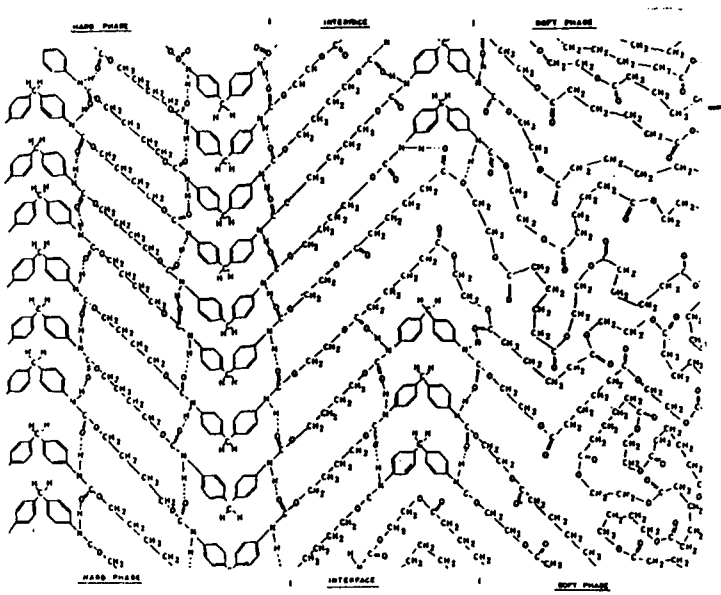

Figure (7) Schematic representation of a segmented polyurethane elastomer

PHASE SEPARATION PROCESSES

The dielectric method is not only capable of providing information on the mobility of dipoles in the system but can also indicate the extent to which phase separation has occured. In a system such as styrene-butadiene-styrene phase separation figure (8) can produce a well defined morphology which will conribute to the dielectric relaxation spectrum of this material. It is not possible to cover the complete theory of the so-called Maxwell Wagner Sillers process in the article, however it can be modelled using a knowledge of the length to breadth ratio of the microphase and the ratio of the conductivities of the two phases. In many copolymers, a low frequency dielectric process can be observed which is associated with the interfacial polarization process. The processes itself involves the transport and trapping of charge carriers to the interfacial region. Broadly speaking, the amplitude and

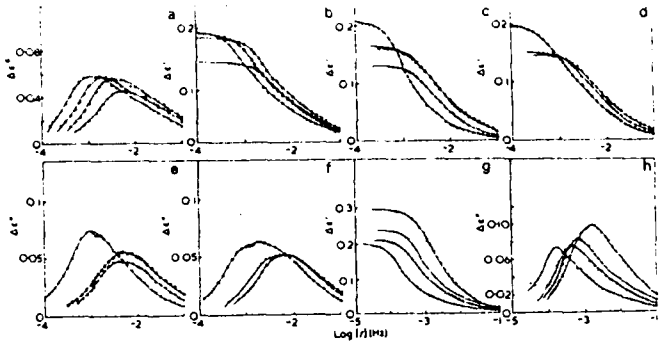

Figure(8) Low frequency dielectric relaxation in doped samples ofstyrene-butadiene-styrene triblock copolymers

time of the process are directly proportional to the distance vector in the direction of the field. In the context of curing systems examination of a novolac system during cure clearly indicates the point at which phase separation is detecte and this can be associated with a model of gelation in which the matrix is non-uniformly crosslinked and hence is an inhomogeneous structure.

CONCLUSION

Dielectric methods can provide useful information on both the local mobility of dipoles in the matrix and also on the extent to which phase separation has occured in the system. The method is however less useful for the estimation of the extent to which crosslinking has occured, however recently it has been shown that in certain systems it is possible to correlate changes in the dielectric spectrum with the reptation motion of polymer molecules and hence is in a way giving information on diffusive motions in the system.

Recommended reading

1)R.T.Bailey, A.M.North and R.A.Pethrick, Molecular Motion in High Polymers Oxford University Press (1983)
2)A.M.North R.A.Pethrick and A.D.Wilson Polymer 19, 913 (1978)
3)L.Bunton,J.H.Daly and R.A.Pethrick J.Materials Science 18, 2817 (1983)
4)R.A.Pethrick and A.R.Eastwood European Polymer J 19, 43 (1983)
5)M.G.B.Mahboubian Jones D.Hayward and R.AS.Pethrick European Polymer J. 11 855 (1987)

ULTRASONIC AND VISCOELASTIC STUDIES OF CHAIN ENTANGLEMENT IN POLYMER SOLUTIONS

RICHARD A. PETHRICK
Department of Pure and Applied Chemistry
University of Strathclyde, Cathedral Street
Glasgow G1 1XL

INTRODUCTION

Whether a polymer chain forms a permanent or temporary entanglement or crosslink; one of the most drammatic effects which is observed is the modification of the dynamic spectrum exhibited by the polymer chain. The other manifestation of network formation is the observation of a modulus value which is directly related to the number of network points per unit volume. In general, we can divide networks into two types; firstly, those in which the chains between the network points are topographically defined in space - "rigid networks" and secondly, those that have flexible regions between junction points - "flexible networks". The most characteristic feature of the dynamics of a polymer chain is its glass transition temperature - T_g. Above T_g, elements of the polymer chain can undergo co-operative molecular motion, below Tg only the uncorrelated motion of short elements of the backbone and side chains are possible. The division of the networks into rigid and flexible can be made on the basis of the glass transition temperature of the backbone polymer structure. In order to understand how the network formation influences the dynamic properties of the matrix it is appropriate to review the measurements which have been made on isolated polymer chains and the way in which their properties are modified on the formation of three dimensional network structures.

DYNAMIC PROPERTIES OF ISOLATED POLYMER CHAINS IN SOLUTION

A polymer chain will adopt a statistical structure which depends on the nature of polymer solvent interactions. In a poor solvent system the chain will collapse and the nature of the interactions between neighbouring bonds will increase and this is reflected in the chain dynamics. For simplicity we will consider the dynamics of an ideal flexible chain in a good solvent. An example of such a system would be polydimethylsiloxane dissolved in toluene. A wide range of techniques exist for the study of the dynamic properties of polymer solutions and include; nuclear magnetic resource, fluorescence lifetime measurements, dynamic light scattering, viscoelastic, ultrasonic and dielectric measurements. In this chapter we will consider the use of ultrasonic and viscoelastic measurements as a method of characterising chain dynamics.

ULTRASONIC RELAXATION MEASUREMENTS ON POLYMER SOLUTIONS

The frequency dependence of the alternation of high frequency sound waves has been used for the study of the dynamic properties of small and large molecules. Sound energy is transmitted through a liquid via the translational motion of molecules in the solution. A pressure wave can induce, by adiabatic compression of the media, an increase in the translational temperature of the solution. If the molecules undergo inelastic collisions it is possible to convert a proportion of the excess translational energy into rotational, vibrational or conformational energy. The dissipation of energy depends on the rate at which energy is returned from the excited state to the pool of translational energy. The rate at which this occurs is a characteristic of the natural relaxation rate of the system and is a function of the energy states of the molecular system. The ultrasonic attenuation (α/f^2) can be described as a function of frequency by the relation:

$$\frac{\alpha}{f^2} = \frac{A}{1+(f/f_c^2)} + B \qquad (1)$$

where A is the amplitude of the process, f_c is the characteristic frequency and B is, for a low molecular weight system the viscothermal loss, characterised by the Navier-Stokes equation which has the form:

$$B = \frac{4\pi^2}{\rho c^3}\left\{(\eta_s + {}^4/_3\eta_v) + \frac{K(\gamma-1)}{C_p}\right\} \qquad (2)$$

where η_v and η_s are respectively the shear and volume viscosities of the solution, ρ is the density, c is the velocity of sound, γ is the ratio of the specific heats; C_p at constant pressure to that at constant volume C_v and K is the thermal conductivity of the solutions. The sound attenuation coefficient (α/f^2) will depend on frequency for a system capable of undergoing conformational change, figure (1). As the temperature of the system is changed so the values of A and f will also vary. The temperature dependence of f_c is related to the relaxation rate (τ) by the relation $\tau = 1/2\pi f_c$. The temperature dependence for a simple thermally activated process is described by an Arrehius relationship:-

$$\tau = A\exp(\Delta H^{\ddagger}/kT)\exp(\Delta S^{\ddagger}/k) \qquad (3)$$

where A is the pre-exponential factor and $\Delta H^{\ddagger}$ and $\Delta S^{\ddagger}$ are respectively the enthalpy and entropy of activation for the rotational isomeric process from the excited to the ground state. This approach has been used for the study of a wide range of substituted ethane molecules.

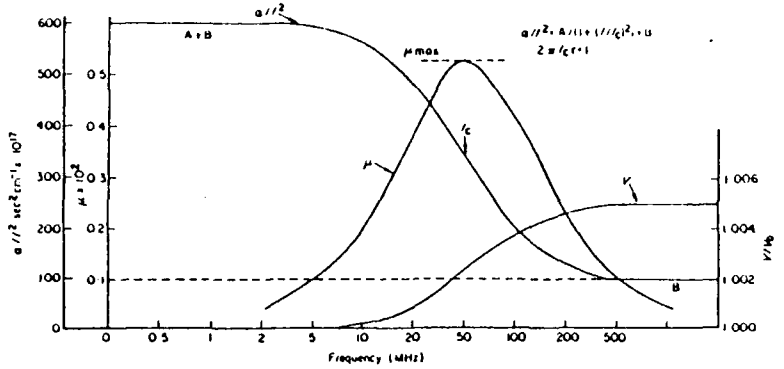

Figure (1) Frequency dependence of the sound propagation in the region of an ultrasonic relaxation

substituted propanes and butanes, cyclic substantiated structures, dioxanes, sulphites and sulphates. The study of polymer molecules in solution is however more complex and this is a direct consequence of the number of degrees of freedom for internal motion possible in a long chain structure. Studies of the activation energy for the processes vary with chain length, table (1). In the case of ethane, no energy

Table 1 Activation energies for internal rotation in hydrocarbons

		Activation energy, $H^{\ddagger}$(kJ.mole^{-1})	
Molecule	n	Internal rotation	Viscous flow
Ethane	2	13.4	-
Propane	3	14.8	-
Butane	4	14.6	-
Pentane	5	16.3	-
Hexane	6	14.2	8.0
Heptane	7	13.6	8.5
Octane	8	13.0	9.0
Nonane	10	13.8	10.9
Decane	11	11.2	11.9
Dodecane	12	15.5	14.0
Tetradecane	13	19.3	15.9

n.b. the first four molecules are gases at room temperature

difference exists between conformational states sound energy. Butane will have two iso energetic higher energy states when the molecule adopts a cis structure and a lower energy true state. Exchange between these structures will lead to the absorption or dissipation of energy and a consequent attenuation of the sound wave. The rate of exchange is a direct measure of the natural frequency of thermal deactivation of the excited state. Whilst the energy states of butane can be described in terms of three energy values, two of which are iso energetic; the addition of a further bond to create propane produces system which is complex. The conformational states can be described in terms of rotational angles associated with bonds two (Φ_2) and three (Φ_3) and lead to an energy surface. The minimum and maximum stable energy states will now be generated by the rotation of both (Φ_2) and (Φ_3), figure (2). The potential energy barrier is a function of the

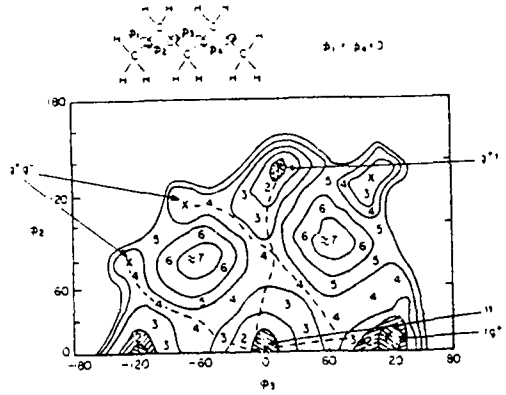

Figure (2) Potential energy contour diagram for pentane.

The terminal bonds are assumed to be fixed with Φ=0; the number indicate the most probable paths for the exchange between isomeric forms, trans = t, gauche = g, + and - refer to right and left handed rotations respectively.

environment created by surrounding molecules. A study of the effects of molecular weight on the amplitude and frequency of the relaxation of narrow molecular weight polystyrene in toluene exhibits a marked dependence on mass upto a value of 10^4 , figure (3). This observation can be explained on the basis of end group effects. The potential energy profile associated with the conformational changes of the bonds at the end of the chains are different and in this case lower than these associated with the centre of the polymer chain. At a molecular weight of about 10^4 the contribution from the ends of the polymer is small and it is only the relaxation of the centre chain which influences the ultrasonic relaxation. Careful analysis of the absorption curves indicate that in addition to the conformational relaxation, the attenuation through a frequency dependent component to B of equation (1).

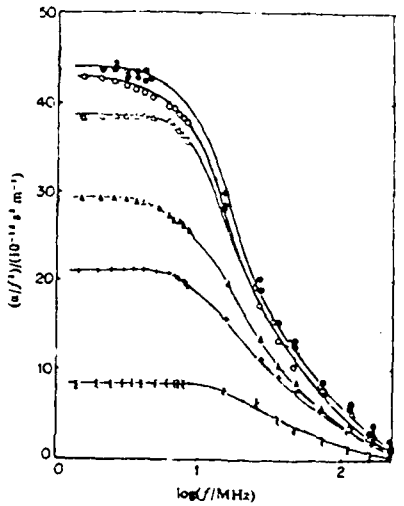

Figure (3a) Ultrasonic relaxation in narrow molecular weight samples of polystyrene in toluene

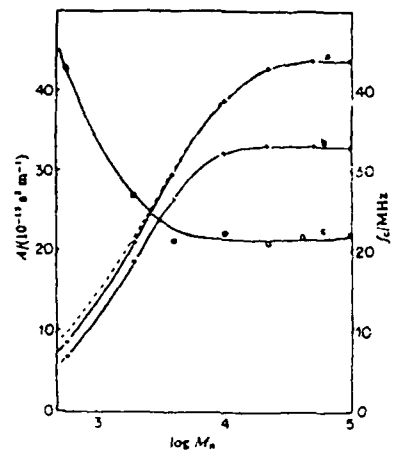

Figure(3b) Plot of the amplitude,characteristic frequency and reduced amplitude as a function of molecular weight for polystyrene

VISCOELASTIC PROCESSES

The frequeny dependence of the low viscosity of a polymer solution reflects the cooperative motions of the whole polymer chain. The first normal mode for the polymer chain is a cooperative distortion of the chain which generates a mode at the centre of the molecule.Higher normal modes have associated with them an increasing number of modes and there is a consequent reduction in the frequency dependent flow viscosity. The behaviour of an ideally flexible polymer chain is illustrated in figure (4). The tail of the normal mode processes

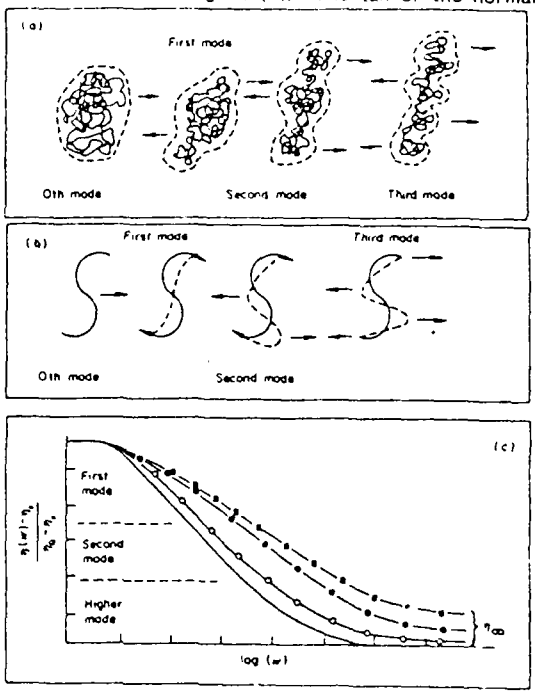

Figure (4) Schematic diagram of viscoelastic relaxation.

extends into the MHz frequency range and contribute a small, but significant, contribution to the ultrasonic attenuation. The mode distribution in an isolated polymer chain is purely a function of the normal mode spectrum and as such is only a property of the

end-to-end distance of the random chain structure. In more concentrated solutions the effects of polymer-polymer chain contents have to be considered. Two factors should be considered; molecular weight of the polymer and the intrinsic backbone flexibility. In the ideal case, the ultrasonic attenuation, corrected for the effects of normal mode relaxation should be independent of concentration, i.e., the attenuation directed by the segment density should be a constant. Studies of polystyrene solutions have shown that this is not the case and have lead to speculations about the origins of these derivations. In order to understand these effects it is useful to examine the viscoelastic properties of polydimethyl siloxane -PDMS. A study of the viscosity of PDMS as a formation of molecular mass indicates that the polymer behaviour can be divided into two regions. Low molecular weights, values below about 14,000, exhibit a viscosity - molar mass dependence of the form; $\eta=KM$, figure 5. Above 14,000 a higher dependence of the molecular weight is observed;$\eta=KM^{3.5}$.

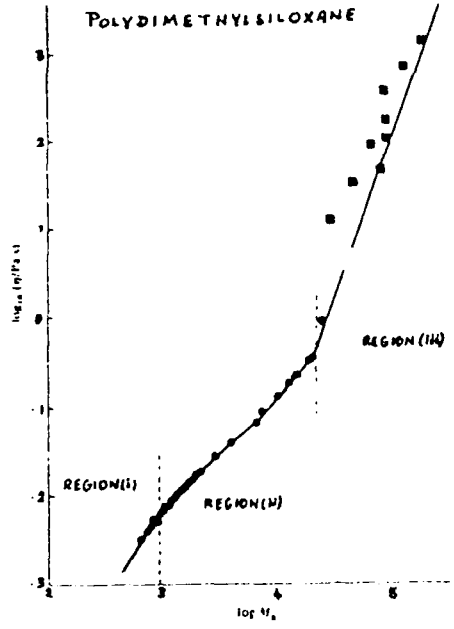

Figure(5) Variation of viscosity with molecular weight for polydimethlsiloxane

This higher order coefficient is believed to be a consequence of polymer-chain entanglements. In the model of Doi and Edwards it is proposed that the long time-low frequency viscoelastic relaxation of the melt is a consequence of the reptational motion of a polymer chain through a tube formed from the entanglements created by the surrounding polymer chains. The rate of the relaxation will depend on the number of entanglements and these will in turn also dictate the magnitude of the observed viscosity component. The classical Doi Edwards theory only considers the contributions to the viscosity arising from the reptation motion and a full explanation of the observed behaviour requires the addition of two further contributions. The first of these is the contribution due to the cooperative normal mode motions of the lengths of chain between entanglements and the final contribution is due to the resistance generated by the freezing out of the local motions of short elements of the backbone.

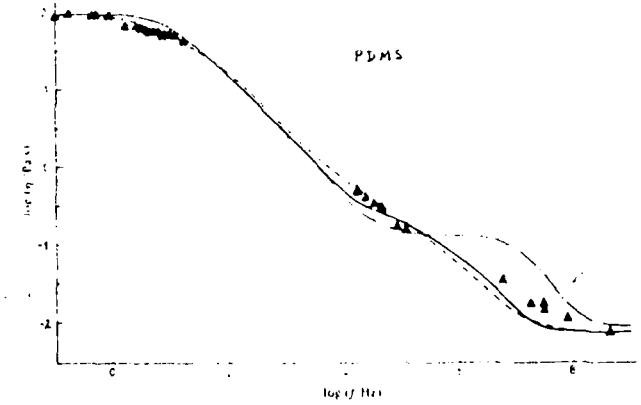

Figure (6) Viscoelastic relaxation in linear polydimethysiloxane.

These three regions of the viscoelastic spectrum can be observed experimentally, figure (6) and will introduce a source of frequency dependence to the ultrasonic relaxation spectrum. Studies of the viscoelastic properties of PDMS have shown the essential correctness of the "reptation" model but have also highlighted the fact that the basic Doi Edwards theory requires modifications to allow for the molecular mass distribution before it is possible to attain an acceptable fit of the experimental data.

ULTRASONIC STUDIES OF ENTANGLED POLYMER SYSTEMS

An increase in the molar mass of a polymer will be expected to increase the normal mode relaxation time and hence shift this relaxation

contribution to lower frequencies. Studies of polystyrene have supported this analysis. If however concentrated solutions or melts are used then other effects can be identified. In the case of PDMS, the local sequential motions of the backbone will occur at frequencies above 1GHz and hence the ultrasonic relaxation is purely a result of the normal mode processes. Initially an increase in molar mass leads to shift in the spectrum to lower frequency, however, around the values for critical entanglement an additional contribution to the relaxation spectrum is observed, figure (7).

A theoretical analysis of the dynamic spectrum indicates that the observed spectrum can be described in terms of a super position of two features. The two entangled chains will have an effective molecular weight corresponding to the combined value of the chains minus the free ends.

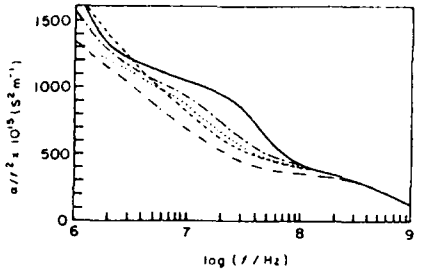

Figure (7a) Ultrasonic relaxation curves for linear polydimethylsiloxane

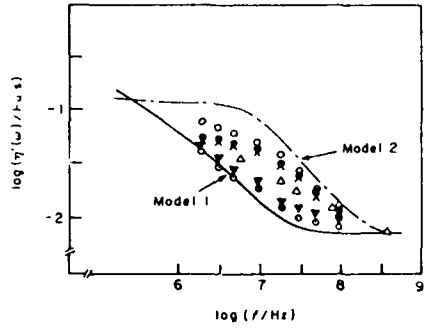

Figure (7b) Dynamic shear viscosity for linear polydimethylsiloxanes

The entanglement will also dictate the mode spectrum and the first normal mode and subsequent mode spectra will have to exhibit a node at the entanglement point. The "ends" of the chains will however be able to exhibit normal mode spectra characteristic of these low molecular weight free ends, figure (8).

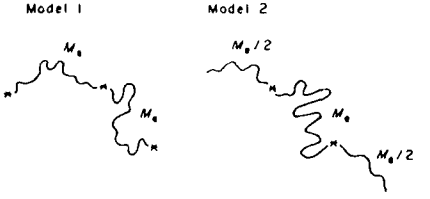

Figure(8) Representation of the mode structures for entangled polymers

This latter motion explains the observation of the additional contribution figure (7) and accounts for the molar mass sensitvity. Once the critical entanglement value has been achieved the main part of the mode spectrum is shifted to lower frequencies and the average value between entanglements becomes constant. This latter process gives an apparently molecular weight independent contribution to the attenuation. The effects of end groups will only be observed for chains with molar mass close to the critical value and as the "effective" molecular mass of the entangled matrix increases, the contribution from the end groups will rapidly decrease. Comparison of viscoelastic and ultrasonic measurements have unambiguously demonstrated the validity of this description of polymer chain dynamics. These experiments illustrate the way in which the creation of a physical entanglement or network point leads to a modification of the relaxation spectrum exhibited by an ideal polymer chain. The same processes will be expected to occur when a polymer chain is crosslinked and are similar to those observed in the case of the ideal isolated flexible chain i.e., the generation of a high value low frequency component characteristic of the overall matrix and increase of the high frequency spectrum corresponding to cooperative motions of the chain elements between entanglement points. There is an additional effect of the formation of interaction points in the matrix which is often not recognised and this is illustrated by a recent study of the process of phase separation in styrene-butadiene-styrene triblock copolymer. -(SBS).

PHASE SEPARATION IN SBS SOLUTIONS

The relaxation spectra of SBS triblock copolymer in solution may be described in terms of the superposition of contributions to the relaxation spectrum from processes associated with motion of the styrene and butadiene blocks and normal mode relaxation of the whole polymer chain. At the point at which the triblock copolymer phase separates to form a three dimensional network is identified by the observation of a marked increase in the high frequency attentuation coefficient as the temperature decreases, figure (9). This contribution is

not a result of scattering of the sound wave by the islands of styrene but is a direct result of the generation of regions of dense polymer structure which is impermeable to the flow of solvent molecules. The styrene domains become like billiard balls joined by permeable elastic structures and the effect is to create an additional component ot the viscosity term of the Navier-Stokes equation which will become frequency dependent at a value close to that for the solvent. In a network we may anticipate that there should exist a high frequency component associated with the rigid network structure of the matrix.

Ultrasonic studies have been reported recently on the changes which occur in the relaxation spectrum as an aliphatic isocyanate is cured with a reactive diol-triol mixture. Initially the ultrasonic attenuation is relatively low, however as the molecular weight of the structure increases so a significant contribution to the attenuation due to normal mode relaxation can be identified.

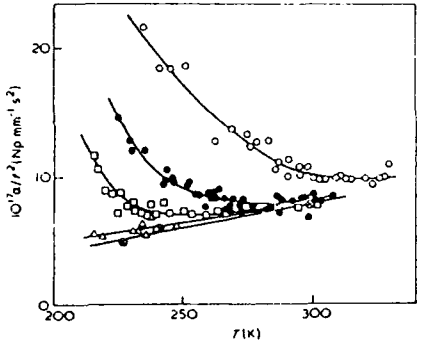

Figure (9) Temperature dependence of attenuation at 740 MHz for SBS solutions in toluene

Since the relaxing unit corresponding to the chain extended isocyanate forms into a gel by the incorporation of the triol, the size of the normal mode is relatively large in these systems and hence the contribution to the ultrasonic attenuation in the MHz range. It is therefore possible, in principle, to correlate the ultrasonic attenuation with the extent of network formation. These studies on flexible gel structures are still in their infancy.

ULTRASONIC STUDIES OF NETWORK FORMATION IN RIGID NETWORKS

The study of rigid networks has been very limited and this is probably a consequence of the difficulty of these measururements. Two systems; novolacs and epoxy resins have however been studied to a limited extent.

i) NOVOLAC RESINS

Novalacs resins have typically a molecular mass of the order of a couple of thousand and are cured by the addition of a methylating-crosslinking agent such as tetra methylene tetra amine. If the measurements are carried out at the temperature of the core characteristic changes are observed in both the attenuation and velocity of sound. The initial increase in the attenuation can be associated with a coincidence of the frequency of local motion of the chain and also normal mode motion with the observation frequency. As the cure process proceeds so the length of the elements COVALENTLY linked increases, but this is modulated by the formation of the three dimensional network. As cure proceeds the rigidity of the matrix increases and this decreases the amplitude of the segmental rotation with a consequent desraux in the ultrasonic attenuation. As the matrix approaches the gel point then the overall rigidity increases markedly with a corresponding increase in the sound velocity. The compressibility of the matrix can be simply related to the sound velocity by the relationship:-

$$K = 1/\rho c^3 \qquad -(4)$$

where K is the adiabatic compressibility, ρ is the density and c is the sound velocity. Initially the matrix is fluid, has a high compressibility and a velocity in the region of 1400 m/sec. Cure decreases the compressibility and raises the sound velocity to a value of approximately 3000 m/sec. The point at which the attenuation changes will not coincide with that for the velocity as they sense different aspects of the system. The attenuation contains information on both the mode structure of the matrix and also the extent to which the backbone can undergo internal rotation. The velocity changes associated with the variation of the molecular motion is small compared with the much larger changes which occur between the fluid and rigid states.

ii) EPOXY RESINS

A study of solid epoxy resins has been performed in which cure is produced by reaction of the diglycydl ether of bisphenol A with a solid diamine. The matrix is solid at the start and cure does not change the state of matter and hence the changes in the velocity are not very large. Similarly, since the attenuation is dominated by the local motion of the backbone, the changes which occur are also not very marked. The initial decrease in the velocity can be associated with changes which occur in the matrix during cure. The density decreases as a result of the generation of voids in the matrix and this also leads to a reduction in the sound velocity. As the cure proceeds so these voids are eventually removed and the velocity is once more observed to increase as a homogeneous solid matrix is generated.

In summary, ultrasonics is useful for the study of cure and network formation in flexible systems but is of limited application in the characterisation of solid matrices.

RECOMMENDED READING

1 RA Pethrick, Ultrasonic Studies of Macromolecules, Prog Polym Sci 9 197-295 (1983)
2 JD Ferry Viscoelastic Properties of Macromolecules Interscience New York London 1978
3 RT Bailey AM North and RA Pethrick Molecular Motion in High Polymers Pergamon Oxford 1981

SPECIFIC PAPERS

1 RA Pethrick and AM Abubaker Polymer Communications 27 194-196 1986
2 RA Pethrick RR Rahalker J Lamb G Harrison AJ Barlow W Hawthorne JA Semlyen and AM North Proc Roy Soc London A394 207-222 1984

MOLECULAR WEIGHT CHANGES AND NETWORK FORMATION BY SCISSION AND CROSSLINKING

A . Charlesby , Watchfield , SWINDON SN 6 8TF. , UK

INTRODUCTION

Many of the physical properties of a polymer can be profoundly modified by changes in molecular weight due to main chain scission , resulting in a reduction in molecular weight , or by crosslinking which at first results in a slight increase in molecular weight , and then by the formation of a network , which can result in a complete change in mechanical behaviour .

Network formation can be produced by chemical means , or by radiation which has great advantages for quantitative analysis and study of resultant physical behaviour .

Outlines are given of several possible methods of providing such network structures .

MAIN CHAIN SCISSION OF POLYMERS

Main chain scission of long chain polymers (degradation , which does not imply any social or moral lapses) is to be distinguished from depolymerization although both involve a reduction in average molecular weight , and corresponding change in physical properties . The conditions understood by main chain scission involve a random distribution along molecular length , so that whatever the initial molecular weight distribution , it rapidly tends towards a random molecular weight distribution , with the weight average M_w and "z" average M_z being twice and three times the number average M_n

A number of important polymers including polyisobutylene (PiB) Teflon (PTFE) , cellulose and poly methyl methacrylate (PMMA) show this behaviour If M_{no} is the initial number average M_n , it will decrease to a value M_{nr} after a dose of r kGy of high energy radiation , where

$$1 / M_{nr} = 1 / M_{no} + 1.04 \times 10^{-4} G(s) r$$

where G(s) represents the number of scission per 100 ev absorbed. This is often about 1 - 2 , and varies little if at all with molecular weight over a very wide range . It can therefore be related to the intrinsic viscosity [η]

$$[\eta] = K M_n^a = K (M_w / 2)^a$$

for a random distribution . Plotting log [η] or any other measure of molecular weight against log r should therefore give a linear plot from which G(s) can be deduced .

This simple exposition leaves open a wide range of questions which will be presented briefly .

(1) Fracture of the main chain leaves two radicals at the side of scission . Which chemical changes then occur to stabilise these highly reactive ends ?

(2) Side shains can also be broken off . Does this occur at the side of main chain scission , or do they occur as independent reactions anywhere along the chain?

(3) Is there some form of chain repair , so that not all initial scissions become permanent ? Evidence for some form of repair is shown by polyisobutylene , where G(s) rises from 2.2 at -196 °C to 10 at 90 °C .(Ref.) Presumably at the higher temprature the initial chain ends can move apart more readily , or react and stabilize . For PMMA the corresponding values are 0.5 to 2.2 again an increase of 4.5 times . (Ref.)

It is highly significant that the same behaviour is shown in a number of bacteria when irradiated in dry form . This would indicate that radiation - induced inactivation in such systems is associated with main - chain breaks or some closely related radiation - chemical reaction , and is not at all specific to biological systems .

(4) In wiew of the similarity in scission behaviour as between PiB (a rubbery material at room temperature) and PMMA (a glass) how do the broken ends migrate away from each other in the glassy state . This poses an interesting question on molecular

mobility in the frozen state , which would of great interest to follow the changes in radical nature and concentration with time after irradiation , using E.S.R techniques for example .

It is interesting to note that in glassy PMMA gas bubbles form if an irradiated specimen is subsequently warmed , allowing gaseous fragments to move together . Are these fragments held separately or do they form from the polymer radicals only when the latter acquires adequate mobility ?

Another interesting feature is that these bubbles do not form near the surface of a piece of PMMA . It must be surmised that this distance of about 1 - 2 mm is the distance for agglomeration and gases formed near the surface can escape . Is there some form of selection or segregation according to gaseous molecular size or nature ?

(5) PTFE is a largely crystalline polymer at room temperature , and irradiation causes main chain scission and a small increase in degree of crystallinity . One may then enquire as to whether scission occurs equally readily in the crystalline and in the amorphous regions which separate them .

(6) If irradiated PTFE is subsequently heated above its melting point , and then recrystallised , there is a considerable increase in the density and degree of crystallisation . It can be assumed that many molecular chains can take part in several crystalline regions , and therefore keep them apart . When scissioned in the amorphous regions , these chains no longer participate in several crystals , which can therefore grow further without this form of interference . Main chain scission can therefore serve as a method of investigating crystallization reactions .

(7) An extremely important aspect of main chain scisson is in radiobiological work involving DNA . Single strand breaks occur naturally and can be repaired , but in the helix form , to become permanent both strand must be broken , and presumably in close proximity. With the radiation doses involved this is extremely unlikely and another explanation must be sought allowing some form of correlation between such scissions . One suggestion is that energy is departed from high energy radiation along short secondary tracks . If each causes several ionizations / excitations along its very short trajectory scissions may be found in close proximity. However as yet there is no evidence of such track effects in simple polymers , although the interaction with incident radiation would be very similar

The nature and characterization of these single and double strand breaks in DNA is of fundamental importance in radiobiology and cancer research and considerable information might be transferred from the simple but related work on scission in long chain polymers .

CROSSLINKING

The physical behaviours and especially the mechanical properties of long chain polymers depend not only on chemical structure and chain mobility (and therefore on temperature) , but also on the association between adjacent molecules . This can take the form of crystallinity , rigidity as in the glassy state , chain entanglements , hydrogen bonding etc. An extremely important form of such intermolecular binding is by crosslinks , representing permanent chemical bonds between what were originally separate molecules . They can occur either directly from one polymer chain to another such as by C - C bonds , or indirectly via a short chemical chain as in the S bonds in rubber vulcanization .

The effect of such bonds depends not only on their density and on the chemical structure of the individual bonds , or even on the molecular mobility and mophology , but also on the distribution of these crosslinks . They may be distributed at random , they may be random except in special regions e. g. crystalline regions , or they may be correlated - i. e. if polymer A is linked to polymer B near a point P , there is an above - average chance of B being linked to polymer molecule C near the same point P . The distribution of crosslinks must also be compared in the crystalline regions with those in the more flexible , amorphous regions . Suitable additive (fillers) such as carbon in rubber may also play an important role . The theory of high elasticity is well-known and is dependent on a statistical approach to molecular arrangement , with corrections for mutually excluded volume , chain rigidity , end effects etc. The theory of tensile strength is less well-understood , and the transition from highly elastic to glassy behaviour can be traced quantitatively for the identical polymer , merely by extending the radiation dose over perhaps a 50 fold range .

Many of these physical properties dependent on crosslink density are also influenced by chain entanglements , which can behave for limited periods as equivalent to permanent crosslinks . The mechanical behaviour of a crosslinked and entangled network will be a composite of permanent elongation plus flow , the latter being due largely to the changes in entanglements under stress . This opens an intriguing possibility of analysing the mechanical behaviour of such crosslinked and entangled networks in terms of their density of links

Crosslinking can be produced in long chain polymers by a number of chemical reagents , but also by high energy radiation , which has a number of advantages , the

reaction shows relatively little dependence on temperature , it leaves no chemical residues similar to those left by chemical catalysts , it can be induced over an enormous range of intensities and ranges , so that the reaction can be studied in the greatest detail at any stage . Furthermore many of these crosslinking reactions are in direct proportion to the dose , so that a quantitative analysis can be achieved , and this allows a direct link between crosslink density and physical properties .

RANDOM CROSSLINKING

The simplest form of crosslinking is one where two radicals on adjacent molecules are linked together to form a direct crosslink . The first change is merely an increase in molecular weight , as when two linear molecules are linked at random to form an X type of structure (with unequal lengths of course) . This is shown by a small increase in viscosity , although the weight average M_w , if measured by light scattering , will show a greater change .

A drastic change occurs when there is an average (δ) of one crosslinked unit (= 0.5 crosslink since each crosslink requires a crosslinked unit on each of the chains) per weight average molecule M_w . At this concentration , termed the gel point , there is an incipient three dimentional network , whose properties are inherently different form the original polymer . This network is essentially a single three - dimensional molecule , and one cannot therefore say that it is a solid , liquid or gas . With increasing radiation dose or degree of crosslinking , this network (or gel) forms an increasing (gel) fraction of the total , while the residue of soluble molecules (sol) shrinks rapidly . A mathematically important relationship exists between this residual soluble fraction s and the crosslink density . This may be expressed in terms of the average number of crosslinks δ per weight average molecule , or when this average becomes very large and the sol fraction or ends of each chain is almost negligible , it becomes more convenient to express it in terms of the average molecular weight between successive links M_c .

Several methods are available to determine the crosslink density under these simple conditions of a random distribution , with no interfering effect such as partial crystallinity , and direct proportionally to dose .

(1) determination of gel dose (by extrapolation of the soluble fraction s, down to s =1 Then δ=1 whatever the molecular weight distribution , for a random crosslink distribution

(2) determination of sol fraction in relation to dose r. This will depend on the molecular weight distribution i.e. weight average M_w , z average , M_z, ... The general expression is

$$g = \delta_g - \frac{1}{2i}\delta^2 g^2 \frac{M_z}{M_w} + \frac{1}{3i}\delta^3 g^3 \frac{M_4 M_z}{M^2_w} - \cdots$$

where δ is the average number of crosslinked unit per weight average M_w (δ = 1 - s , where s is the soluble fraction) .
If the initial distribution is uniform

$$S = \exp(-\delta\sqrt{1-s})$$

which if is random

$$S + \sqrt{S} = 2/\delta$$

and if it is pseudo random ($M_w = M_z/2 = M_4/3 = \cdots M_i/(i-1)$)

$$S = 1/\delta \ .$$

where even a very slight degree of crosslinking initiates formation of a network .

(3) *Swelling of the network*
For a completely crosslinked system

$$\ln(1-x) + x + \mu x^2 + \rho\upsilon(x^{1/3} - x/2)\rho\upsilon / M_c = 0$$

Where ρ is the polymer density , υ is the molar volume of the solvent , and x is the original volume / swollen volume , or for large degrees of swelling (with V = 1/x = swelling ratio)

$$v^{5/3} = (0.5 - \mu) M_c / \rho\upsilon$$

so that once the constants are known , M_c can be deduced directly from the swelling ratio V . In this relation any soluble fraction or chain end effects are ignored .

(4) If the specimen is well above the glass temperature or crystal melting point , the crosslinked network acquires highly elastic properties , and the elastic modulus E is inversely proportional to the crosslink density or its reciprocal M_c .

$$E = 3\rho RT / M_c$$

with ρ = density , RT are gas constant and absolute temperature , a correction should be applied for chain ends (i.e. the portion of the chains containing only one linked unit, and therefore not constituting part of the elastic network) . The value of this correction depends not only on M_c but also on the molecular weight distribution .

(5) More recenty evidence has been found showing that pulsed NMR can be used to distinguish between network (gel = 1 - s) and soluble fraction s , also provide measures of M_c . This will be discussed separately .

By following the changes in mechanical properties with crosslink density over a very wide range - as can be achieved by radiation one can pass through the following physical changes

(a) At low crosslink densities ($\delta < 1$) the polymer is completely soluble . At low temperature it may be somewhat flexible if it is partly crystalline , or rigid as in a glassy state . At high temperature it becomes a viscous fluid , though it may retain a shape for short periods due to chain entanglements .

(b) At higher crosslink densities ($\delta > 1$) it is almost unchanged in mechanical properties while still crystalline or glassy but at higher temparatures it takes on rubber - like properties of high elasticity . The modulus is proportional to radiation dose i.e. crosslink density .The tensile strength also increases .

(c) At even higher crosslink densities, the elastic modulus continues to increase , but the properties are successively those of an overcured rubber , a cheesy, leathery and finally glassy state .

ENHANCED CROSSLINKING

In many crosslinking reactions , there is a direct proportionality between the number of crosslinks and the chemical reagents or better the radiation dose . This is best illustrated by the radiation dose r_g (expressed in kGy) needed to form an incipient network with a random distribution

$$G\, r_g\, M_w = 0.47 \times 10^7$$

where G (the number of crosslinked units per 100 ev absorbed) and M_w is the weight average molecular weight . Typically $G \approx 1$, so that if $M_w = 5 \times 10^5$, r_g = 9.4 kGy approximately . In the case of polystyrene G is very much smaller for radiation chemical reasons, but much higher values are very unusual.

For a series of polyfunctional monomers , or unsaturated polymers , a high degree of crosslinking , giving a rigid or glassy structure , is obtained at far smaller doses , even if M_w is low , say 10^4 . Obviously a very different crosslinking system is involved , with a G value for crosslink formation amounting to perhaps one - hundred times that expected from the energy input . This behaviour is termed enhanced crosslinking , and is in fact a combination of crosslink and a polymerization or grafting reaction . It requires multiple unsaturation either in the polymer P itself, or in a low molecular weight additive known as a sensitizer, S

What is involved is a reaction of the following character

$$P \longrightarrow P\cdot + H \text{ etc. or } \quad S \longrightarrow S\cdot +$$

$$P\cdot + S \longrightarrow PS\cdot$$

$$PS\cdot + P \longrightarrow PSP$$

$$PSP + S + P \longrightarrow PSPSP. \text{ etc . or variants}$$

A single initation step can therefore result in a number of crosslinks associated with each other in close proximity . The relation between network formation and radiation dose is quite different from that applicable to random crosslinking , as outlined above . In particular the network first begins to appear at a greatly reduced radiation dose or initiating chemical concentration . This is the behaviour found in unsaturated polyesters for example , and is also present to some extent in polyisobutene .

Since this is in part a polymerization reaction proceeding through a series of polymers , some means must be found to terminate the reaction , once commenced . This can be achieved for example by the combination of two such crosslinking chains. If i is the chance of a given link being the last one (i.e. reciprocal of the number of links per initiating species) and $i \ll 1$, $\delta_g \approx i/2$ as against 1 for random crosslinking. The required radiation dose $r_{\ }$ is now

$$G\, r_g\, M_w \approx i^2\ 0.47 \times 10^7$$

Then the value of G(crosslinks) at the gelation dose appears to have increased by a factor of the order of i^2 . The plot of sol / dose curve is also very different .

The use of irradiated linear polymers such as polyethylene and rubber is usually to enhance their radiation stability at higher temperatures , or to make use of the memory effect . For the polymers utilised in enhanced crosslinking it is usually to obtain a much higher degree of crosslinking with a very modest dose , though sometimes at the cost of a more expensive sensitizing monomer .

The relationship between such highly crosslinked systems and the resultant physical properties has not been studied to the same extent as have those for lightly crosslinked polymers showing high elasticity . The transition from a very lightly crosslinked polymer , through maximum tensile strength until eventually a glass-like state is reached , deserves far greater attention .

One may enquire why polytransisoprene shows this tendency towards enhanced crosslinking , though it is absent in the equally unsaturated polyisoprene . One possibility is that for a chain crosslinking reaction to occur there must be a suitable morphological arrangement of adjacent molecular chains and this is possibly present in the trans configuration , whereas with the cis form links between polymer molecules A and B place A and B locally in a geometric arrangement where they cannot approach adjacent molecules to allow crosslinking .

The use of so - called sensitizers , notably trifunctional unsaturated monomers , to crosslink linear polymers which would otherwise be resistant to this reaction - e.g. P.V.C. , may involve a link from one polymer molecule to another via the sensitizer , but the doses involved appear low . Another possibility is that the sensitizer forms a three - dimensional network very readily , and that the polymer is trapped within its pores, appearing insoluble as a result . Measurements on low molecular weight PVC , polystyrene etc. might answer this important question. Another matter for study is how these polyunsaturated systems build up a three - dimensional network so readily . A simple polymerization reaction should not , at the low doses involved do more than form largely linear polymerization chains .

OTHER FORMS OF CROSSLINKING

A number of possibilities occur in the formation a network . One of these is by H bonding , which involves a special chemical structure Another is termed endlinking , where a scissioned molecule can , via a reactive radical end, link to a linear molecule to give a T type of intermolecular bond . It is assumed that of all polymer molecules scissioned , a fraction α can form endlinks . In this case the sol fraction depends on α

$$s = (1 - \alpha / 3 \alpha)^2$$

so that for gel formation ($s < 1$) , α must exceed 0.25 . The relation for network formation with $\alpha = 0.25$

$$G r_g M_w = 0.64 \times 10^7 \quad (r \text{ in kGy})$$

as compared with

$$G r_g M_w = 0.47 \times 10^7$$

for simple random crosslinking

The full plot of soluble fraction s versus dose for endlinking is not very different from that for random crosslinking , and the two may well be confused .

COMBINED CROSSLINKING AND SCISSION

In spite of the random absorption of energy by irradiated polymers , there is a very sharp distinction between those which crosslink and those which scission. It must therefore be accepted that a number of intervening steps before the final chemical changes involving selective bond rupture and formation (usually) of reactive radicals .

To see how far the two processes take place on a polymer, one can most conveniently use the Charlesby - Pinner relation $s + \sqrt{s} = 2 / \delta = 2 r_g / r$, which is strictly only applicable to polymers , initially of a random molecular weight distribution ($M_w = 2 M_n$) , and for a random distribution of crosslinks . Then a plot of $s + \sqrt{s}$ versus r^{-1} should give a straight line , passing through the origin ($s = 0$) and r_g . This simple relation has been widely used , often where it is inappropriate , instead of the more general relations for other initial distributions . However if crosslinking and scission occur in the same polymer , and in proportion to dose (with crosslinking predominating) , the distribution will rapidly become a random one and an approximately straight line plot of $s + \sqrt{s}$ is still obtained , but extrapolating to the ratio of scission to crosslinking . This is notably the situation for polypropylene intermediate between the crosslinking polyethylene and the scissioning polyisobutylene .

ANTIOXIDANTS

Crosslinking reactions especially in linear or branched polyolefins , can be greatly affected by the presence of oxygen , which reacts with the radicals which would otherwise provide crosslinks . This is reduced by the addition of antioxidants such as sterically hindered phenols or aromatic amines .

The effect of these and other antioxidants may not only reduce the oxygen effect , it may also reduce the degree of crosslinking , so that higher doses are needed for the same degree of crosslinking . This could be by the transfer of energy to the antioxidant , or the scavenging of polymer radicals which might otherwise result in a crosslinked species . Another question to determine is whether in either of these two patterns of behaviour , the antioxidant molecule is itself modified and can no longer take up this function .

As an example one may quote a LDPE polyethylene whose crosslinking is enhanced by about 35 % using a sensitizer. This sensitizing effect is reduced to 16 % by only 0.25 % of an antioxidant to 10 % with 0.5 % and to 6 % with 1%

FILLERS

The introduction of very small particles such as carbon into highly elastic networks can profoundly influence its mechanical properties , and there are several theories available to explain this behaviour .(Ref.) One assumes that additional crosslinks are formed between carbon particles and rubber for example , but such additional links could also result from an increased dose in the abse ıce of such particles , and this does not appear to be the case . Other formes of intervention can also be considered , but the one favoured by the author is a largely physical one , in which the particles are embedded into the pores the rubber network and therefore reduce its deformability .

REFERENCES

The basic equations relating crosslink or scission density to radiation dose or radical concentration have been published in the early days of the subject of radiation of polymers , and are summarized in " Atomic Radiation and Polymers " by A. Charlesby (Pergamon 1960) which also gives the original references e. g.

Proc Roy Soc (London) A (1954) 222 , 60 , 542 , A(1954) 224 ,120 ;A (1955) 231 , 521 , A (1957) 241 , 495

Flory , P J Principles of Polymer Chemistry (Cornell) 1953

THE USE OF PULSED NMR TO DETERMINE NETWORK FORMATION BY CROSSLINKING AND ENTANGLEMENT

A. Charlesby , Silver Spring , Watchfield , Swindon SN6 8TF , UK

INTRODUCTION

Although nuclear magnetic resonance has been used fo .ny years as a powerful technique for chemical analysis , its use for the determination of arrangement and mobility of high molecular weight systems is almost unknown . Yet it promises a powerful method of investigating such matters as molecular weight , mobility in a solvent , network formation by crosslinks or entanglements and other physical properties without any detailed knowledge of chemical structure . In what follows we shall be primarily concerned with the spin - spin relaxation curve (T_2) using a pulsed NMR technique

The spin - spin relaxation curve (free induction decay , F.I.D) can consist of components representing the rigid structure (crystalline or glassy) , the mobile molecules in a flexible network , and the individual free molecules. At first we consider the relaxation curve for polymer molecules of low molecular weight (typically less than about 10^4) and in a mobile state , either because of a temperature well above the crystalline or glassy state , or because of a solvent. For the simplest case (no solvent) , the curve is usually a simple exponential decay , characterized by a time T_{2L} : $\exp(- t / T_{2L})$. T_{2L} is found to depend on average molecular weight M

$$T_{2L} \alpha M^{-1}$$

Since for such polymers its viscosty η varies approximately as M , it follows that T_2^{-1} measures the mobility of the polymer molecule. This is best shown with polyisobutylene, a polymer which suffers main chain scission in direct proportion to the radiation dose . In a series of samples of diminishing molecular weight, the product $T_{2L} M_n^{0.5}$ remains constant (at 150 ° C) with a scatter of a few percent over a range in M_n from 5200 to 88

For flexible polymers crosslinked to give a partially soluble network , the spin - spin relaxation curve is no longer a simple exponential , but can be represented by the sum of two exponentials

$$A(t) = f \exp(-t / T_{2L}) + (1 - f) \exp (-t / T_{2S})$$

and for initially low molecular weight polymer, the parameter f is found to correspond to the soluble fraction s as determined by the usual solvent technique . The paremeter T_{2S} appears to be determined by M_c the average molecular weight between successive links in the network fraction , while T_{2L} refers to the mobility of the residual free molecules , obviously modified by their dispersion within the polymer network . Thus pulsed NMR appears to offer a rapid , simple and non-destructive method of measuring crosslinking and network formation . The value of T_{2S} is usually of the order of 0.1 to 10 ms , while T_{2L} is often far longer , sometimes about 100 to 1000 ms, so the two components can be readily distinguished . Since crosslinks are permanent chemical bonds , the sol and gel (network) fractions are independent of temperature , the quantities f and 1-f do not vary with temperature , although T_{2L} and T_{2S} do so vary since they depend on molecular mobility .

The importance of the limiting molecular weight (typically about 10^4, depending on factors such as temperature) is because above this value , the spin - spin relaxation curve shows two component f and 1-f (T_{2L} and T_{2S}) even for a polymer which is not crosslinked , and is completely soluble . The explanation is that chains are entangled on a temporary basis , but long enough to appear as crosslinks during the very short time span needed for the NMR pulse measurement . Thus pulsed NMR measures crosslinks + entanglements and in the absence of the former , a temporary network can still appear to be formed at a sufficiently high concentration of entanglements, namely an average of at least one entangled unit per weight average molecule . For some polymers this occurs at room temperature at a molecular weight of about 10^4 , i.e. there are 6×10^{19} entangled units per g of polymer .

Although entangled and crosslinked units appear to behave similary as far as network formation is concerned , at least for a period of less then 1s , they can be readily distinguished since the crosslinks are permanent bonds , while the density of entangled units decrease rapidly with temperature , and the limiting molecular weight rises rapidly above 10^4 . Thus the value of 1-f (due to both crosslinks and entangled units forming a network) decreases rapidly with rising temperature , but reaches a limiting value when all the effective entangled units have disappeared , and only the crosslinks remain . In this manner one can measure not only the number of entanglements , but also their variation with temperature In fact it may be that the number of entanglements remains constant , but their lifetime is diminished , and new entanglements replace them Only the entanglements of lifetime longer than that needed for the pulsed NMR are effective for this

technique . Thus it appears that we can measure entanglement concentrations , their dependence on temperature and their average lifetime .

As might be expected the introduction of a solvent greatly increases molecular mobility and diminishes the number of effective entanglements detected by NMR This can be clearly demonstrated by the reduction of (1 -f) , equivalent to that obtained by a temperature rise . If it is assumed that polymer mobility is what these measurements involve , an equivalence can be posed between temperature rise , and increase in volume due to solvent . It can therefore be shown that the mobility is simply a function of the free volume obtained by either of these two means , and since this NMR measurement parallels viscosity , it appears that viscosity also depends on the free volume (as well as molecular weight).

The above refers to molecules in a highly flexible state , either as in highly elastic network , or as free molecules , these being characterized by the two exponential decays with characteristic times T_{2L} and T_{2S} , with typical times of the order of ms or even sec . For polymer of which a fraction may appear rigid (as in crystals or a glassy system) , a third component appears denoted by T_{2C} , of the order of μs . Moreover unlike T_{2L} and T_{2S} , this free induction decay is no longer exponential (Lorentzian) but is approximately Gaussian , i.e. $\exp(-t^2 / T^2_{2C})$ or more generally $\exp (- t^a / T^a_{2C})$. Here T_{2C} is far smaller than T_{2S} , of the order of 10 μs , so that it can only be picked up from the log (intensity) / log time curve for the shortest times , and it may appear less certain . The transition from T_{2C} to T_{2S} can be readily seen , and it becomes possible to use its measurement to determine crystallization rates . The results thus obtained with pulsed NMR agree with those derived from thermal analyses , but cover a much wider range of times , and the measurements can be made very quickly .

Many attempts have been made to deduce the effect of additive acting as stabilizers for irradiated polymer , and their effect can be readily followed using the FID curves to follow the effect of irradiation for a series of samples . They have also been used to determine the effect of fillers such as carbon particles in rubber .

In one or two polymers subjected to this type of NMR analysis , and well above the crystallization or glass transition temperatures (T_c or T_g) , a third relaxation component has been noted , with a T_m value between T_{2S} and T_{2C} . Its amplitude is usually very small , but its origin is as yet unknown , and indeed its occurence is not fully confirmed . There is of course room (or even possibly a requirement) for an additional component corresponding to the motion of the fractions of a chain , thus into the network at only one point , and for which M_c has no meaning It may also originate from some other form of structure , due to H bonding for example , since it does not occur in most polymers , and is in any case small Some measurements indicate that it only appears above the gel point

The technique can also be used to follow polymerization rates at various temperatures , showing a rapid drop in T_{2L} and f after a certain time (which depends on temperature) as the monomer polymerizes to give polymer which can then entangle to form a network .

The use of pulsed NMR has also been extended to study radiation effect in some biological systems , such as Bovine Serum Albumin , in water . This shows the expected simple exponential decay , whose slope is greatly increased with a relatively small dose . The presence of a very small amount of protector such as thiourea almost completely eliminates this effect of radiation - far more than might be expected if it only intervenes in protecting the biomolecule against the radiation products of the water .

REFERENCES

(a) Generai

A. Charlesby ; Rad. Phys. and Chem. ,14 , 919 (1979)
Tihany Symposium , Budapest , 843 (1983)
A. Charlesby ; Jnl of Radioanalytical and Nuclear Chem. Articles 101 (2) 401 (1986)
A. Charlesby , R Folland ; Rad .Phys. and Chem. , 15 , 393 (1980)
Rad .Res .Conf. , (Tokyo) 336 (1979)
A. Charlesby (Polym. and Biological Macromol.) Polymer J.,19 (5) 649 (1987)

(b) Polyethylene

R Fallow , A Charlesby , Europ Polym J. , 15 , 953 (1979)
J. Polymer Sci. Let Ed ., 16 , 339 (1978)
B J. Bridges , A Charlesby , R Folland , Proc. Roy. Soc. (London) A (1979)
367 , 343
I Kamel , A Charlesby , J Polym Sci. (Phys. Ed) 19 ,803 (1981)
A Charlesby , R Raefer , R. Folland , Rad. Phys. Chem ,11, 83 (1978)

(c) Poly dimethyl Silicones

R Folland , A Charlesby Int J Rad Phys Chem , 8 ,555 (1976)
R Folland . A. Charlesby Rad . Phys. Chem. 10, 61(1977)
J. Poly Sci .,16, 1041 (1978)

(d) Poly Isobutylene

A Charlesby , J . Steven , Int . J. Rad . Phys . Chem ., 8 , 585 (1976)
A. Charlesby , B J. Bridges ,Rad. Phys . Chem., 19. 155 (1982)

(e) Poly Styrene

A. Charlesby , E. M. Joroszkiewicz , Europ. Pol. J . ,21 , 55 (1985)

(f) Poly cis Isoprene

R. Folland , A. Charlesby , Polymer, 20 , 207 , 211 (1979)
A. Charlesby , B.J. Bridges, Europ . Pol. J. , 17 , 645 (1981)

END